Mechanisms of myosin regulation and function during tissue folding

Claudia G. Vasquez
B.S. Biology
Brandeis University (2010)

Submitted to the Department of Biology in partial fulfillment of the requirements for the degree of

Doctor of Philosophy in Biology
Massachusetts Institute of Technology

[September 2015]

Signature of author: Signature redacted
Department of Biology
September 8, 2015

Certified by: Signature redacted
Adam C. Martin
Assistant Professor of Biology
Thesis Advisor

Accepted by: Signature redacted
Amy E. Keating
Professor of Biology
Co-Chair, Biology Graduate Committee

Mechanisms of myosin regulation and function during tissue folding

Claudia G. Vasquez

Abstract

Throughout organismal development, precise three-dimensional organization of tissues is required for proper tissue function. These three-dimensional forms are generated by coordinated cell shape changes that induce global tissue shape changes, such as the transformation of an epithelial sheet into a tube. A model for this transformation occurs early in *Drosophila* development where approximately 1,000 cells on the ventral side of the embryo constrict their apical sides. Apical constriction drives the formation of a furrow that invaginates, forming a tube, and consequently, a new cell layer in the embryo. Constriction of ventral cells is driven by cycles of assembly and disassembly of actin-myosin networks at the cell apex, called pulses. Pulsatile myosin leads to phases of cellular contraction and cell shape stabilization that result in step-wise apical constriction. While many of the key components of the pathway have been identified, how pulsatile myosin is regulated was previously not well understood. The results presented in this thesis identify mechanisms of regulation of these myosin pulses. First, we demonstrated that cycles of phosphorylation and dephosphorylation of the myosin regulatory light chain are required for myosin pulsing and step-wise apical constriction. Uncoupling myosin from its upstream regulators resulted in loss of pulsatile myosin behavior and continuous, instead of incremental, apical constriction. A consequence of persistent, non-pulsatile myosin is a loss of myosin network integrity as the tissue invaginated. Thus, pulsatile myosin requires tight coordination between its activator and inactivator to generate cycles of myosin assembly, coupled to cellular constriction, and myosin disassembly, associated with cell shape stabilization. Second, we demonstrated that myosin motor activity is required for efficient apical constriction and for effective generation of tissue tension. This work defines essential molecular mechanisms that are required for proper cellular constriction and tissue invagination.

Thesis Supervisor: Adam C. Martin
Title: Assistant Professor of Biology

Acknowledgements

I would like to thank my advisor, Adam Martin, for his mentorship. I have had the honor of being the first graduate student in the Martin Lab. As a result, I received a large amount of attention in my first years as a graduate student that really benefitted my development as a scientist. This attention manifested itself in Adam literally teaching me basic experimental skills, from how to orient, mount, and image embryos, to how to pour protein gels (the latter because he discovered I had only used manufactured ones). Importantly, every time Adam taught me a new technique he ensured that I knew the fundamental principles underlying the process and the advantages and limitations of each technique. Additionally, I would like to thank Adam for while at the same time encouraging me to be rigorous with my own work somehow always finding something new to be excited about after I dumped a series of movies that I had deemed "uninteresting." This excitement and passion for inquiry is the skill I am most grateful to have learned from Adam.

To all the members of the Martin Lab (Mike, Frank, Mimi, Jonathan, Natalie, Jeanne, Clint, Hannah, and Elena), thank you for forming a fantastic environment to spend my graduate career. Specifically, I would like to thank Mike for patiently explaining anything I wanted to know about fly genetics, meticulously helping me troubleshoot whatever PCR trouble I found myself in. I would also like to thank Frank (though he will vehemently deny it) for his continuous encouragement and advice, especially when I needed it most. Mimi, thanks for being the resident anything-related-to-math-computer-or-cats-guru, I cannot imagine having a better lab companion for the past 4 years. Jonathan, thanks for finally getting Mimi and me to stop laughing at the mere mention of blebs, but more importantly thanks for pushing us to elevate lab discussions and for really generating a lab environment that is at the same time discerning and welcoming. Soline, thanks for teaching me how to make beautiful embryo cross-sections, tackling the tissue-cutting experiments with me, and for always being there to talk about experiments, grab a coffee (or a beer), or offer a fun dance move.

To my thesis committee members, Terry Orr-Weaver, Frank Gertler, and Roger Kamm — thanks for your time, advice, and encouragement throughout my time at MIT. I would like to thank Terry and Frank for bearing with the more mechanical aspects of my project, and accordingly, I would like to thank Roger for enduring the nitty-gritty biological aspects of my thesis to proffer advice on these aforementioned mechanical aspects.

I would also like to express thanks to our collaborators, Sarah Heissler and Jim Sellers, at the NIH, for their rigorous biochemical characterization of *Drosophila* myosin phosphomutants.

I would also like to thank my family for their support throughout my time at MIT. Mamita, muchas gracias por siempre buscar la parte buena de cualquiera situación, y por continuamente buscarme soluciones cuando yo ya me rendía. Papito, gracias por iniciar mi amor de la ciencia, por incentivarme a perseguir investigaciones científicas en MIT, y por siempre acordarme de evaluar todos las perspectivas de un problema antes de tomar acción. Camila, thanks for your continuous encouragement and, despite being 7 years younger than me, thanks for often being the voice of reason and for helping me see the big picture.

And finally thank you to my friends and teammates, without whom I quite literally would have forgotten to eat while writing this thesis. But more lastingly, thanks for patiently enduring my incessant rambling about flies and myosin, and for always providing an enticing alternative for my non-scientific activities throughout my time at MIT.

Table of Contents

Abstract 3

Acknowledgements 4

Chapter 1: Introduction—Force Transmission in Epithelial Tissues 7

Abstract 8

Introduction 9

Molecular components critical to transmit force in tissues 11

Cell-Cell Junctions 11

The Actomyosin cytoskeleton 15

Transmitting forces across a cell-cytoskeletal network 21

Magnitudes of forces transmitted in a tissue 23

Transmitting forces across a tissue 26

Conclusion 30

References 31

Findings presented in this thesis 39

Chapter 2: Dynamic myosin phosphorylation regulates contractile pulses and tissue integrity during epithelial morphogenesis 40

Abstract 41

Introduction 42

Results 45

Myo-II pulses correlate with fluctuations in apical Rok localization 45

RLC mutants that mimic mono- or di-phosphorylation result in constitutive Myo-II oligomerization independent of Rok 48

RLC phosphorylation dynamics do not trigger changes in Myo-II apical-basal localization 52

Phospho-mimetic RLC mutants disrupt polarized actomyosin condensation 55

Myo-II phospho-mutants exhibit defects in Myo-II assembly/disassembly cycles 59

Myosin phosphatase localizes to the Myo-II contractile network and is required for contractile pulses 63

Myo-II pulses are important for maintaining tissue integrity during morphogenesis 66

Discussion 70

Dynamic Myo-II phospho-regulation organizes contractile pulses 70

Role of pulsatile Myo-II contractions during tissue morphogenesis 73

Materials and Methods 76

Acknowledgments **82**
References **83**
Supplementary Information **88**

Chapter 3: *Drosophila* Myosin ATPase activity limits the rate of tissue folding **91**
Abstract **92**
Introduction **93**
Results **96**
Myosin RLC phosphomutants have reduced actin-activated ATPase activity 96
Myosin RLC phosphomutants have slower cellular contractions than wildtype myosin 98
Myosin ATPase activity contributes to tissue tension 101
Discussion **104**
Materials and Methods **106**
Acknowledgements **108**
Supplementary Information **109**
References **110**

Chapter 4: Discussion **112**
Key conclusions of this thesis **113**
Myosin pulsing is regulated by cycles of myosin phosphorylation and dephosphorylation 113
Cellular force-generation depends on myosin motor activity 113
Unanswered questions and future directions **115**
What are the dynamics of the myosin binding subunit of the myosin phosphatase? 115
Does ROCK regulate MP activity via MBS phosphorylation during apical constriction? .. 116
What are upstream regulators of MBS? 118
Concluding Remarks **119**
References **120**

Chapter 1: Introduction—Force Transmission in Epithelial Tissues

Authors: Claudia G. Vasquez and Adam C. Martin

Review submission to *Developmental Dynamics* for a special issue on "Mechanisms of Morphogenesis." Submitted on August 6th, 2015.

Abstract

In epithelial tissues, cells constantly transmit forces between each other. Force generated by the actomyosin cytoskeleton regulates tissue shape and structure and also provides signals that influence cells' decisions to divide, die, or differentiate. Force transmission in epithelia requires that cells are mechanically linked through adherens junction complexes and that force can propagate through the cell cytoplasm. Here we review molecular mechanisms responsible for force transmission and discuss how such processes are coordinated between cells in tissues.

Introduction

During development, epithelial tissues undergo dramatic shape changes to generate three-dimensional forms that are essential for organ function. For many of these processes, epithelial cells remain adhered to each other as they undergo shape changes. Furthermore, tissues utilize many of the same mechanisms used to shape developing organisms for the maintenance and modification of tissue properties in adulthood. For example, in developing embryos actomyosin-induced contractions drive cell shape changes to generate new tissue morphologies. In adult mammals, endothelial cells line blood vessels and function to provide a barrier between blood and surrounding tissues. In response to vasoactive compounds, like thrombin and histamine, activation of actomyosin induces endothelial cell contraction and increases endothelial tissue permeability (Lum and Malik, 1996).

Force transmission and mechanical signals are factors that influence cell survival and cell fate. The extent to which a single cell spreads influences the magnitude of force generated and affects a cell's decision either to undergo programmed cell death or to enter the cell cycle (Chen et al., 1997; Oakes et al., 2014). Accordingly, cells in an epithelial sheet respond to mechanical stress, and proliferation occurs in the regions of highest stress; these responses are dependent on tension generated by the actomyosin cytoskeleton and transmitted through cell-cell junctions (Nelson et al., 2005; Rauskolb et al., 2014). The degree of cell spreading can also influence cell differentiation in a manner that is dependent on cytoskeleton-dependent signals (McBeath et al., 2004). Stem cells can be biased to adopt certain cellular morphologies and transcriptional profiles by differences in substrate stiffness; this substrate-directed differentiation is dependent on myosin activity (Engler et al., 2006). Thus, intracellular and intercellular mechanical cues influence a variety of cell and tissue behaviors.

This Introduction provides a "bottom-up" discussion of the principles of force transmission through a tissue. First, we discuss the molecular components essential for force

transmission between and within cells, specifically adherens junctions and the actomyosin cytoskeleton. We then discuss how cells organize the actomyosin cytoskeleton to transmit forces across the cytoplasm. We discuss measurements of the forces that cells can transmit in pairs and in tissues. Finally, we provide some examples of how adherens junctions and actomyosin integrate forces across a tissue, and evidence for their requirement *in vivo*.

Molecular components critical to transmit force in tissues

Cell-Cell Junctions

Effectively transmitting force across a tissue requires cells to be mechanically coupled; this coupling is achieved via junctional complexes. Adherens junctions (AJs) link neighboring cell membranes and their internal actin cytoskeletons. Cadherin-family proteins are the transmembrane elements of the AJ complex; the extracellular domains of cadherin proteins can interact with each other, linking neighboring cells (Figure 1A) (Oda et al., 1994; Yap et al., 1997). Because cadherin and its associated proteins connect to the cell's actin cytoskeleton, the AJ can be considered as a mechanical coupler, which connects the actin cytoskeleton of adjacent cells.

Cadherin proteins are composed of extracellular (EC) domains arranged in tandem; E-Cadherin, the vertebrate epithelial cadherin isoform, has 5 EC domains, named EC1-EC5 (Ringwald et al., 1987; Shapiro and Weis, 2009; Shirayoshi et al., 1986). Structural analysis of the extracellular domains of cadherins demonstrated that these domains bind to each other in two distinct conformations, X-dimers (Figure 1B, top) or strand-swapped dimers (Figure 1B, bottom). X-dimers were characterized by interactions between EC1 and EC2 domains of adhering partners (Harrison et al., 2010). Strand-swap dimers were mediated by insertion of a β-strand of the EC1 domain into a pocket on the EC1 domain of the trans-binding partner (Haussinger et al., 2004). *In vitro* force measurements of the different conformations provided insight into the functional difference of the two conformations. While X-dimers became longer-lived upon application of tensile force, behaving like catch bonds, strand-swap dimers were short-lived under tensile force, and thus behave like slip bonds (Rakshit et al., 2012). These results suggested that trans-cellular cadherin interaction conformations respond to mechanical forces, switching from X-dimers with catch-bond behavior under load, to more stable strand-swap dimers in the absence of load. Studies in epithelial cell culture demonstrated that

conformational switching is a mechanism for cadherins to remodel junctions (Hong et al., 2011). Cells expressing a cadherin mutant locked in the X-dimer state displayed increased cadherin mobility at cellular junctions; conversely, cells expressing a mutant that only forms strand-swap dimers, stabilized cadherin at the junctions. Thus, force-sensitive conformational changes of trans-cellular cadherin interactions could be a mechanism to modulate AJ stability (Hong et al., 2011). Regardless of the conformation of trans-cellular cadherin interactions, these extracellular interactions are required to maintain tissue integrity (Kintner, 1992).

While the extracellular domains of cadherins are required for cell-cell adhesion, they are not sufficient to mechanically couple cells. The intracellular domain of cadherin interacts with α- and β-catenin, proteins that connect the cytoplasmic side of cadherins to the actin cytoskeleton (Figure 1A). In *in vitro* experiments, β-catenin bound the cytoplasmic domain of E-Cadherin with high affinity while α-catenin bound β-catenin and actin filaments but not E-Cadherin. These findings suggested the existence of a tetracomplex between E-Cadherin, β-catenin, α-catenin, and actin filaments; however, until recently only a complex between E-Cadherin, β-catenin, and α-catenin (tricomplex) could be isolated or reconstituted (Aberle et al., 1994; Rimm et al., 1995). Application of tensile force on the E-Cadherin, β-catenin, and α-catenin complex resulted in strong binding between the tricomplex and actin filaments; thus, tensile force is required for tetracomplex formation (Figure 1C) (Buckley et al., 2014). *In vivo* studies suggested that this tension-dependent interaction of the AJs components with actin filaments is due to force-sensitive conformational changes in α-catenin. Under low-tension α-catenin adopted an inhibited conformation that obstructs the binding sites of some its binding partners; when tension was applied to the junction, α-catenin adopted a different conformation that revealed these binding sites (Yonemura et al., 2010). Furthermore, measurement of cellular velocity, deformation rate, intercellular, and intracellular rates of cells in an epithelial sheet expressing siRNAs against α- or β-catenin demonstrated that both catenins were required to transmit

tension through an epithelial sheet and to maintain epithelial cohesiveness (Bazellieres et al., 2015).

The components of AJs are important for generation and maintenance of tissues *in vivo*. During development of vertebrate and invertebrate organisms, mutations in cadherin genes caused defects in epithelial organization and morphogenetic movements (Larue et al., 1994; Tepass et al., 1996). Additionally, inhibition of trans-cellular cadherin interactions, via calcium chelation or antibodies, caused tissues to lose adhesion and dissociate (Damsky et al., 1983; Takeichi et al., 1981). Mutation of either α- or β-catenin resulted in tissue adhesion defects. In *C. elegans*, cadherin, α- or β-catenin (HMR-1, HMP-1, and HMP-2, respectively) are required for morphogenetic movements, including cell migration and tissue elongation (Costa et al., 1998). Structure-function analysis of α-catenin in *Drosophila* tissues found that both the β-catenin binding domain and the actin-binding domain of α-catenin are required for AJ formation (Desai et al., 2013). Furthermore, expression of an E-Cadherin–α-catenin fusion could rescue defects caused by α-catenin mutations in developing tissues as well as cell adhesion in cell culture systems (Nagafuchi et al., 1994; Sarpal et al., 2012). Thus, cadherins, catenins, and the actin cytoskeleton all function to not only adhere neighboring cells, but also, to mechanically couple the cytoskeletons of cells.

Figure 1

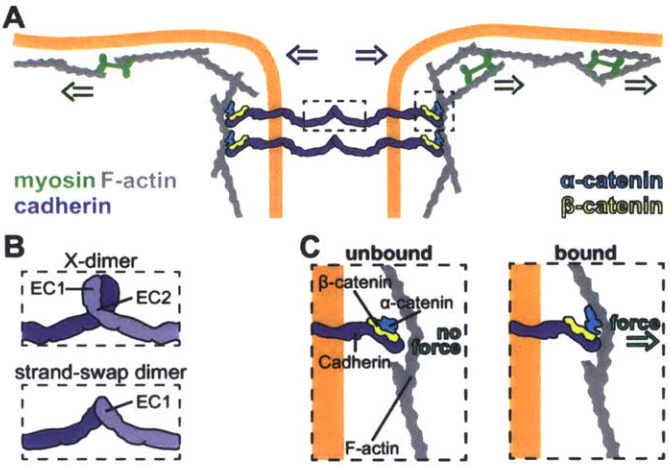

Figure 1 Adherens junctions mechanically couple adjacent cells. (A) AJs are composed of cadherins, α-catenin, and β-catenin. The extracellular domains of cadherins can interact with each other to link adjacent cells. Together α-catenin and β-catenin form a scaffold that links the AJ to the actin cytoskeleton. In this way the intracellular force from actomyosin contraction (green arrows) is transmitted to adjacent cells (purple arrows). (B) Schematic of two different conformations for trans-interaction of vertebrate E-Cadherin highlighting the regions of interest. E-Cadherin can adopt the X-dimer form (top) or the strand-swapped dimer form (bottom). (C) Components of the AJs complex interact in a force dependent manner. β-catenin binds directly to the intracellular domain of E-cadherin in the presence or absence of force. In the absence of force, α-catenin adopts a folded conformation and does not bind strongly to actin filaments (F-actin) (left). When tensile force is applied to the junction, α-catenin adopts a new conformation and binds F-actin tightly (right).

The Actomyosin cytoskeleton

For a tissue to propagate force, force must be transmitted across the volumes of cells. The actomyosin cytoskeleton provides a means to generate and transmit force across a cell. Actin filaments (F-actin) are polymers composed of subunits that have an intrinsic polarity, such that filaments have a plus-end (barbed end) and a minus-end (pointed end) (Figure 2A). Assembly and disassembly occurs at both ends of a filament; however, *in vivo*, actin monomers preferentially add to F-actin plus-ends and disassembly occurs preferentially at the minus-end (Pollard et al., 1982; Pollard and Borisy, 2003). F-actin is assembled in a meshwork just below the plasma membrane in a structure called the F-actin cortex (Bovellan et al., 2014). The F-actin cortex resists and generates force such that cells can maintain or change their shapes.

A key force-generating protein in a cell's cortex is the molecular motor non-muscle myosin II (myosin), which has roles in cell migration, cell-cell adhesion, and morphogenesis (Vicente-Manzanares et al., 2009). Myosins are a superfamily of motors that utilize energy from ATP hydrolysis to move along F-actin tracks (Howard, 2001). Myosin is a hexameric complex that consists of two myosin heavy chains (MHC) and two pairs of light chains called the regulatory light chain (RLC) and the essential light chain (ELC) (Sellers and Knight, 2007) (Figure 2B). The N-terminal head domain of MHC binds F-actin and ATP. The head domain couples energy from ATP hydrolysis to myosin movement along F-actin. Each enzymatic cycle of the motor domain results in its displacement towards the plus-end of F-actin, (refer to (De La Cruz and Ostap, 2004) for a detailed review of the actin-activated ATPase cycle). Compared to other molecular motors, myosin heads spend a relatively short time bound to actin during the ATPase cycle. This characteristic means that individual myosin heads have a low duty-ratio, defined as the proportion of the ATPase cycle a head domain is bound to F-actin. To enable processive movement along F-actin, myosin hexamers assemble into bipolar minifilaments via

the C-terminal coiled-coil domain of the MHC. Bipolar minifilament assembly increases the effective duty ratio of the minifilament structure.

Myosin has to perform diverse functions in tissues, including dynamic cell shape changes and stable generation of tension (Vicente-Manzanares et al., 2011). In mammals there are three isoforms of myosin (myosin-IIA, myosin-IIB, myosin-IIC). These isoforms are differentially expressed during development and in different cell types, suggesting that differences in function are reflected in the molecular behavior and assembly of these motors (Ma et al., 2010; Maupin et al., 1994; Rochlin et al., 1995). Myosin-IIA has the fastest ATPase cycle of the three isoforms and the lowest duty ratio (Table 1) (Kovacs et al., 2003). In contrast, myosin-IIB has a significantly greater duty ratio and has the highest affinity for F-actin of the three isoforms, suggesting it is suited for long-term maintenance of tension instead of short-term force generation, like myosin-IIA (Table 1) (Billington et al., 2013; Wang et al., 2003). The less well-studied myosin-IIC has an intermediate duty ratio; however, in comparison to myosin-IIA, its minifilaments have fewer heads, and as such, myosin-IIC has the lowest probability of the three isoforms of binding F-actin at any given time (Billington et al., 2013; Heissler and Manstein, 2011). Interestingly, *Drosophila* only expresses one non-muscle myosin-II isoform, whose kinetics are most like the fast-acting myosin-IIA isoform, with a low duty ratio (Heissler et al., 2015; Kiehart and Feghali, 1986; Kiehart et al., 1989; Mansfield et al., 1996). Given that the three mammalian myosin isoforms have different kinetic behaviors and thus provide varying functionality to the organism, how *Drosophila* prevails with one isoform is not understood. One possible mechanism is that myosin heads tune their actin-binding kinetics in response to load. An *in vitro* study of two-headed myosin motors exploited the fact that the leading head and trailing head experience different loads to demonstrate that ADP release, the rate-limiting step of the ATPase cycle for myosin motors, is sensitive to load (Kovacs et al., 2007). A resistive load slows ADP release and thus increases the lifetime of F-actin binding, while an assisting load increases the rate of ADP release, resulting in decreased F-actin attachment lifetimes

(Figure 2C). Thus, tension in the cytoskeleton would be expected to slow myosin dynamics and promote a more stable myosin-actin association. There is some indication that the application of force or tension in tissues leads to myosin stabilization and accumulation (Fernandez-Gonzalez et al., 2009; Pouille et al., 2009). However, whether this build-up is due to direct mechanical regulation of the motor, modulation of upstream signaling pathways, or both is not clear.

Myosin activity is primarily regulated by phosphorylation of the RLC (Bresnick, 1999; Sellers, 1991). Dephosphorylated myosin is inactive, where the MHC tail adopts a folded (10S) conformation that blocks productive association of the motor domain with F-actin (Jung et al., 2008; Lowey and Trybus, 2010; Wendt et al., 2001). Phosphorylation of the RLC, primarily on Serine-19 but secondarily on Threonine-18, shifts myosin equilibrium towards an extended conformation (6S), which allows myosin to oligomerize, form bipolar minifilaments, and bind F-actin (Craig et al., 1983; Scholey et al., 1980) (Figure 2B and 2D). The kinases primarily responsible for phosphorylation of the RLC, and consequently myosin activation, are the Rho-associated and coiled-coil kinase (ROCK), myosin light chain kinase, and citron kinase (Amano et al., 1996; Ikebe and Hartshorne, 1985; Totsukawa et al., 2000; Yamashiro et al., 2003). Additionally, ROCK can activate myosin by phosphorylating and inhibiting the myosin binding subunit of myosin phosphatase, the phosphatase that dephosphorylates RLC (Hartshorne et al., 1998; Kimura et al., 1996).

The polarity of F-actin and assembly of myosin into bipolar minifilaments enables plus-end-directed movement of myosin along opposing F-actin to mediate filament sliding (Figure 2E). In muscle, the contractile unit is a sarcomere, which is composed of overlapping arrays of F-actin and myosin, where F-actin plus-ends are fixed at the boundaries of sarcomeres, which themselves are arranged in series. Myosin activation results in movement towards F-actin plus ends, decreasing sarcomere length, and muscle contraction (Huxley, 1963). Models of non-muscle contraction do not rely on ordered arrays of F-actin and myosin, but rely on the physical and biochemical properties of myosin and F-actin (Murrell and Gardel, 2012; Soares e Silva et

al., 2011). Using a reconstituted actin cortex attached to a membrane surface, it was shown that a network, composed of F-actin, myosin, and other actin cross-linking proteins, can contract in the absence of initial F-actin order (Murrell and Gardel, 2012). The initiation of network contraction depended on breaking the balance between compressive and tensile stresses exerted on F-actin by myosin motors. F-actin resists tensile stresses, with the force required to break a single F-actin via extension being approximately 100 pN (Kishino and Yanagida, 1988). Therefore, pulling and filament extension most often result in translocation of F-actin. In contrast, the force required to buckle and break F-actin under compressive stresses is 0.16 pN, almost 4 orders of magnitude less than that required to break F-actin via extension (Lenz et al., 2012). Thus, in a disordered network the compressive stresses on F-actin, generated by myosin, were asymmetrically relieved by F-actin buckling, while the remaining tensile stresses were retained and promoted network contraction via shortening of F-actin segments via F-actin sliding.

Importantly, contraction of this pseudo-cortex has no requirement for a precise or ordered actin filament organization, demonstrating that contraction could be an intrinsic property of actomyosin networks. In non-muscle cells, actomyosin networks most often do not demonstrate a high degree of order and yet still contract (Verkhovsky et al., 1997). Thus, this *in vitro* work provides a physical model for how actomyosin networks without defined polarity and organization contract *in vivo*.

Table 1: Comparison of mammalian myosin isoforms and *Drosophila* myosin properties

Myosin	D.R. of a head	<# of heads per filament>	Effective filament D.R.*	Actin-activated ATPase activity (s^{-1})	F-actin affinity (nM)	% of myosin filaments bound to F-actin
myosin-IIA	~0.1[a]	58[e]	0.95	0.41[e]	<10[a]	72[e]
myosin-IIB	~0.4[b]	60[e]	0.99	0.23[e]	<3[b]	89[e]
myosin-IIC	~0.26[c]	28[e]	0.98	0.13[e]	~3.5[c]	47[e]
***Drosophila* myosin-II**	~0.1[d]	32[d]	0.81	0.82[f]	~60[d]	unknown

[a](Kovacs et al., 2003)

[b](Wang et al., 2003)

[c](Heissler and Manstein, 2011)

[d](Heissler et al., 2015)

[e](Billington et al., 2013)

[f]per-communication with S. Heissler and J. Sellers

* effective filament $D.R. = p$(myosin filament is attached to F-actin), at any given time

effective filament $D.R. = 1 - (1 - D.R.)^{\frac{n}{2}}$

$D.R.$ = duty ratio

n = total number of heads per myosin mini-filament

Figure 2

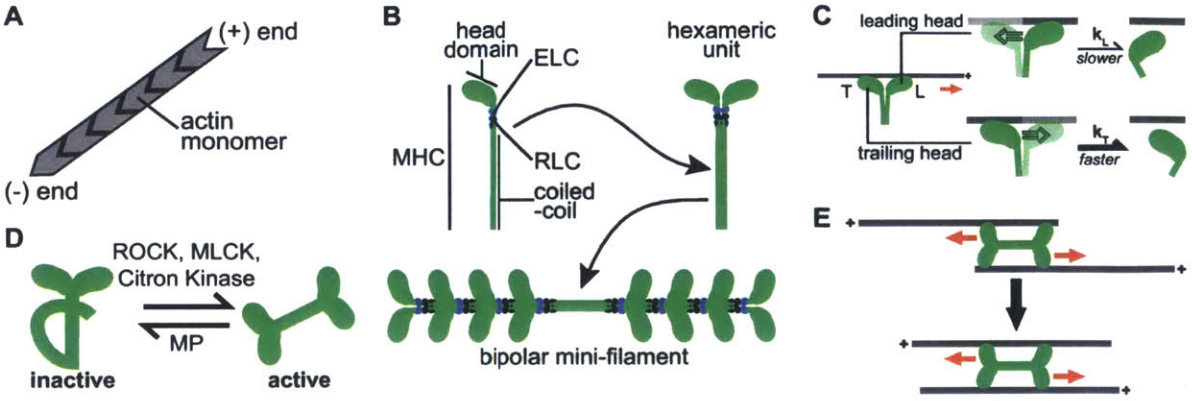

Figure 2 Properties and regulation of the actomyosin cytoskeleton. **(A)** Actin monomers assemble into polar filaments with plus-ends and minus-ends. **(B)** Myosin is a hexameric complex composed of 2 myosin heavy chains (MHCs), 2 essential light chains (ELCs), and 2 regulatory light chains (RLCs). The MHC contains the head or motor domain, which binds and translocates F-actin, and a coiled-coil region that assembles with other coiled-coil tails to form bipolar minifilaments (bottom). **(C)** Leading and trailing heads experience different loads, which affect F-actin attachment lifetime. Unlike the trailing head (bottom), the leading head (top) experiences a resistive load, which slows the rate of ADP release (k_L) and increases the lifetime of F-actin binding, compared to the trailing head ($k_T > k_L$). **(D)** Phosphorylation of the RLC by Rho-kinase (ROCK), myosin light chain kinase (MLCK), or Citron kinase promotes activation of motor activity and bipolar minifilament assembly. Dephosphorylation of the RLC by myosin phosphatase (MP) inactivates and disassembles myosin minifilaments. **(E)** Bipolar myosin minifilaments promote contraction of anti-parallel F-actin filaments because myosin heads walk towards the plus-ends of F-actin. In this schematic we have minimized the number of myosin heads in the bipolar minifilament for simplicity.

Transmitting forces across a cell-cytoskeletal network

The ability to transmit force across a cell is essential for force generation on a cellular scale; transmission requires transduction of force across the cell's cytoplasm through a coherent mechanical network. Myosin inhibition caused the cell's cytoplasm to fragment as it lost circumferential actin bundles and stress fibers (Cai et al., 2010). Thus, myosin activity is essential to maintain a coherent actin network that spans an entire cell.

Advances in microscopy have uncovered a suborganization of cytoskeletal components required to transmit forces in a cell. Treatment of cells with Latrunculin A, a small-molecule that sequesters actin monomers, revealed "nodes" of actin structures throughout the cortex (Luo et al., 2013). Using super-resolution microscopy, nodes were visible without drug treatment, demonstrating that these node structures were not an artifact of drug treatment. Analysis of node movement demonstrated that nodes do not move by pure diffusion, but movement is best described by a biased random walk, suggesting that node movements are coupled via the actin cytoskeleton. In particular, nodes that were less than 2 μm apart moved towards each other. Myosin localized to actin nodes and myosin motor inhibition with blebbistatin caused nodes to move by pure diffusion, demonstrating that myosin motor activity is required to transmit force between nodes. Actomyosin nodes and their coalescence was also observed in contractile rings of fission yeast (Vavylonis et al., 2008). Here, high-speed microscopy of node movements uncovered a mechanism where myosin in nodes stochastically "captured" F-actin growing from a nearby node, exerted force on it, and then released it. These transient connections between nodes were sufficient to generate a contractile ring that could separate daughter cells during cytokinesis. These studies demonstrated that, while non-muscle cells may not display highly-ordered actomyosin organizations (like those observed in muscle cells), they do display supramolecular complexes that are essential for force transmission through a cell.

Supramolecular structures, such as nodes, are integrated into larger cellular structures that transmit forces across a cell. For example, stress fibers are 10-200 μm long bundles of cross-linked actin and myosin that can consist of a repeated sarcomere-like structure and can transmit force across a cell (Katoh et al., 1998). Ablation of a single stress fiber, in living cells growing on a compliant surface, resulted in viscoelastic retraction of the cut ends, compensatory relaxation of the extracellular surface, cell shape change, and actin cytoskeleton remodeling (Kumar et al., 2006). These results demonstrated that individual stress fibers play a role in stabilizing cell shape and exerting force on extracellular adhesions via contractile forces. Cells grown on soft matrices form contractile lamellar networks, characterized by myosin nodes dispersed in a randomly polarized branched F-actin meshwork and without any stress fibers (Verkhovsky et al., 1997; Yeung et al., 2005). These lamellar networks also generate and transmit force with lamellar networks contributing up to 60% of a cell's total traction stress (Aratyn-Schaus et al., 2011). These results demonstrated that a range of actomyosin organizations generate and transmit forces, providing mechanisms for cells to modulate force generation in the context of a tissue.

Magnitudes of forces transmitted in a tissue

To highlight the significance of transmitting forces in tissues, we first discuss the magnitude and nature of measured forces transmitted between cells. One approach to measure forces transmitted between cells is to examine the force balance for a pair of adherent cells in which cell-substrate traction forces are known. Maruthamuthu et al. found that the tensile force between pairs of isolated epithelial cells was approximately 100 nN and oriented perpendicularly to the interface (Maruthamuthu et al., 2011). This magnitude of force would require on the order of thousands of myosin minifilaments (Finer et al., 1994). Using fabrication techniques to adhere endothelial cell pairs to each other by a single contact and measuring the traction forces exerted by these cells, Liu et al. determined that the tugging force exerted by a cell at a single cell contact is approximately 40 nN (Liu et al., 2010). Additionally, the size of the cell-cell contact is determined by the magnitude of the tugging force generated by the neighboring cells, which is dependent on myosin activity. Activation of myosin contraction, by inhibition of myosin phosphatase or addition of vasoactive compounds, increased the intercellular tugging force and resulted in a larger cell-cell contact. Conversely, inhibition of myosin activity decreased tugging force and diminished the size of the cell-cell contact. Furthermore, contractile force induces F-actin assembly at the junction, providing a possible mechanism for tension-dependent cell-cell contact size (Leerberg et al., 2014). Thus, studies examining the forces exerted by cells in cell pairs, demonstrated that there is coordination between actomyosin-generated mechanical forces and cell-cell contacts.

The principles of cellular force balance can also be used to quantify forces in epithelial sheets (Tambe et al., 2013). Measurement of the traction forces exerted by individual cells in a spreading epithelial monolayer demonstrated that tensile stress increases from the sheet edge to the sheet center (~300 pN μm^{-2} to ~1,000 pN μm^{-2}) (Trepat et al., 2009). Thus in a cell sheet

with 2 mm in diameter, an enormous amount of force is transmitted across cells and through junctions.

An important question is whether similar levels of force are experienced in the tissues of an organism. Previously, force inference in living tissues has relied on laser ablation techniques to infer tissue tension from the initial recoil velocity of the tissue following a cut (Hutson et al., 2003; Kiehart et al., 2000). These studies have provided insight into the relative tensile state of a tissue prior to the cut, and the directionality of tension generation in a tissue; however, ablation techniques do not allow absolute measurement of force in a tissue. To study forces dynamically generated by a tissue during morphogenesis, Zhou et al. embedded embryonic dorsal tissue of *Xenopus* in an agarose gel of known mechanical properties (Zhou et al., 2015). By tracking the displacement of fluorescent beads embedded in the gel as the dorsal tissue underwent convergent extension (convergence along the mediolateral embryonic axis and extension along the anterio-posterior axis), the authors were able to map the stress field surrounding the tissue. Through this analysis, the authors found that the dorsal tissue produces approximately 5 pN μm^{-2} of stress during convergent extension. A recent study optically trapped cell-cell interfaces in the early *Drosophila* embryo and found that they generate 100 pN of tension, which could be generated by about fifteen myosin minifilaments (Bambardekar et al., 2015). Furthermore, by measuring the deflection of an interface after release from an optical trap, the authors found that the embryonic tissue behaves as a viscoelastic material, with a combination of elastic components (springs) and viscous components (dashpots) (for a review and detailed description of these mechanical components see (Davidson et al., 2009)). These studies and others have begun to provide information on the magnitude of forces generated in living tissues and organisms. Overall, it appears that tissues have to manage a high magnitude of force, with forces *in vivo* being lower than cultured cells. One possible explanation for the discrepancy in these force measurements could be due to varying degrees of stiffness of the extracellular matrix. However, more *in vivo* studies will elucidate the range of forces that tissues

produce and furthermore will determine key properties of cells and their surrounding environments that are required to tune force generation in a tissue.

Transmitting forces across a tissue

To transmit force across a tissue cells must couple intracellular force transmission with mechanical coupling across intercellular contacts. Model systems, such as *Drosophila,* have provided a means to experimentally test the importance of each of these mechanisms. An excellent model of epithelial sheet contraction and folding is formation of the *Drosophila* ventral furrow. At the onset of furrow formation, the ellipsoid embryo consists of a single epithelial sheet that surrounds the yolk. Cells of the prospective mesoderm constrict their apical (outside) ends, which promotes furrowing, or folding, of the epithelial sheet into a tube (Figure 3A). Another model for epithelial sheet contraction is *Drosophila* dorsal closure, whereby amnioserosa cells, a squamous epithelium on the dorsal face of the embryo, apically constrict, and the lateral epidermis moves dorsally such that they meet and fuse over the amnioserosa cells. The lateral epidermis forms a supracellular actomyosin cable that surrounds the amnioserosa and shortens throughout dorsal closure (Figure 3C) (Kiehart et al., 2000; Peralta et al., 2007). From laser cutting experiments, it has been inferred that both ventral furrow formation and dorsal closure involve relatively high tension transmitted across the tissue (Hutson et al., 2003; Martin et al., 2010).

During ventral furrow formation and tissue folding, AJs are required to transmit tension across the tissue. Depletion of any component of the AJ, E-Cadherin, β-catenin, or α-catenin during ventral formation, resulted in tears in the normally supracellular myosin meshwork that spans the ventral tissue (Martin et al., 2010) (Figure 3B). Depletion of E-Cadherin or β-catenin during dorsal closure resulted in separations between the amnioserosa and the epidermis and also disrupts the actomyosin cable (Gorfinkiel and Arias, 2007). Tearing of the tissue-wide cytoskeletal meshwork in embryos with weakened AJs, demonstrates that AJs are required to mechanically integrate the cytoskeleton across a tissue.

Myosin is required not only to generate force, but also to maintain cell shape. Depletion of the myosin heavy chain during dorsal closure caused the apically constricting amnioserosa cells to separate from each other, as well as disrupted the organization of the supracellular cable (Franke et al., 2005). Generation of an animal with mosaic myosin expression resulted in the stretching of myosin-null cells adjacent to cells expressing myosin (Figure 3D). Thus, cells that do not express myosin cannot generate resistive tensile forces from the supracellular cable and are passively stretched by the neighboring cells contracting their sections of the supracellular cable.

A surprising property of contraction in many systems, including the ventral furrow and dorsal closure, is that actomyosin activity is pulsatile (for review see (Martin and Goldstein, 2014)). Myosin pulses involve cycles of myosin accumulation and subsequent remodeling, which can result in incremental cell constriction (Martin et al., 2009) (Figure 3E). Myosin pulses require dynamic regulation of the myosin motor by regulatory light chain phosphorylation, with cycles of phosphorylation and dephosphorylation (Vasquez et al., 2014). Interestingly, abrogation of myosin pulses either via depletion of a subunit of myosin phosphatase (a negative regulator of myosin activity) or by expression of myosin regulatory light chain phosphomutants resulted in tears in the supracellular myosin meshwork (Vasquez et al., 2014). Thus, dynamic regulation of myosin activity is somehow required to maintain stable mechanical connections between cells, although the mechanism is not yet clear.

The observation of pulsatile contraction, where it is thought that myosin activity periodically ebbs, leads to the question, how do cells transmit forces between myosin pulses. Analysis of pulsatile behavior of ventral cells reveals that myosin pulses can generate different types of cellular responses: ratcheted pulses (cell constricts and stabilizes constricted area), oscillating or unratcheted pulses (cell constricts but relaxes area), and unconstricting pulses (cell does not constrict, or minimally constricts) (Figure 3E) (Xie and Martin, 2015). Myosin persists in the apical domain during ratcheted pulses, but does not persist during unratcheted

pulses, suggesting that, specifically during ratcheted pulses, a cell's myosin network is stabilized (Martin et al., 2010; Xie and Martin, 2015). Interestingly, ratcheted pulses seem to be required for cells to cooperatively contract in a tissue (Xie and Martin, 2015). If a cell is undergoing an unratcheted pulse, neighboring pulses appear to slow the cell's constriction, suggesting competition between neighboring contractions. However, for a cell undergoing a ratcheted pulse, neighboring contractions enhance its constriction rate, suggesting that ratcheting allows cells to cooperate during tissue shape change. A model for this effect is that the persistence of myosin structures that follow ratcheted pulses bear tensile force, allowing forces in neighboring cells to propagate across a ratcheting cell, and thus add up, instead of dissipating. Consistent with this model, depletion of a gene that increases the frequency of unratcheted pulses dramatically reduced epithelial tension (Martin et al., 2010); thus, ratcheted pulses, but not unratcheted pulses, promote epithelial tension during tissue shape change. In addition, there is a transition from unratcheted to ratcheted pulses and the onset of ventral furrow formation (Xie and Martin, 2015).

Another example of pulsatile and ratchet-like apical constriction occurs in amnioserosa cells during dorsal closure. Early in dorsal closure, amnioserosa cell areas oscillate in a manner that correlates with pulsatile myosin behavior; as dorsal closure proceeds, area oscillations are dampened and apical constriction is more ratcheted (Figure 3E) (Blanchard et al., 2010; David et al., 2010; Solon et al., 2009). Thus, like ventral cells, amnioserosa cellular behavior transitions from a phase where there are more unratcheted or unconstricting pulses to a phase where ratcheted pulses are the dominant cellular behavior. David et al. identified a negative feedback loop with a delay that is responsible for cycles of myosin assembly and disassembly in amnioserosa cells (David et al., 2010). This delay is sufficient for amnioserosa cells to build up a persistent actomyosin network, inducing cellular constrictions to become more ratcheted (David et al., 2010; David et al., 2013). Thus, in both dorsal closure and the ventral furrow, effective

force transmission across a tissue requires a transition from unratcheted or oscillatory cellular constrictions to ratcheted constrictions that sustain cell spanning cytoskeletal structures.

Figure 3

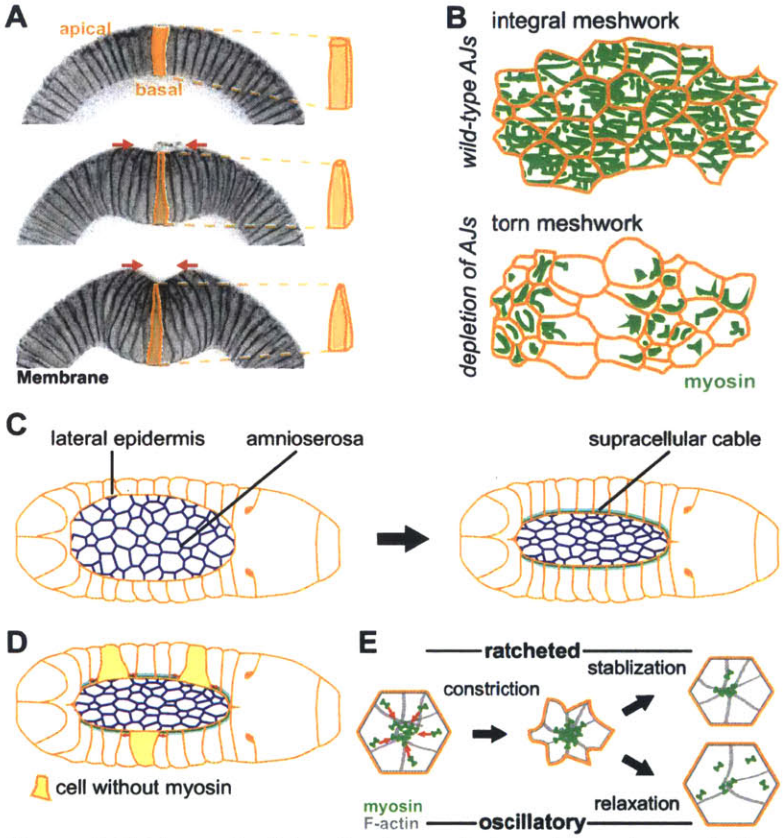

Figure 3 Evidence for AJ and actomyosin based force transmission *in vivo*. (A) Apical constriction drives folding of the ventral tissue (ventral furrow formation) in the early *Drosophila* embryo. The left panels are cross-sections of staged embryos, stained for a membrane marker, undergoing ventral furrow formation. Cells are initially columnar (top) and then apically constrict to become wedged shape (middle and bottom), driving invagination of the tissue. (B) Illustration showing importance of AJs in transmitting tension across a constricting tissue. Myosin forms a supracellular meshwork that spans the constricting tissue (top). Depletion of any AJs component results in tears in the supracellular cytoskeletal meshwork (bottom). (C) Schematic of dorsal closure process. Amnioserosa cells apically constrict, while lateral epidermis forms a supracellular actomyosin cable (green) that also contracts the amnioserosa tissue. (D) In a mosaic animal, epidermal cells that express myosin stretch (red arrows) cells that do not express myosin (yellow cells). (E) Schematic of the apical surface of a cell undergoing ratcheted or oscillatory constriction. Initially, both cells constrict, however the decrease in cell area is stabilized and epithelial tension is facilitated by ratcheted constriction (top). In contrast, the cell shape is not stabilized and relaxes during oscillatory constrictions (bottom).

Conclusion

Effective transmission of force in between cells and through a tissue requires three properties: (1) Attachments between neighboring cells. In this review we only discussed cadherins but tight junctions and desmosomes also play a role in force transmission (Bazellieres et al., 2015); (2) Coupling between the adhesion complex and the force-generating machinery; (3) A coherent intracellular meshwork, like the actomyosin cortex (Figure 4). Together, these features mechanically couple cells to each other such that they can generate forces (4), react to forces, and ultimately, generate tissue-wide shape changes.

Figure 4

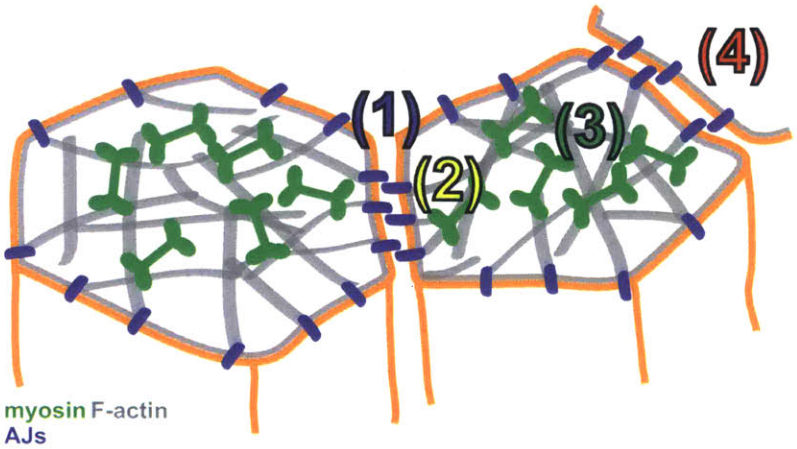

Figure 4 Summary of components required to transmit forces across a tissue.
(1) Adherens junctions mediate cell-cell attachment.
(2) Adherens junctions couple the cell membrane to F-actin cytoskeleton.
(3) Actin and myosin form a coherent network across the cell, called the cortex. Myosin can contract F-actin networks to transmit force to the neighboring cell **(4)**.

References

Aberle, H., Butz, S., Stappert, J., Weissig, H., Kemler, R., and Hoschuetzky, H. (1994). Assembly of the cadherin-catenin complex in vitro with recombinant proteins. J Cell Sci *107 (Pt 12)*, 3655-3663.

Amano, M., Ito, M., Kimura, K., Fukata, Y., Chihara, K., Nakano, T., Matsuura, Y., and Kaibuchi, K. (1996). Phosphorylation and activation of myosin by Rho-associated kinase (Rho-kinase). J Biol Chem *271*, 20246-20249.

Aratyn-Schaus, Y., Oakes, P.W., and Gardel, M.L. (2011). Dynamic and structural signatures of lamellar actomyosin force generation. Mol Biol Cell *22*, 1330-1339.

Bambardekar, K., Clement, R., Blanc, O., Chardes, C., and Lenne, P.F. (2015). Direct laser manipulation reveals the mechanics of cell contacts in vivo. Proc Natl Acad Sci U S A *112*, 1416-1421.

Bazellieres, E., Conte, V., Elosegui-Artola, A., Serra-Picamal, X., Bintanel-Morcillo, M., Roca-Cusachs, P., Munoz, J.J., Sales-Pardo, M., Guimera, R., and Trepat, X. (2015). Control of cell-cell forces and collective cell dynamics by the intercellular adhesome. Nat Cell Biol *17*, 409-420.

Billington, N., Wang, A., Mao, J., Adelstein, R.S., and Sellers, J.R. (2013). Characterization of three full-length human nonmuscle myosin II paralogs. J Biol Chem *288*, 33398-33410.

Blanchard, G.B., Murugesu, S., Adams, R.J., Martinez-Arias, A., and Gorfinkiel, N. (2010). Cytoskeletal dynamics and supracellular organisation of cell shape fluctuations during dorsal closure. Dev *137*, 2743-2752.

Bovellan, M., Romeo, Y., Biro, M., Boden, A., Chugh, P., Yonis, A., Vaghela, M., Fritzsche, M., Moulding, D., Thorogate, R., *et al.* (2014). Cellular control of cortical actin nucleation. Curr Biol *24*, 1628-1635.

Bresnick, A.R. (1999). Molecular mechanisms of nonmuscle myosin-II regulation. Curr Opin Cell Biol *11*, 26-33.

Buckley, C.D., Tan, J., Anderson, K.L., Hanein, D., Volkmann, N., Weis, W.I., Nelson, W.J., and Dunn, A.R. (2014). Cell adhesion. The minimal cadherin-catenin complex binds to actin filaments under force. Science *346*, 1254211.

Cai, Y., Rossier, O., Gauthier, N.C., Biais, N., Fardin, M.A., Zhang, X., Miller, L.W., Ladoux, B., Cornish, V.W., and Sheetz, M.P. (2010). Cytoskeletal coherence requires myosin-IIA contractility. J Cell Sci *123*, 413-423.

Chen, C.S., Mrksich, M., Huang, S., Whitesides, G.M., and Ingber, D.E. (1997). Geometric control of cell life and death. Science *276*, 1425-1428.

Costa, M., Raich, W., Agbunag, C., Leung, B., Hardin, J., and Priess, J.R. (1998). A putative catenin-cadherin system mediates morphogenesis of the Caenorhabditis elegans embryo. J Cell Biol *141*, 297-308.

Craig, R., Smith, R., and Kendrick-Jones, J. (1983). Light-chain phosphorylation controls the conformation of vertebrate non-muscle and smooth muscle myosin molecules. Nature *302*, 436-439.

Damsky, C.H., Richa, J., Solter, D., Knudsen, K., and Buck, C.A. (1983). Identification and purification of a cell surface glycoprotein mediating intercellular adhesion in embryonic and adult tissue. Cell *34*, 455-466.

David, D.J., Tishkina, A., and Harris, T.J. (2010). The PAR complex regulates pulsed actomyosin contractions during amnioserosa apical constriction in Drosophila. Dev *137*, 1645-1655.

David, D.J., Wang, Q., Feng, J.J., and Harris, T.J. (2013). Bazooka inhibits aPKC to limit antagonism of actomyosin networks during amnioserosa apical constriction. Dev *140*, 4719-4729.

Davidson, L., von Dassow, M., and Zhou, J. (2009). Multi-scale mechanics from molecules to morphogenesis. Int J Biochem Cell Biol *41*, 2147-2162.

De La Cruz, E.M., and Ostap, E.M. (2004). Relating biochemistry and function in the myosin superfamily. Curr Opin Cell Biol *16*, 61-67.

Desai, R., Sarpal, R., Ishiyama, N., Pellikka, M., Ikura, M., and Tepass, U. (2013). Monomeric alpha-catenin links cadherin to the actin cytoskeleton. Nat Cell Biol *15*, 261-273.

Engler, A.J., Sen, S., Sweeney, H.L., and Discher, D.E. (2006). Matrix elasticity directs stem cell lineage specification. Cell *126*, 677-689.

Fernandez-Gonzalez, R., Simoes Sde, M., Roper, J.C., Eaton, S., and Zallen, J.A. (2009). Myosin II dynamics are regulated by tension in intercalating cells. Dev Cell *17*, 736-743.

Finer, J.T., Simmons, R.M., and Spudich, J.A. (1994). Single myosin molecule mechanics: piconewton forces and nanometre steps. Nature *368*, 113-119.

Franke, J.D., Montague, R.A., and Kiehart, D.P. (2005). Nonmuscle myosin II generates forces that transmit tension and drive contraction in multiple tissues during dorsal closure. Curr Biol *15*, 2208-2221.

Gorfinkiel, N., and Arias, A.M. (2007). Requirements for adherens junction components in the interaction between epithelial tissues during dorsal closure in Drosophila. J Cell Sci *120*, 3289-3298.

Harrison, O.J., Bahna, F., Katsamba, P.S., Jin, X., Brasch, J., Vendome, J., Ahlsen, G., Carroll, K.J., Price, S.R., Honig, B., *et al.* (2010). Two-step adhesive binding by classical cadherins. Nat Struct Mol Biol *17*, 348-357.

Hartshorne, D.J., Ito, M., and Erdodi, F. (1998). Myosin light chain phosphatase: subunit composition, interactions and regulation. J Muscle Res Cell Motil *19*, 325-341.

Haussinger, D., Ahrens, T., Aberle, T., Engel, J., Stetefeld, J., and Grzesiek, S. (2004). Proteolytic E-cadherin activation followed by solution NMR and X-ray crystallography. EMBO J *23*, 1699-1708.

Heissler, S.M., Chinthalapudi, K., and Sellers, J.R. (2015). Kinetic characterization of the sole nonmuscle myosin-2 from the model organism Drosophila melanogaster. FASEB journal : official publication of the Federation of American Societies for Experimental Biology *29*, 1456-1466.

Heissler, S.M., and Manstein, D.J. (2011). Comparative kinetic and functional characterization of the motor domains of human nonmuscle myosin-2C isoforms. J Biol Chem *286*, 21191-21202.

Hong, S., Troyanovsky, R.B., and Troyanovsky, S.M. (2011). Cadherin exits the junction by switching its adhesive bond. J Cell Biol *192*, 1073-1083.

Howard, J. (2001). Mechanics of Motor Proteins and the Cytoskeleton, First edition edn (Sunderland, MA: Sinauer Associates, Inc.).

Hutson, M.S., Tokutake, Y., Chang, M.S., Bloor, J.W., Venakides, S., Kiehart, D.P., and Edwards, G.S. (2003). Forces for morphogenesis investigated with laser microsurgery and quantitative modeling. Science *300*, 145-149.

Huxley, H.E. (1963). Electron Microscope Studies on the Structure of Natural and Synthetic Protein Filaments from Striated Muscle. J Mol Biol *7*, 281-308.

Ikebe, M., and Hartshorne, D.J. (1985). Phosphorylation of smooth muscle myosin at two distinct sites by myosin light chain kinase. J Biol Chem *260*, 10027-10031.

Jung, H.S., Komatsu, S., Ikebe, M., and Craig, R. (2008). Head-head and head-tail interaction: a general mechanism for switching off myosin II activity in cells. Mol Biol Cell *19*, 3234-3242.

Katoh, K., Kano, Y., Masuda, M., Onishi, H., and Fujiwara, K. (1998). Isolation and contraction of the stress fiber. Mol Biol Cell *9*, 1919-1938.

Kiehart, D.P., and Feghali, R. (1986). Cytoplasmic myosin from Drosophila melanogaster. J Cell Biol *103*, 1517-1525.

Kiehart, D.P., Galbraith, C.G., Edwards, K.A., Rickoll, W.L., and Montague, R.A. (2000). Multiple forces contribute to cell sheet morphogenesis for dorsal closure in Drosophila. J Cell Biol *149*, 471-490.

Kiehart, D.P., Lutz, M.S., Chan, D., Ketchum, A.S., Laymon, R.A., Nguyen, B., and Goldstein, L.S. (1989). Identification of the gene for fly non-muscle myosin heavy chain: Drosophila myosin heavy chains are encoded by a gene family. EMBO J *8*, 913-922.

Kimura, K., Ito, M., Amano, M., Chihara, K., Fukata, Y., Nakafuku, M., Yamamori, B., Feng, J., Nakano, T., Okawa, K., *et al.* (1996). Regulation of myosin phosphatase by Rho and Rho-associated kinase (Rho-kinase). Science *273*, 245-248.

Kintner, C. (1992). Regulation of embryonic cell adhesion by the cadherin cytoplasmic domain. Cell *69*, 225-236.

Kishino, A., and Yanagida, T. (1988). Force measurements by micromanipulation of a single actin filament by glass needles. Nature *334*, 74-76.

Kovacs, M., Thirumurugan, K., Knight, P.J., and Sellers, J.R. (2007). Load-dependent mechanism of nonmuscle myosin 2. Proc Natl Acad Sci U S A *104*, 9994-9999.

Kovacs, M., Wang, F., Hu, A., Zhang, Y., and Sellers, J.R. (2003). Functional divergence of human cytoplasmic myosin II: kinetic characterization of the non-muscle IIA isoform. J Biol Chem *278*, 38132-38140.

Kumar, S., Maxwell, I.Z., Heisterkamp, A., Polte, T.R., Lele, T.P., Salanga, M., Mazur, E., and Ingber, D.E. (2006). Viscoelastic retraction of single living stress fibers and its impact on cell shape, cytoskeletal organization, and extracellular matrix mechanics. Biophysical Journal *90*, 3762-3773.

Larue, L., Ohsugi, M., Hirchenhain, J., and Kemler, R. (1994). E-cadherin null mutant embryos fail to form a trophectoderm epithelium. Proc Natl Acad Sci U S A *91*, 8263-8267.

Leerberg, J.M., Gomez, G.A., Verma, S., Moussa, E.J., Wu, S.K., Priya, R., Hoffman, B.D., Grashoff, C., Schwartz, M.A., and Yap, A.S. (2014). Tension-sensitive actin assembly supports contractility at the epithelial zonula adherens. Curr Biol *24*, 1689-1699.

Lenz, M., Gardel, M.L., and Dinner, A.R. (2012). Requirements for contractility in disordered cytoskeletal bundles. New J Phys *14*.

Liu, Z., Tan, J.L., Cohen, D.M., Yang, M.T., Sniadecki, N.J., Ruiz, S.A., Nelson, C.M., and Chen, C.S. (2010). Mechanical tugging force regulates the size of cell-cell junctions. Proc Natl Acad Sci U S A *107*, 9944-9949.

Lowey, S., and Trybus, K.M. (2010). Common structural motifs for the regulation of divergent class II myosins. J Biol Chem *285*, 16403-16407.

Lum, H., and Malik, A.B. (1996). Mechanisms of increased endothelial permeability. Can J Physiol Pharmacol *74*, 787-800.

Luo, W., Yu, C.H., Lieu, Z.Z., Allard, J., Mogilner, A., Sheetz, M.P., and Bershadsky, A.D. (2013). Analysis of the local organization and dynamics of cellular actin networks. J Cell Biol *202*, 1057-1073.

Ma, X., Jana, S.S., Conti, M.A., Kawamoto, S., Claycomb, W.C., and Adelstein, R.S. (2010). Ablation of nonmuscle myosin II-B and II-C reveals a role for nonmuscle myosin II in cardiac myocyte karyokinesis. Mol Biol Cell *21*, 3952-3962.

Mansfield, S.G., al-Shirawi, D.Y., Ketchum, A.S., Newbern, E.C., and Kiehart, D.P. (1996). Molecular organization and alternative splicing in zipper, the gene that encodes the Drosophila non-muscle myosin II heavy chain. J Mol Biol *255*, 98-109.

Martin, A.C., Gelbart, M., Fernandez-Gonzalez, R., Kaschube, M., and Wieschaus, E.F. (2010). Integration of contractile forces during tissue invagination. J Cell Biol *188*, 735-749.

Martin, A.C., and Goldstein, B. (2014). Apical constriction: themes and variations on a cellular mechanism driving morphogenesis. Dev *141*, 1987-1998.

Martin, A.C., Kaschube, M., and Wieschaus, E.F. (2009). Pulsed contractions of an actin-myosin network drive apical constriction. Nature *457*, 495-499.

Maruthamuthu, V., Sabass, B., Schwarz, U.S., and Gardel, M.L. (2011). Cell-ECM traction force modulates endogenous tension at cell-cell contacts. Proc Natl Acad Sci U S A *108*, 4708-4713.

Maupin, P., Phillips, C.L., Adelstein, R.S., and Pollard, T.D. (1994). Differential localization of myosin-II isozymes in human cultured cells and blood cells. J Cell Sci *107 (Pt 11)*, 3077-3090.

McBeath, R., Pirone, D.M., Nelson, C.M., Bhadriraju, K., and Chen, C.S. (2004). Cell shape, cytoskeletal tension, and RhoA regulate stem cell lineage commitment. Dev Cell *6*, 483-495.

Murrell, M.P., and Gardel, M.L. (2012). F-actin buckling coordinates contractility and severing in a biomimetic actomyosin cortex. Proc Natl Acad Sci U S A *109*, 20820-20825.

Nagafuchi, A., Ishihara, S., and Tsukita, S. (1994). The roles of catenins in the cadherin-mediated cell adhesion: functional analysis of E-cadherin-alpha catenin fusion molecules. J Cell Biol *127*, 235-245.

Nelson, C.M., Jean, R.P., Tan, J.L., Liu, W.F., Sniadecki, N.J., Spector, A.A., and Chen, C.S. (2005). Emergent patterns of growth controlled by multicellular form and mechanics. Proc Natl Acad Sci U S A *102*, 11594-11599.

Oakes, P.W., Banerjee, S., Marchetti, M.C., and Gardel, M.L. (2014). Geometry regulates traction stresses in adherent cells. Biophysical Journal *107*, 825-833.

Oda, H., Uemura, T., Harada, Y., Iwai, Y., and Takeichi, M. (1994). A Drosophila homolog of cadherin associated with armadillo and essential for embryonic cell-cell adhesion. Dev Biol *165*, 716-726.

Peralta, X.G., Toyama, Y., Hutson, M.S., Montague, R., Venakides, S., Kiehart, D.P., and Edwards, G.S. (2007). Upregulation of forces and morphogenic asymmetries in dorsal closure during Drosophila development. Biophysical Journal *92*, 2583-2596.

Pollard, T.D., Aebi, U., Cooper, J.A., Fowler, W.E., and Tseng, P. (1982). Actin structure, polymerization, and gelation. Cold Spring Harb Symp Quant Biol *46 Pt 2*, 513-524.

Pollard, T.D., and Borisy, G.G. (2003). Cellular motility driven by assembly and disassembly of actin filaments. Cell *112*, 453-465.

Pouille, P.A., Ahmadi, P., Brunet, A.C., and Farge, E. (2009). Mechanical signals trigger Myosin II redistribution and mesoderm invagination in Drosophila embryos. Sci Sign *2*, ra16.

Rakshit, S., Zhang, Y., Manibog, K., Shafraz, O., and Sivasankar, S. (2012). Ideal, catch, and slip bonds in cadherin adhesion. Proc Natl Acad Sci U S A *109*, 18815-18820.

Rauskolb, C., Sun, S., Sun, G., Pan, Y., and Irvine, K.D. (2014). Cytoskeletal tension inhibits Hippo signaling through an Ajuba-Warts complex. Cell *158*, 143-156.

Rimm, D.L., Koslov, E.R., Kebriaei, P., Cianci, C.D., and Morrow, J.S. (1995). Alpha 1(E)-catenin is an actin-binding and -bundling protein mediating the attachment of F-actin to the membrane adhesion complex. Proc Natl Acad Sci U S A *92*, 8813-8817.

Ringwald, M., Schuh, R., Vestweber, D., Eistetter, H., Lottspeich, F., Engel, J., Dolz, R., Jahnig, F., Epplen, J., Mayer, S., *et al.* (1987). The structure of cell adhesion molecule uvomorulin. Insights into the molecular mechanism of Ca2+-dependent cell adhesion. EMBO J *6*, 3647-3653.

Rochlin, M.W., Itoh, K., Adelstein, R.S., and Bridgman, P.C. (1995). Localization of myosin II A and B isoforms in cultured neurons. J Cell Sci *108 (Pt 12)*, 3661-3670.

Sarpal, R., Pellikka, M., Patel, R.R., Hui, F.Y., Godt, D., and Tepass, U. (2012). Mutational analysis supports a core role for Drosophila alpha-catenin in adherens junction function. J Cell Sci *125*, 233-245.

Scholey, J.M., Taylor, K.A., and Kendrick-Jones, J. (1980). Regulation of non-muscle myosin assembly by calmodulin-dependent light chain kinase. Nature *287*, 233-235.

Sellers, J.R. (1991). Regulation of cytoplasmic and smooth muscle myosin. Curr Opin Cell Biol *3*, 98-104.

Sellers, J.R., and Knight, P.J. (2007). Folding and regulation in myosins II and V. J Muscle Res Cell Motil *28*, 363-370.

Shapiro, L., and Weis, W.I. (2009). Structure and biochemistry of cadherins and catenins. Cold Spring Harb Perspect Biol *1*, a003053.

Shirayoshi, Y., Hatta, K., Hosoda, M., Tsunasawa, S., Sakiyama, F., and Takeichi, M. (1986). Cadherin cell adhesion molecules with distinct binding specificities share a common structure. EMBO J *5*, 2485-2488.

Soares e Silva, M., Depken, M., Stuhrmann, B., Korsten, M., MacKintosh, F.C., and Koenderink, G.H. (2011). Active multistage coarsening of actin networks driven by myosin motors. Proc Natl Acad Sci U S A *108*, 9408-9413.

Solon, J., Kaya-Copur, A., Colombelli, J., and Brunner, D. (2009). Pulsed forces timed by a ratchet-like mechanism drive directed tissue movement during dorsal closure. Cell *137*, 1331-1342.

Takeichi, M., Atsumi, T., Yoshida, C., Uno, K., and Okada, T.S. (1981). Selective adhesion of embryonal carcinoma cells and differentiated cells by Ca2+-dependent sites. Dev Biol *87*, 340-350.

Tambe, D.T., Croutelle, U., Trepat, X., Park, C.Y., Kim, J.H., Millet, E., Butler, J.P., and Fredberg, J.J. (2013). Monolayer stress microscopy: limitations, artifacts, and accuracy of recovered intercellular stresses. PLoS One *8*, e55172.

Tepass, U., Gruszynski-DeFeo, E., Haag, T.A., Omatyar, L., Torok, T., and Hartenstein, V. (1996). shotgun encodes Drosophila E-cadherin and is preferentially required during cell rearrangement in the neurectoderm and other morphogenetically active epithelia. Genes Dev *10*, 672-685.

Totsukawa, G., Yamakita, Y., Yamashiro, S., Hartshorne, D.J., Sasaki, Y., and Matsumura, F. (2000). Distinct roles of ROCK (Rho-kinase) and MLCK in spatial regulation of MLC phosphorylation for assembly of stress fibers and focal adhesions in 3T3 fibroblasts. J Cell Biol *150*, 797-806.

Trepat, X., Wasserman, M.R., Angelini, T.E., Millet, E., Weitz, D.A., Butler, J.P., and Fredberg, J.J. (2009). Physical forces during collective cell migration. Nat Phys *5*, 426-430.

Vasquez, C.G., Tworoger, M., and Martin, A.C. (2014). Dynamic myosin phosphorylation regulates contractile pulses and tissue integrity during epithelial morphogenesis. J Cell Biol *206*, 435-450.

Vavylonis, D., Wu, J.Q., Hao, S., O'Shaughnessy, B., and Pollard, T.D. (2008). Assembly mechanism of the contractile ring for cytokinesis by fission yeast. Science *319*, 97-100.

Verkhovsky, A.B., Svitkina, T.M., and Borisy, G.G. (1997). Polarity sorting of actin filaments in cytochalasin-treated fibroblasts. J Cell Sci *110 (Pt 15)*, 1693-1704.

Vicente-Manzanares, M., Ma, X., Adelstein, R.S., and Horwitz, A.R. (2009). Non-muscle myosin II takes centre stage in cell adhesion and migration. Nature reviews Molecular cell biology *10*, 778-790.

Vicente-Manzanares, M., Newell-Litwa, K., Bachir, A.I., Whitmore, L.A., and Horwitz, A.R. (2011). Myosin IIA/IIB restrict adhesive and protrusive signaling to generate front-back polarity in migrating cells. J Cell Biol *193*, 381-396.

Wang, F., Kovacs, M., Hu, A., Limouze, J., Harvey, E.V., and Sellers, J.R. (2003). Kinetic mechanism of non-muscle myosin IIB: functional adaptations for tension generation and maintenance. J Biol Chem *278*, 27439-27448.

Wendt, T., Taylor, D., Trybus, K.M., and Taylor, K. (2001). Three-dimensional image reconstruction of dephosphorylated smooth muscle heavy meromyosin reveals asymmetry in the interaction between myosin heads and placement of subfragment 2. Proc Natl Acad Sci *98*, 4361-4366.

Xie, S., and Martin, A.C. (2015). Intracellular signalling and intercellular coupling coordinate heterogeneous contractile events to facilitate tissue folding. Nat Commun *6*, 7161.

Yamashiro, S., Totsukawa, G., Yamakita, Y., Sasaki, Y., Madaule, P., Ishizaki, T., Narumiya, S., and Matsumura, F. (2003). Citron kinase, a Rho-dependent kinase, induces di-phosphorylation of regulatory light chain of myosin II. Mol Biol Cell *14*, 1745-1756.

Yap, A.S., Brieher, W.M., and Gumbiner, B.M. (1997). Molecular and functional analysis of cadherin-based adherens junctions. Annu Rev Cell Dev Biol *13*, 119-146.

Yeung, T., Georges, P.C., Flanagan, L.A., Marg, B., Ortiz, M., Funaki, M., Zahir, N., Ming, W., Weaver, V., and Janmey, P.A. (2005). Effects of substrate stiffness on cell morphology, cytoskeletal structure, and adhesion. Cell Motil Cytoskeleton *60*, 24-34.

Yonemura, S., Wada, Y., Watanabe, T., Nagafuchi, A., and Shibata, M. (2010). alpha-Catenin as a tension transducer that induces adherens junction development. Nat Cell Biol *12*, 533-542.

Zhou, J., Pal, S., Maiti, S., and Davidson, L.A. (2015). Force production and mechanical accommodation during convergent extension. Dev *142*, 692-701.

Findings presented in this thesis

During my graduate work I identified a regulatory mechanism of pulsatile myosin behavior. I demonstrated that cycles of phosphorylation and dephosphorylation of the myosin regulatory light chain are required for assembly and disassembly of apical myosin networks and consequently for step-wise apical constriction during *Drosophila* ventral furrow formation. I demonstrated this requirement for phospho-regulation of myosin in two ways: first, by generating myosin regulatory light chain phosphomutants that uncouple myosin from its upstream regulators; and second, by depletion of a negative regulator of myosin activity (myosin binding subunit). In both cases, disruption of the myosin phosphorylation cycle caused persistent accumulation of myosin apically and continuous apical constriction. One consequence of loss of pulsatile myosin behavior is that abrupt separations in the myosin meshwork formed, suggesting that pulsatile myosin behavior is a mechanism of cellular coordination during tissue invagination.

Additionally, by coupling my *in vivo* analysis of myosin regulatory light chains phosphomutants with *in vitro* biochemical analysis of motor activity of these mutants by Sarah Heissler and James Sellers (NIH, Bethesda, Maryland, USA), we found that force-generation at the cellular- and tissue-scales depends on myosin motor activity.

Chapter 2: Dynamic myosin phosphorylation regulates contractile pulses and tissue integrity during epithelial morphogenesis

Reprinted from Rockefeller University Press:
Claudia G. Vasquez, Michael Tworoger, Adam C. Martin. 2014. Dynamic myosin phosphorylation regulates contractile pulses and tissue integrity during epithelial morphogenesis. *J Cell Biol.* 3:435-450
MT carried out preparation and imaging of *rok* germline clone embryos expressing *sqh-TS* and *sqh-EE* transgenes and initial characterization of MBS depletion phenotype.
CV performed all other work shown in figures.
CV and AM wrote manuscript.

Abstract

Apical constriction is a cell shape change that promotes epithelial bending. Activation of non-muscle myosin II (Myo-II) by kinases such as Rho-associated kinase (Rok) is important to generate contractile force during apical constriction. Cycles of Myo-II assembly and disassembly, or pulses, are associated with apical constriction during *Drosophila* gastrulation. It is not understood whether Myo-II phospho-regulation organizes contractile pulses or whether pulses are important for tissue morphogenesis. Here, we show that Myo-II pulses are associated with pulses of apical Rok. Mutants that mimic Myo-II light chain phosphorylation or depletion of myosin phosphatase inhibit Myo-II contractile pulses, disrupting both actomyosin coalescence into apical foci and cycles of Myo-II assembly/disassembly. Thus, coupling dynamic Myo-II phosphorylation to upstream signals organizes contractile Myo-II pulses in both space and time. Mutants that mimic Myo-II phosphorylation undergo continuous, rather than incremental, apical constriction. These mutants fail to maintain intercellular actomyosin network connections during tissue invagination, suggesting that Myo-II pulses are required for tissue integrity during morphogenesis.

Introduction

Epithelial morphogenesis is critical for organs and embryos to change shape during development (Heisenberg and Bellaiche, 2013; Leptin, 2005). A cell shape change that often accompanies epithelial remodeling is apical constriction, which promotes epithelial sheet bending and cell invagination (Martin and Goldstein, 2014; Sawyer et al., 2010). One example of apical constriction-induced tissue remodeling occurs in *Drosophila* gastrulation, when a group of approximately 1,000 cells along the ventral midline of the embryo undergo apical constriction to form a ventral furrow. These constricted cells invaginate to become the mesoderm (Fig. 1 A) (Leptin and Grunewald, 1990; Sweeton et al., 1991). The molecular motor non-muscle myosin II (Myo-II), which localizes apically in *Drosophila* ventral furrow cells and other cell types that undergo apical constriction, is thought to generate the contractile force that facilitates invagination (Dawes-Hoang et al., 2005; Hildebrand, 2005; Lee and Harland, 2007; Lee et al., 2006; Martin et al., 2009; Nance et al., 2003; Nishimura and Takeichi, 2008; Young et al., 1991). While Myo-II is clearly involved in apical constriction, the mechanism of apical actomyosin contraction remains poorly understood.

Myo-II activity is regulated by phosphorylation of its regulatory light chain (RLC, *sqh* in *Drosophila*), which promotes Myo-II oligomerization into minifilaments and activation of the Myo-II motor ATPase activity (Jordan and Karess, 1997; Karess et al., 1991; Sellers, 1991). An effector of the RhoA GTPase (Rho1 in *Drosophila*), Rho-associated coiled-coil kinase (ROCK or Rok in *Drosophila*), can phosphorylate and activate Myo-II via direct RLC phosphorylation or by inhibiting the phosphatase that dephosphorylates the RLC (myosin phosphatase) (Amano et al., 1996; Kawano et al., 1999; Kimura et al., 1996; Winter et al., 2001). In the *Drosophila* mesoderm, the transcription factors Twist and Snail are thought to promote apical constriction and apical Myo-II accumulation by activating Rho1 and its effectors, including Rok (Barrett et al., 1997; Dawes-Hoang et al., 2005; Hacker and Perrimon, 1998) (Fig. S1 A). Mutants or chemical

inhibition of Rok results in loss of apical Myo-II and lack of apical constriction, demonstrating that Rok is necessary for cortical Myo-II localization in the ventral furrow (Dawes-Hoang et al., 2005; Mason et al., 2013). In addition, mutants that mimic Myo-II RLC phosphorylation progress through development and suppress *rok* mutants, suggesting that Rok increases levels of active Myo-II to promote actomyosin contractility and morphogenesis (Jordan and Karess, 1997; Royou et al., 2002; Winter et al., 2001). It is not clear, however, whether coupling of Rok activity to Myo-II activation plays a role in organizing apical actin contraction.

We have developed a system to visualize the dynamics of actomyosin contraction and apical constriction during *Drosophila* gastrulation. In ventral furrow cells, Myo-II undergoes cycles of assembly in the center of the apical surface (medioapical cortex) followed by disassembly or remodeling, which we refer to as pulses (Martin et al., 2009) (Fig. 1 A). Phases of rapid apical constriction are associated with pulses of Myo-II assembly and the coalescence of Myo-II and actin filament (F-actin) structures into medioapical foci, which possibly represent contractions of the actin cortex (Martin et al., 2009; Roh-Johnson et al., 2012). Following Myo-II coalescence, Myo-II structures remodel by either disassembling or changing in morphology. Despite Myo-II remodeling, cell shape is often stabilized between pulses, resulting in incremental apical constriction. While Myo-II still undergoes pulsing in Twist knock-downs, the contracted cell shape following a pulse is not stabilized, resulting in cell shape fluctuations and inefficient constriction (Martin et al., 2010; Martin et al., 2009). Thus, one model for ventral furrow formation is that cells undergo ratcheted apical constriction, whereby pulses drive constrictions that are stabilized via a Twist-dependent mechanism for efficient apical constriction. We proposed that the polarized localization of Rok to medioapical foci results in the persistence of medioapical actomyosin fibers that stabilize cell shape between pulses; we have named this cellular organization radial cell polarity (Mason et al., 2013). The persistence of medioapical Myo-II fibers is important for the formation of a supracellular Myo-II meshwork that transmits tension across the ventral furrow tissue (Martin et al., 2010). However, the roles of

Rok and Myo-II phosphorylation during pulsatile constriction are still unclear. Furthermore, it is not known why cells undergo pulsatile, rather than continuous contraction to promote tissue morphogenesis.

Here, we combined live imaging and quantitative analysis of Myo-II regulators and GFP-tagged Myo-II RLC phospho-mutants to define the role of coupling Myo-II activation to upstream signals during contractile pulses. We show that temporal and spatial control of Myo-II phosphorylation organizes contractile pulses. We suggest that the pulsatile nature of apical constriction is required for the stable transmission of intercellular forces during tissue morphogenesis.

Results

Myo-II pulses correlate with fluctuations in apical Rok localization

Contractile pulses during ventral furrow cell apical constriction are associated with the coalescence and increase in apical Myo-II intensity, after which apical Myo-II structures are remodeled (Fig. 1 A) (Martin et al., 2009). Because Rok is required for cortical Myo-II localization in the *Drosophila* embryo (Dawes-Hoang et al., 2005; Royou et al., 2002), we examined whether dynamic Myo-II localization was correlated with changes in Rok localization. Prior to gastrulation, Rok localizes to basal furrow canals and is relocalized to foci in the center of the apical domain during apical constriction (Mason et al., 2013) (Fig. 1 B). At the onset of apical constriction, we found that Rok intensity exhibited clear fluctuations, with medioapical Rok foci appearing and disappearing in association with Myo-II coalescence (Fig. 1, C and D). Analysis of the time-resolved cross-correlation between Myo-II and Rok intensity during individual pulses demonstrated a significant correlation that peaked at 0 seconds offset (Fig. 1 E). Thus, Myo-II foci appear at the same time as Rok foci. Additionally, apical Rok intensity increased during apical constriction, often in bursts that corresponded with phases of rapid constriction (Fig. S1 B). The pulsatile behavior of Rok during ventral furrow formation suggests that dynamic changes in Myo-II phosphorylation by Rok direct contraction pulses that result in incremental apical constriction.

Figure 1

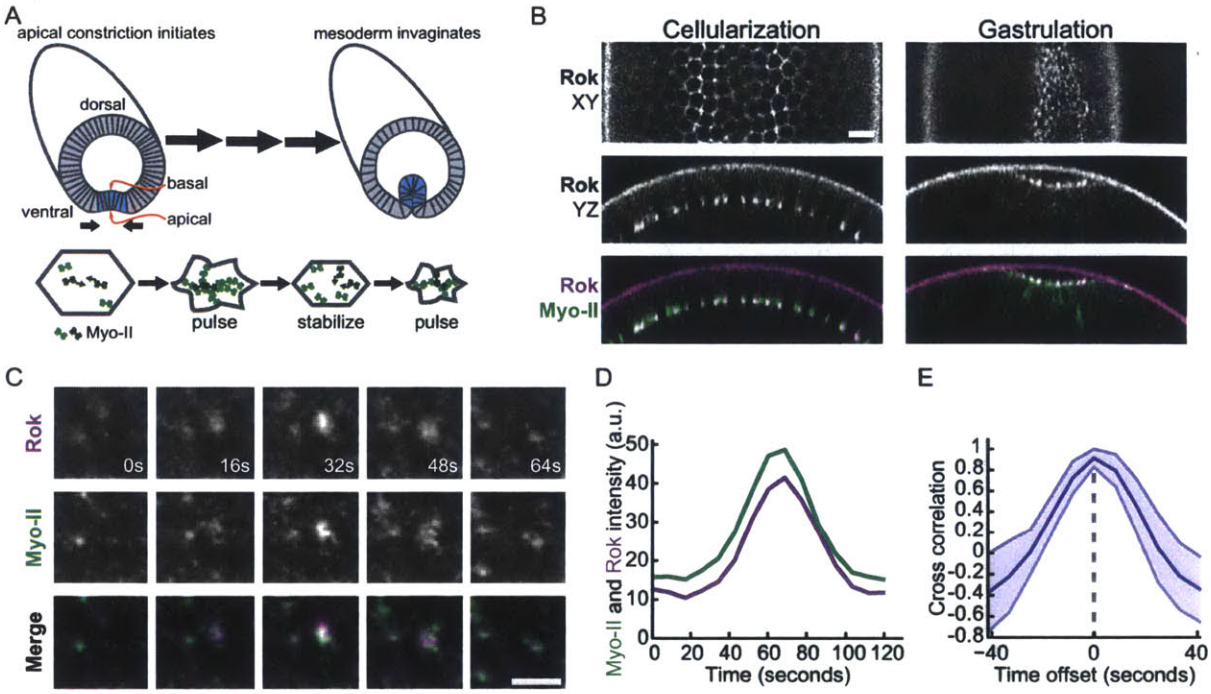

Figure 1 Rok co-localizes with Myo-II pulses. (A) Schematic of apical constriction of prospective mesodermal cells (shaded in blue) during *Drosophila* ventral furrow formation. *Bottom:* An individual cell undergoes pulsatile apical constriction. Myo-II undergoes cycles of assembly and coalescence (indicated by arrows) followed by remodeling. (B) Rok localizes with Myo-II at furrow canals during cellularization and apically during ventral furrow formation. Scale bar = 10 μm. (C) Time-lapse images of Rok and Myo-II intensity during a pulse from *rok*^{2}*; Venus::Rok (WT); sqh::mCherry* embryo. Scale bar = 5 μm. (D) Myo-II and Rok appear simultaneously during pulse. Graph represents signal intensity of Rok and Myo-II within a single pulse event. (E) Rok signal is correlated with Myo-II signal with no temporal lag. Mean cross-correlation for different time offsets between Rok and Myo-II signals from pulses (n = 30 pulses, shaded area is +/- 1 SD).

Figure S1

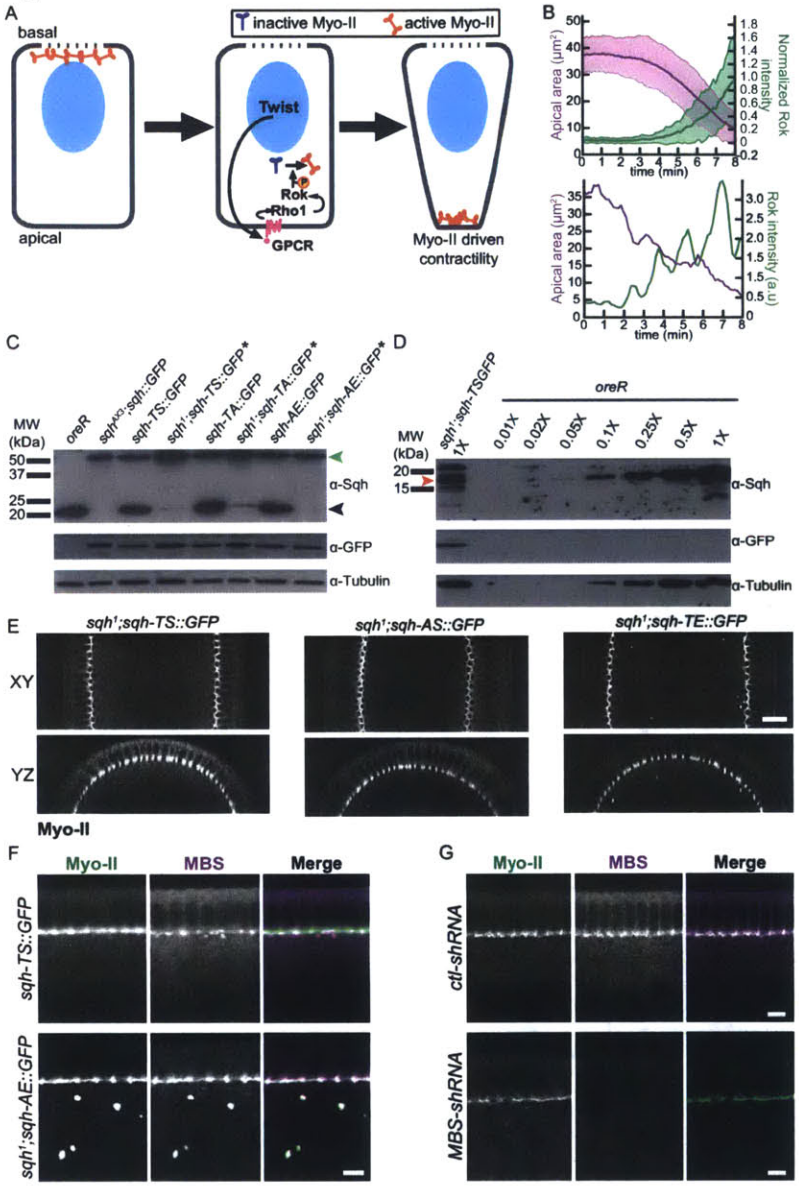

Figure S1 (A) Schematic of changes in Myo-II localization in the ventral furrow. During a process called cellularization, Myo-II is localized to the basal tips of invaginating plasma membranes, called furrow canals. The invaginating membranes compartmentalize nuclei, forming epithelial cells immediately prior to gastrulation. At the onset of gastrulation, the Twist transcription factor activates signaling through the small GTPase Rho1 in ventral furrow cells. Rho1 signaling leads to Rok activation, which is thought to phosphorylate and consequently activate Myo-II contractility. (B) Rok intensity increases throughout apical constriction. Mean apical area (magenta) decreases while mean Rok intensity (green) increases (top) (n = 67 cells, shaded area is +/- 1 standard deviation from the mean (solid line)). Plot of apical area (magenta) and Rok intensity (green) for an individual cell (bottom). (C) GFP-tagged sqh mutants that prevent (mutated to Alanine) or mimic (mutated to Glutamate) phosphorylation are expressed at the same level as endogenous sqh. Western blot of embryo lysates prepared from cellularizing blastoderms probed with α-Sqh, α-GFP or α-Tubulin (loading control). Green arrowhead indicates GFP-tagged Sqh, black arrowhead indicates endogenous Sqh. Germline clones of the sqh1 allele (indicated by asterisk) were estimated to express 1/10th of the endogenous amount of Sqh of wild-type (OreR) embryos. (D) Endogenous sqh expression in sqh1 germline clone embryos is 10% of endogenous sqh expression in OreR embryos. Red arrowhead indicates endogenous Sqh. (E) Representative images of XY semi-sagittal sections and YZ cross-sections for cellularizing live-embryos. Scale bar = 20 μm. (F) Images represent fixed cellularizing embryos expressing sqh::GFP (top) or sqh-AE::GFP (bottom) and stained for MBS. Note that MBS localizes to basal furrow canals and to small or large cytoplasmic aggregates in sqh-TS and sqh-AE, respectively. Scale bar = 5 μm. (G) Representative images of fixed cellularizing ctl-shRNA (top) and MBS-shRNA (bottom) embryos expressing sqh::GFP and stained for MBS. Note that in ctl-shRNA, MBS localized at the cellularization front and in the cytoplasm; however, in the MBS knock-down there is little detectable MBS signal. Scale bars = 5 μm.

RLC mutants that mimic mono- or di-phosphorylation result in constitutive Myo-II oligomerization independent of Rok

To test whether dynamic Myo-II phosphorylation, and thus changes in Myo-II minifilament assembly and motor activity, is required for Myo-II pulses, we generated GFP-tagged *sqh* mutants affecting threonine-20 and serine-21 (Fig. 2 A) (Jordan and Karess, 1997). Alanine substitutions in these residues decrease Myo-II motor ATPase activity *in vitro* (Kamisoyama et al., 1994), and the *sqh-AA* mutant resembles a *sqh* null allele *in vivo* (Jordan and Karess, 1997). Conversely, glutamate substitutions activate Myo-II minifilament assembly and ATPase activity in the absence of phosphorylation *in vitro*, although the ATPase activity of phospho-mimetic myosin mutants is lower than that of phosphorylated Myo-II (Kamisoyama et al., 1994). We differentiated between possible roles of mono- and di-phosphorylation by generating mutants that trap the Myo-II motor in all possible combinations of RLC phosphorylation states that are likely present *in vivo* (Fig. 2 B). The *sqh* phospho-mutants were expressed at similar levels as endogenous *sqh* and did not exhibit gastrulation phenotypes in the presence of the endogenous Sqh (Fig. S1 C and S2 A). We reduced endogenous Sqh protein levels approximately 90 % by making germline clones with the hypomorphic sqh^1 allele (Fig. S1, C and D). The wild-type *sqh* transgene (*sqh-TS::GFP*), but not the inactive *sqh-AA::GFP* allele, rescued nuclear migration and the uneven cellularization phenotypes of sqh^1 mutants (Fig. 2 C) (Royou et al., 2004; Royou et al., 2002; Wheatley et al., 1995). In addition, we obtained gastrulating embryos from all mutants, including the *sqh-AA* allele. Thus, the partial activity of the sqh^1 allele enabled us to examine the function of *sqh* phospho-mutants during gastrulation.

We first determined whether the different *sqh* phospho-mimetic mutants activate Myo-II minifilament assembly *in vivo*. During cellularization, Myo-II localizes to basal furrow canals and cytoplasmic aggregates (Royou et al., 2004). Although we did not observe ectopic cortical Myo-II assembly, phospho-mimetic *sqh* mutants, particularly *sqh-AE* and *sqh-EE*, accumulated Myo-

II in aggregates that are immediately basal to the furrow canals (Fig. 2 C and Fig. S1 E). Myo-II aggregates were reduced in size when wild-type levels of endogenous Sqh were present and Myo-II aggregates also contained the myosin heavy chain (MHC, *Drosophila zipper*), suggesting that these aggregates are not denatured protein (Fig. 2, C and D). Importantly, Sqh aggregates do not contain F-actin, suggesting that the Sqh aggregates do not form by actomyosin contraction, but could result from constitutive Myo-II minifilament assembly (Fig. 2 E). The phospho-mimetic mutants resulted in a decrease in cytoplasmic Myo-II levels relative to wild-type embryos, suggesting that RLC mutants that mimic mono- or di-phosphorylation shift the Myo-II complex towards the active conformation *in vivo*, promoting constitutive oligomerization (Fig. 2 F). Thus, our GFP-tagged phospho-mimetic RLC mutants appear to uncouple activation of Myo-II oligomerization from phosphorylation by Rok.

Figure 2

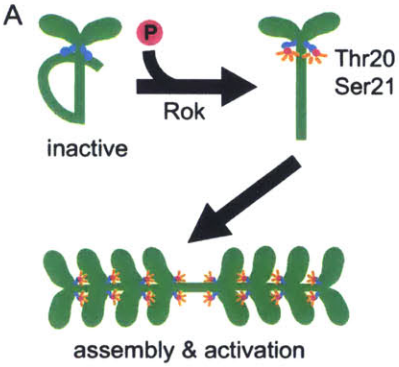

B

phospho-mutant	Thr-20	Ser-21	available states
sqh-TS	+/-	+/-	all states
sqh-AA	-	-	un-P
sqh-TA	+/-	-	un- or mono-P
sqh-AS	-	+/-	un- or mono-P
sqh-TE	+/-	+	mono- or di- P
sqh-AE	-	+	mono-P
sqh-EE	+	+	di-P

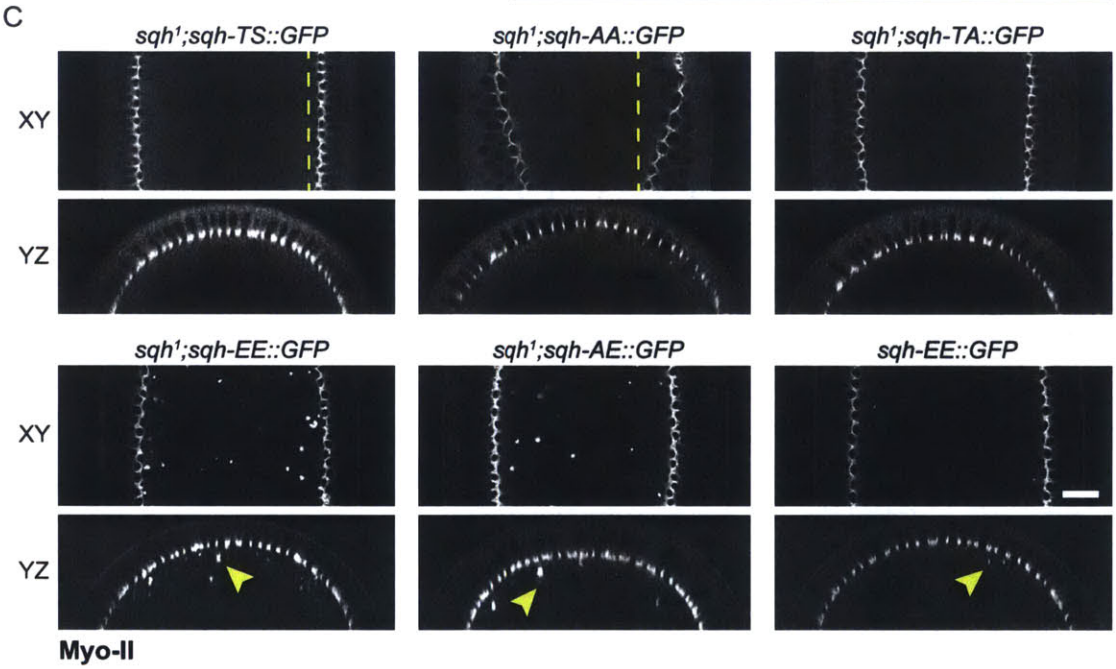

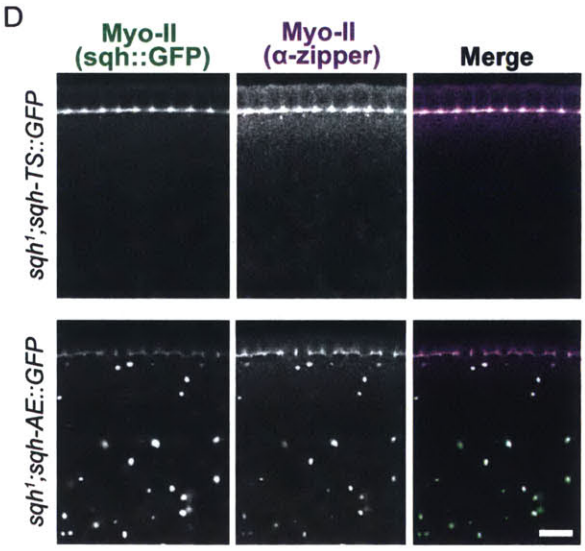

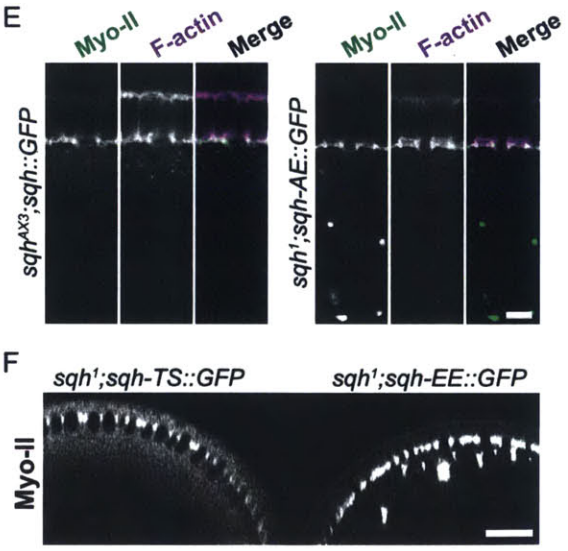

Figure 2 Characterization of *sqh* phospho-mutant oligomerization. (A) Phosphorylation of the *Drosophila* Myo-II RLC, *sqh*, on threonine-20 and serine-21 is predicted to activate motor activity and promote bipolar minifilament assembly. (B) Chart summarizing phosphorylation states available to different Sqh phospho-mutants. (C) Sqh mutants that mimic phosphorylation result in cytoplasmic Myo-II aggregates. Representative images of XY semi-sagittal sections and YZ cross-sections for live cellularizing embryos. Dashed lines highlight evenness (*sqh-TS)* or un-evenness (*sqh-AA*) of cellularization front. Arrowheads indicate examples of cytoplasmic Myo-II aggregates. Scale bar = 20 μm. (D) Basal Sqh aggregates co-localize with Zipper aggregates. Images are fixed embryos stained for Zipper (myosin heavy chain) and endogenous GFP. Scale bar = 10 μm. (E) Basal Sqh aggregates do not co-localize with F-actin. Images are fixed embryos stained for F-actin (phalloidin) and endogenous GFP. Scale bar = 5 μm. (F) Phospho-mimetic Sqh mutants deplete levels of cytoplasmic Myo-II. Image is a YZ cross-section of a live sqh^{1}; *sqh-TS*::GFP embryo immediately adjacent to a sqh^{1}; *sqh-EE*::GFP embryo. Scale bar = 20 μm.

RLC phosphorylation dynamics do not trigger changes in Myo-II apical-basal localization

Apical activation of Rok has been proposed to localize Myo-II assembly during apical constriction (Dawes-Hoang et al., 2005). Thus, mutants that uncouple Myo-II activity from phosphorylation by Rok might disrupt the apical-basal localization of Myo-II. Therefore, we tested whether the apical-basal polarity of Myo-II localization is controlled by RLC phosphorylation and oligomerization. Mutants that mimic mono- or di-phosphorylation localized specifically to the apical surface of ventral furrow cells, despite the presence of Myo-II aggregates throughout the entire embryo (Fig. 3, A and B; S2 B). Furthermore, Myo-II was reduced in basal furrow canals during ventral furrow invagination in phospho-mimetic mutants, similar to wild-type Myo-II, suggesting that dephosphorylation of the RLC is not the mechanism of basal Myo-II loss (Fig. 3, A and B). Inactivation of the RLC phosphorylation sites similarly did not disrupt apical Myo-II localization (Fig. 3 C; S2 B). These results demonstrate that despite the tissue specific apical recruitment of Rok in ventral furrow cells, regulation of oligomerization does not instruct apical Myo-II localization at the onset of gastrulation.

Figure 3

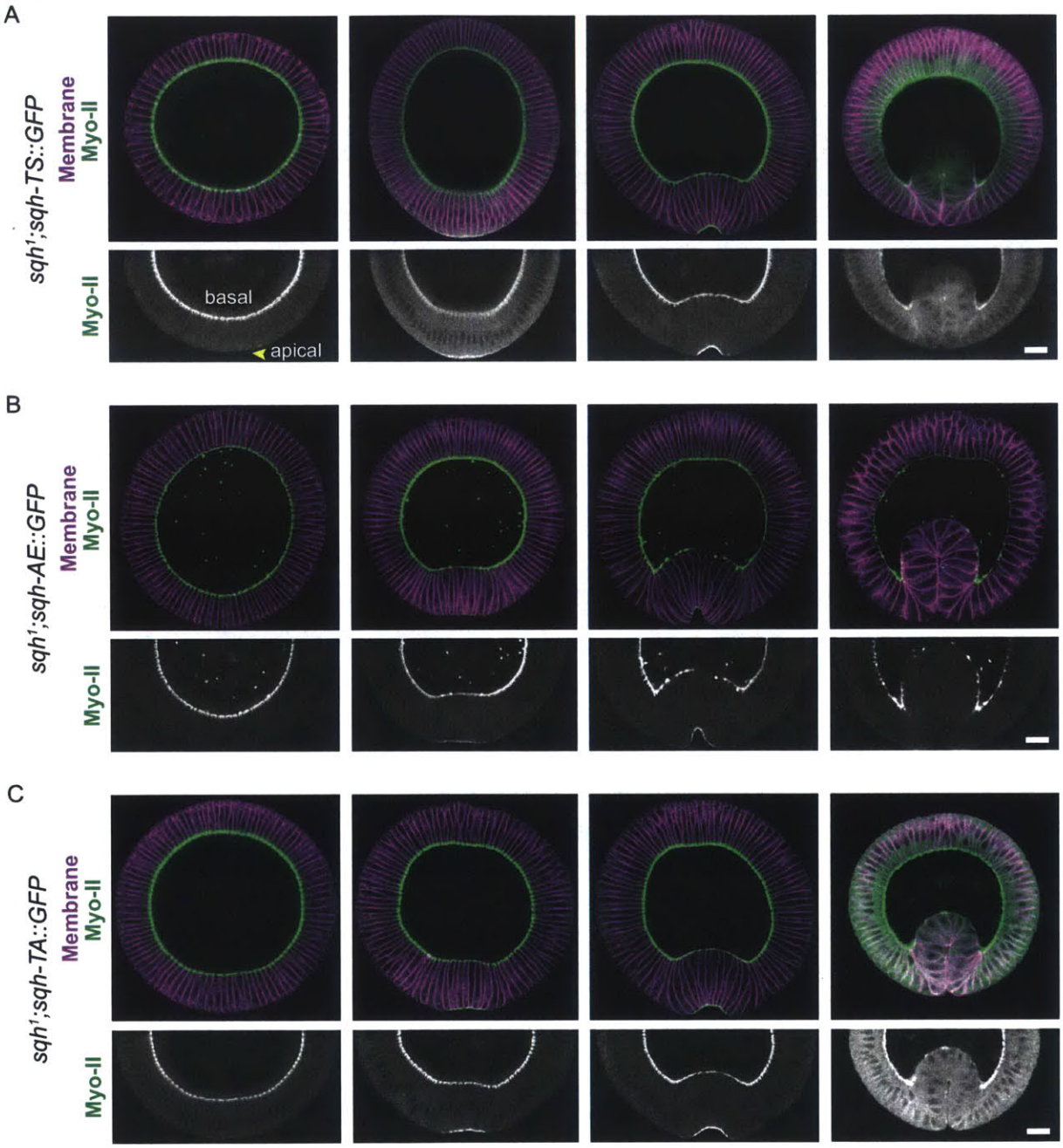

Figure 3 Dynamic RLC phosphorylation is not required to trigger basal to apical relocalization of Myo-II. (A) Wild-type Myo-II localizes to the apical surface and is reduced basally during ventral furrow formation. Images are fixed embryo cross-sections during sequential stages of apical constriction stained for Zipper (myosin heavy chain) and Neurotactin (membrane). (B) and (C) Sqh phospho-mutants do not alter the basal-apical Myo-II redistribution. Embryo preparation was the same as (A), except germline clones expressing *sqh-AE* (B) and *sqh-TA* (C) were fixed. Scale bars = 20 μm.

Figure S2

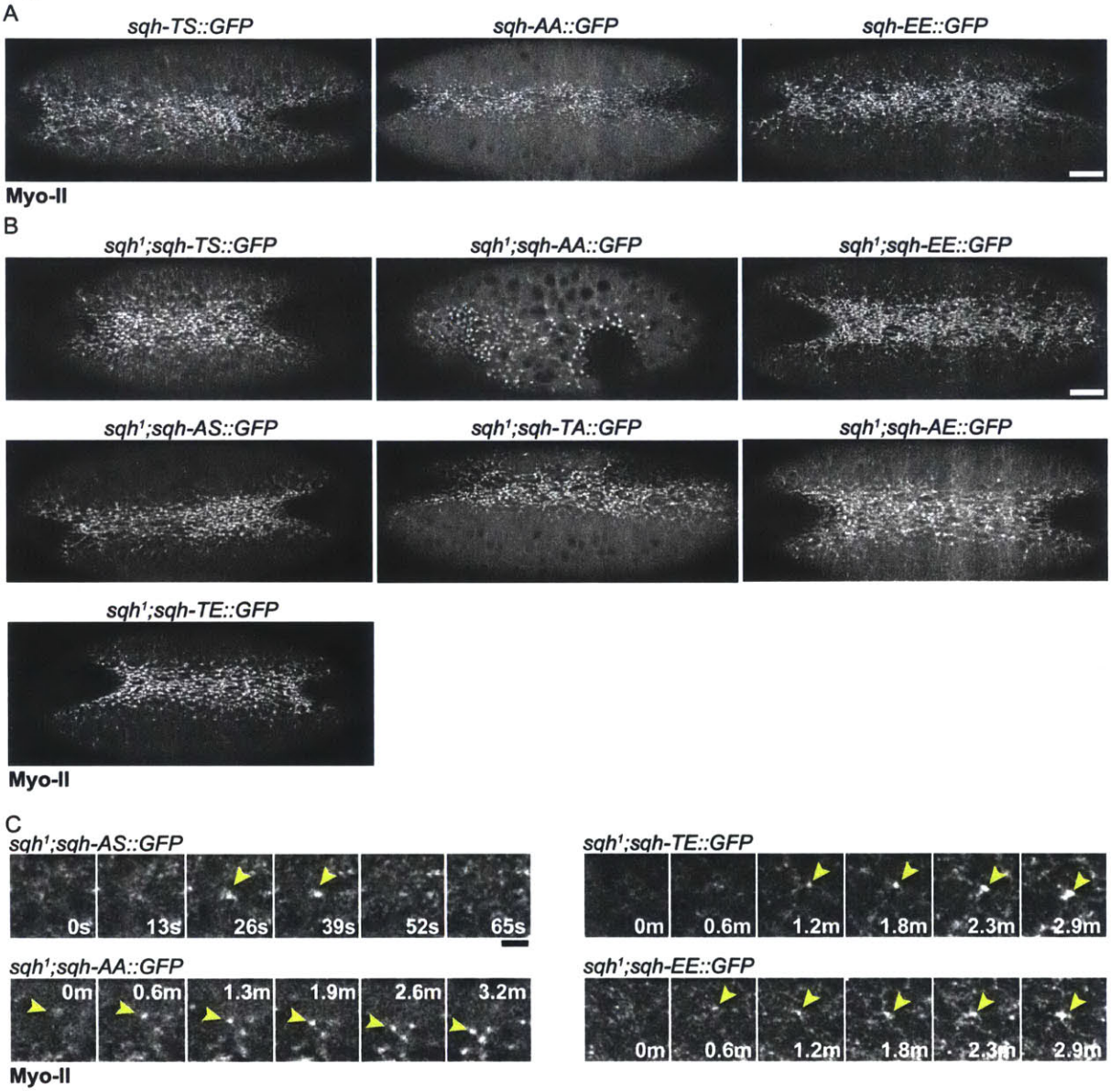

Figure S2 Ventral furrow phenotypes for *sqh* phospho-mutants. (A) Apical Myo-II localization in *sqh* mutants expressed with wild-type levels of endogenous Sqh. Images represent live embryos expressing the indicated *sqh* allele. Scale bar = 20 μm. (B) Sqh phospho-mutants exhibit apical localization specifically in ventral furrow cells. Images represent live embryos expressing the indicated *sqh* phospho-mutant allele expressed in sqh^1 germline clones. Note that *sqh-AA::GFP* localizes to the apical surface of ventral cells, but the tissue fails to form a tissue-wide furrow. Scale bar = 20 μm. (C) Dynamic phosphorylation of serine-21 is critical for contraction pulses. Time-lapse images show *sqh::GFP* structures in sqh^1 germline clone embryos expressing the indicated allele. Note the shorter time scale for the *sqh-AS* mutant. Mutants that inactivate or activate serine-21 exhibit continuous Myo-II assembly without apparent disassembly/remodeling. Yellow arrowheads indicate instances Myo-II assembly. Scale bar = 5 μm.

Phospho-mimetic RLC mutants disrupt polarized actomyosin condensation

Medioapical Myo-II pulses involve the coalescence or condensation of both Myo-II and F-actin into medioapical foci (Martin et al., 2009; Mason et al., 2013). Because Rho1 and Rok are also enriched in medioapical foci, we have proposed that the apical domain of ventral furrow cells exhibits radial cell polarity, with protein localization differing between the apical center to the junctions (Mason et al., 2013). To test whether dynamic regulation of RLC phosphorylation polarizes actomyosin within the apical cortex, we combined *sqh::GFP* transgenes with a membrane marker fused to mCherry (Memb::Cherry) to visualize and quantify the apical organization of Myo-II. Because we have been unable to obtain viable embryos expressing Memb::Cherry and *sqh-EE::GFP*, which exhibits additional oogenesis defects associated with constitutive Myo-II activation, we focused our quantitative analysis on the *sqh-AE* mutant. We observed similar Myo-II localization and mutant phenotypes between *sqh-AE* and *sqh-EE*, consistent with these mutants similarly activating Myo-II oligomerization. The *sqh-TS::GFP* transgene rescued Myo-II coalescence in sqh^1 germline clone mutants, forming medioapical foci during pulses and thus exhibiting radial cell polarity in Myo-II accumulation (Fig. 4 A). In contrast, Myo-II in *sqh-AE* mutants accumulated across the entire apical domain, at both the junctional and the medioapical cortex, but failed to coalesce (Fig. 4 B). Consistent with the defect in Myo-II coalescence, the *sqh-AE* mutant also failed to condense apical F-actin during Myo-II accumulation (Fig. 4, E and F). We quantified this difference in the radial cell polarity of Myo-II localization by calculating the difference between medioapical and junctional/peripheral Myo-II intensity before and after the onset of apical constriction. Because wild-type Myo-II coalesces towards the center of the medioapical cortex, the amount of medioapical Myo-II relative to peripheral Myo-II increases when cells begin constricting (Medioapical polarity > 0) (Fig. 4 D). In contrast, Myo-II in the *sqh-AE* mutant did not exhibit this medioapical enrichment, indicating a defect in medioapical Myo-II coalescence (Fig. 4 D). The defect in the medioapical

polarization of Myo-II was specific to phospho-mimetic mutants because Myo-II in both the *sqh-AA* and *sqh-TA* mutants accumulated as concentrated foci and the *sqh-TA* mutant exhibited medioapical F-actin condensation (Fig. 4, C, D,and G). Thus, the defects in actomyosin coalescence observed in the *sqh-AE* mutants suggest that coupling of Myo-II activation to Rok phosphorylation is critical to polarize actomyosin contractile activity within the apical domain of ventral cells.

Because Myo-II localization in the phospho-mimetic mutants could be influenced by the low (10%) levels of endogenous Sqh, we sought to fully uncouple Myo-II activation from upstream signals by activating Myo-II in a *rok* mutant background. Either rok^1 or rok^2 mutant germline clones result in a loss of Myo-II from the cortex, consistent with Rok and Myo-II phosphorylation being required for Myo-II activation (Fig. S3) (Dawes-Hoang et al., 2005; Mason et al., 2013; Royou et al., 2002). Previous studies suggested that *sqh-EE* can suppress loss of Rok function (Bertet et al., 2004; Winter et al., 2001), suggesting that Rok activates Myo-II minifilament assembly, whereas minifilament localization is dependent on other cortical cues. Consistent with these results, we found that *sqh-EE* rescued cortical Myo-II localization in rok^1 and rok^2 mutant germline clones (Fig. S3). However, despite rescuing cortical localization in *rok* germline clones, *sqh-EE* Myo-II failed to undergo medioapical coalescence and generate cell contractions (data not shown). Instead, Myo-II accumulated uniformly across the apical domain (Fig. S3). Furthermore, the *rok sqh-EE* double mutants failed to undergo mesoderm invagination (data not shown). Although we cannot rule out that the possibility that other Rok substrates are required for Myo-II coalescence, our data suggest that simply activating apical Myo-II is not sufficient for medioapical actomyosin network condensation and radial cell polarity. We favor a model whereby spatial regulation of Myo-II by Rok within the apical domain is required for actomyosin network contraction during a pulse.

Figure 4

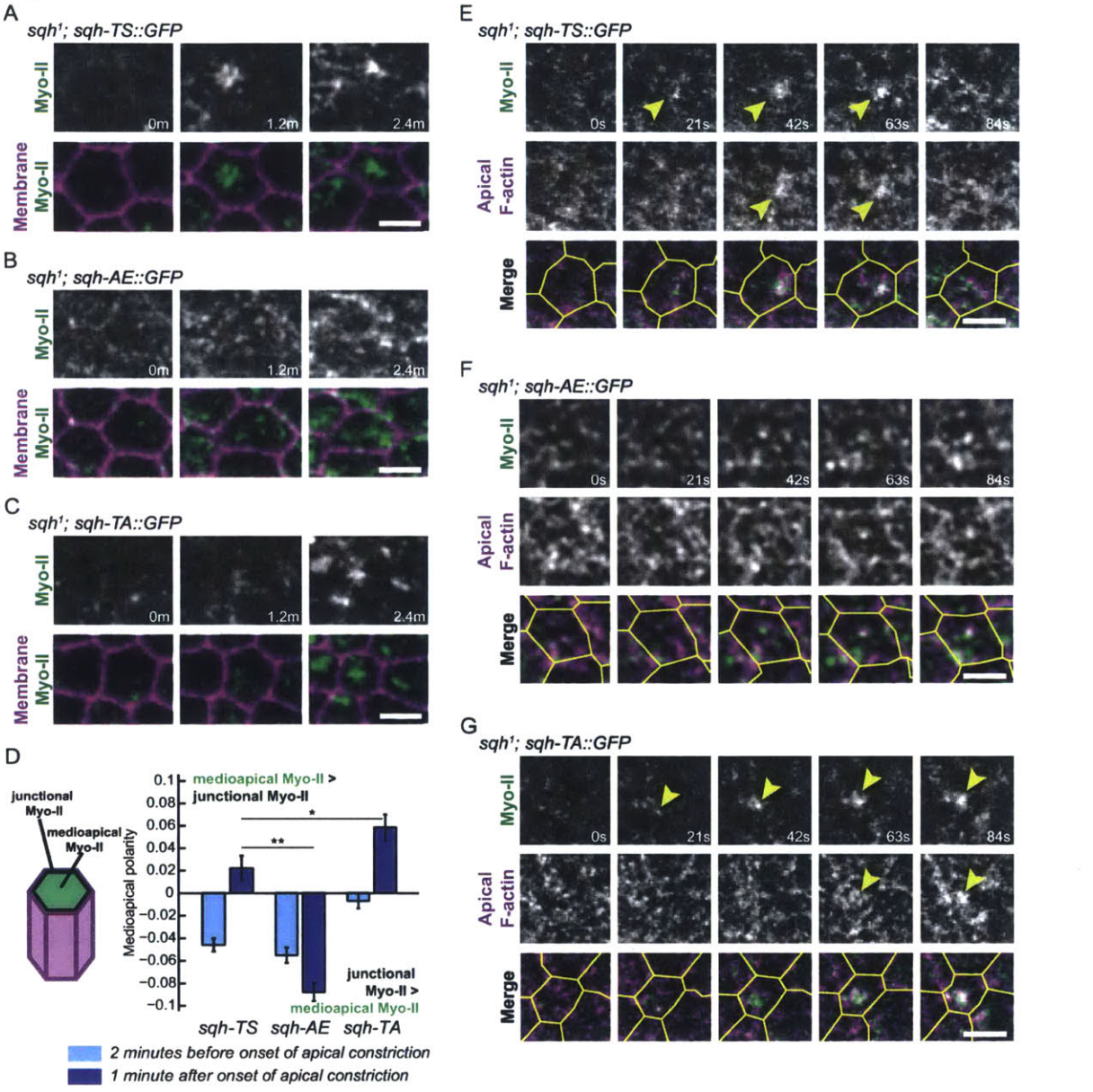

Figure 4 Polarized actomyosin condensation requires dynamic Myo-II phosphorylation. (A-C) Uncoupling Myo-II activation from Rok phosphorylation disrupts medioapical Myo-II coalescence. Time-lapse images are representative cells from *sqh*^{1} germline clone embryos expressing the indicated phospho-mutants and Memb::Cherry (membrane). Scale bars = 5 μm. (D) Quantification of Myo-II "Medioapical polarity", which is the difference between medioapical Myo-II (light green in schematic) and junctional Myo-II (green in schematic) intensities normalized by the total Myo-II intensity in a cell. Error bars are SEM (*sqh-TS* n=120 cells, 2 embryos; *sqh-AE* n= 100 cells, 2 embryos; *sqh-TA* n= 118 cells, 2 embryos). (E-G) The *sqh-AE* mutant fails to condense apical F-actin. Time-lapse images are of representative cells from *sqh*^{1} germline clone embryos expressing the indicated phospho-mutants and Utr::mCherry (F-actin). Arrowheads in (E and G) indicate Myo-II and F-actin condensation. Cell-outlines for (E-G), in yellow, were made by manually segmenting the subapical Utr::mCherry signal 2 μm below the apical meshwork. Scale bars = 5 μm. *, $p < 0.05$; **, $p < 0.01$.

Figure S3

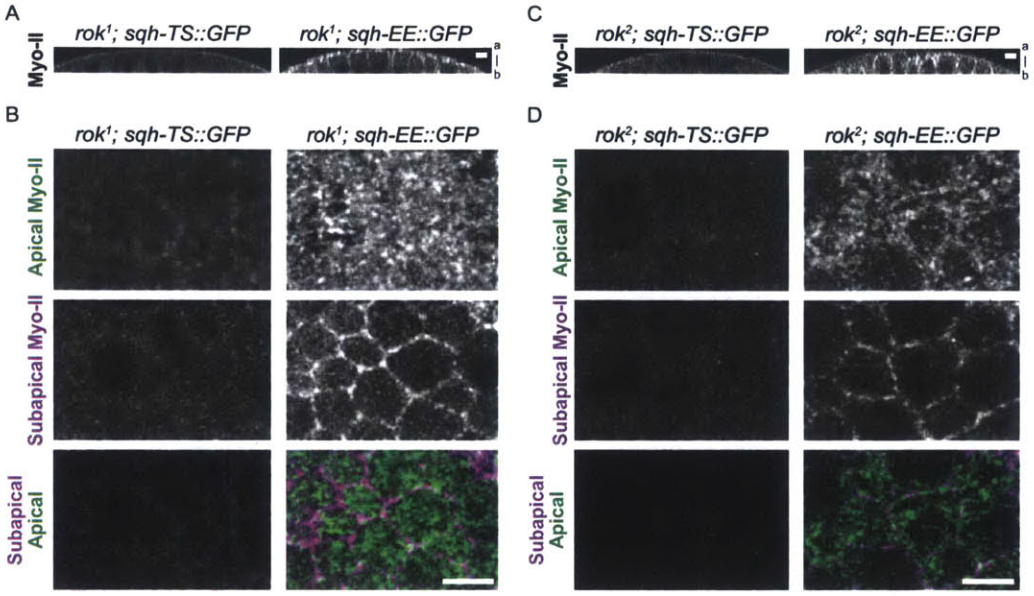

Figure S3 Phospho-mimetic *sqh* fails to suppress ventral furrow defects of *rok* mutants. (A-D) The *sqh-EE* mutant rescues apical Myo-II localization but not polarized contraction in *rok* germline clones. Images represent endogenous GFP fluorescence from live rok^1 (A-B) and rok^2 (D-C) germline clone embryos expressing either *sqh-TS::GFP* or *sqh-EE::GFP*. Representative images of YZ cross-sections (A and C; a = apical, b = basal) or surface views (B and D) are shown. The *rok* mutants disrupt cortical myosin localization, which is partially suppressed by *sqh-EE*. However, *sqh-EE* is present across the entire apical surface in *rok* mutants.

Myo-II phospho-mutants exhibit defects in Myo-II assembly/disassembly cycles

We next determined whether dynamic Myo-II phosphorylation is critical for temporal organization of Myo-II pulses. Similar to Myo-II in wild-type embryos, *sqh-TS::GFP* displayed Myo-II contraction pulses in sqh^1 germline clones, with the appearance of Myo-II structures lasting 20 to 30 seconds before being disassembled or remodeled (Fig. 5 A). In contrast, phospho-mimetic mutants caused a gradual increase in Myo-II accumulation (Fig. 5 B and S2 C). Myo-II persisted long after it initially appeared, failing to undergo disassembly over the course of constriction (Fig. 5 B). Based on the frequency of events involving rapid Myo-II intensity increase, we found that the *sqh-AE* mutant had significantly fewer Myo-II pulses than wild-type embryos (Fig. 5 D). Correspondingly, apical constriction in the *sqh-AE* mutant appeared more continuous, with fewer rapid phases of constriction that were lower in magnitude than those observed in wild-type (Fig. 5, B, E, F and S4 A). During pulsatile constriction, phases of rapid Myo-II accumulation correlate with increased constriction rate (Martin et al. 2009). However, the *sqh-AE* mutant displayed a significantly weaker cross-correlation between Myo-II accumulation and the constriction rate, confirming our observation that mimicking Sqh phosphorylation disrupts contractile pulses and results in more continuous apical constriction (Fig. 5 G).

Mutants that decrease Myo-II phosphorylation resulted in Myo-II dynamics that were distinct from the phospho-mimetic alleles. The *sqh-AS* mutant displayed contractile oscillations and Myo-II disassembly similar to wild-type embryos (Fig. S2 C), suggesting that dynamic phosphorylation of serine-21 is sufficient for Myo-II remodeling. The *sqh-TA* mutant exhibited phases of rapid Myo-II accumulation that were temporally correlated with constriction (Fig 5 C and G), which possibly results from Rok phosphorylating theronine-20. However, the *sqh-TA* and *sqh-AA* mutants did not exhibit Myo-II disassembly after accumulation, demonstrating that dynamic phosphorylation of threonine-20 is insufficient for Myo-II remodeling (Fig. 5, C-G; and

Fig. S2 C and S4 A). These data are consistent with *in vitro* experiments that show phosphorylation of either threonine-20 or serine-21 can promote minifilament formation, but that serine-21 is most important for Myo-II ATPase activity (Bresnick et al., 1995; Kamisoyama et al., 1994), suggesting that high levels of Myo-II motor activity are required to remodel the actomyosin network after a pulse. Thus, cycling between high and low Myo-II activity states is required for contractile oscillations.

Figure 5

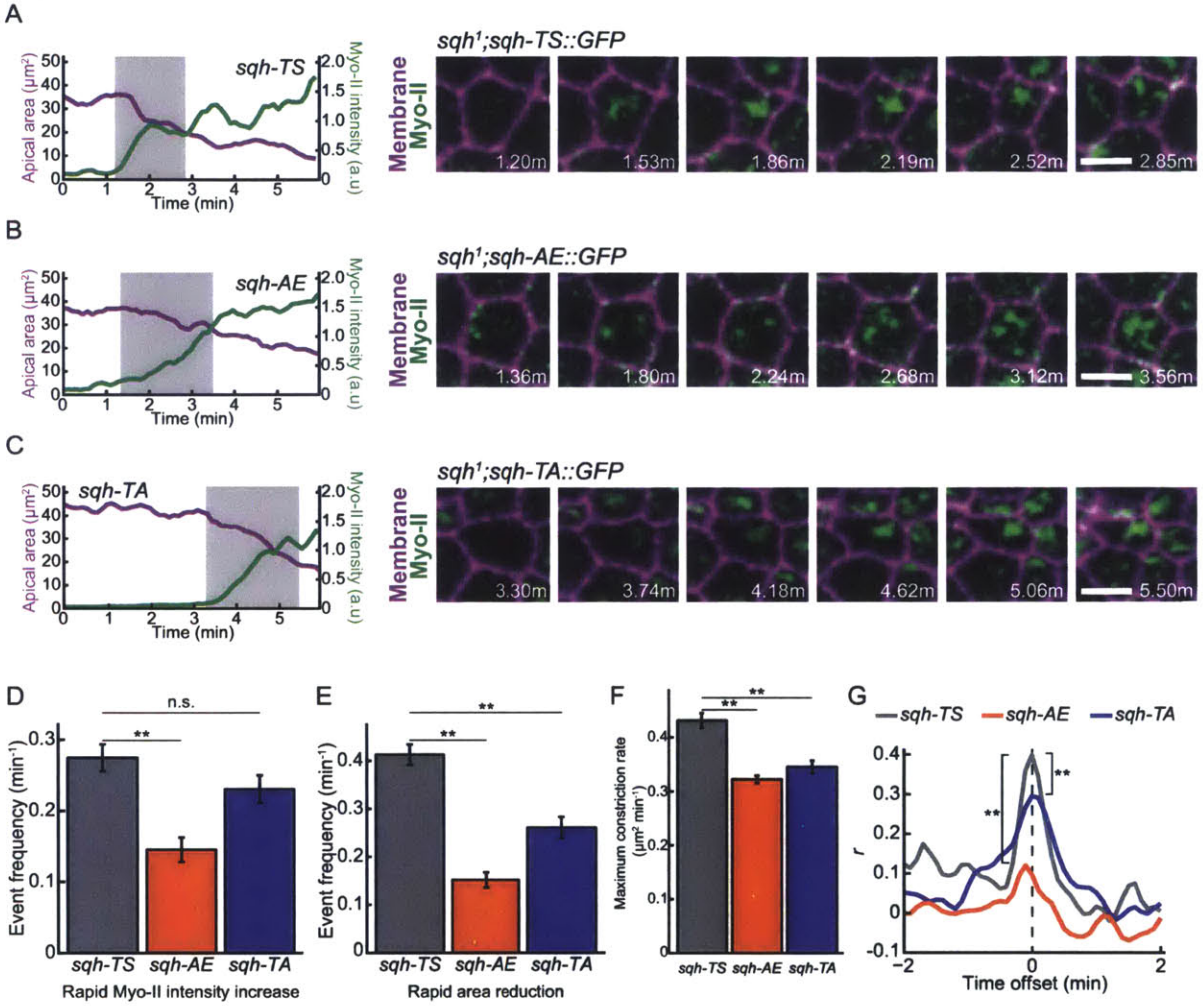

Figure 5 Cycles of Myo-II assembly and disassembly require dynamic RLC phosphorylation. (A-C) The *sqh-AE* and *sqh-TA* mutants inhibit Myo-II remodeling associated with pulses. Time-lapse images are representative cells from *sqh*^{1} germline clone embryos expressing the indicated phospho-mutants and Memb::Cherry (membrane). Plots represent apical area and Myo-II intensity as a function of time for the same cells; the time highlighted in gray corresponds to the time time-lapse shown. Scale bars = 5 μm. (D) Quantification of frequency of instances where there is a rapid increase in Myo-II intensity (*sqh-TS* n=94 cells, 2 embryos; *sqh-AE* n=131 cells, 3 embryos; *sqh-TA* n=92 cells, 2 embryos). (E) Quantification of frequency of instances of rapid apical area reduction (*sqh-TS* n=94 cells, 2 embryos; *sqh-AE* n=131 cells, 3 embryos; *sqh-TA* n=92 cells, 2 embryos). (F) Quantification of maximal instantaneous constriction rate achieved in control or mutant cells (*sqh-TS* n=138 cells, 2 embryos; *sqh-AE* n=187 cells, 3 embryos; *sqh-TA* n=172 cells, 2 embryos). (D-F) Error bars are SEM. (G) Mean cross-correlation between constriction rate and change in Myo-II intensity. (*sqh-TS* n=123 cells, 2 embryos; *sqh-AE* n=143 cells, 3 embryos; *sqh-TA* n=88 cells, 2 embryos). P-values were calculated at 0 time offset. **, $p < 0.01$; n.s., not significant.

Figure S4

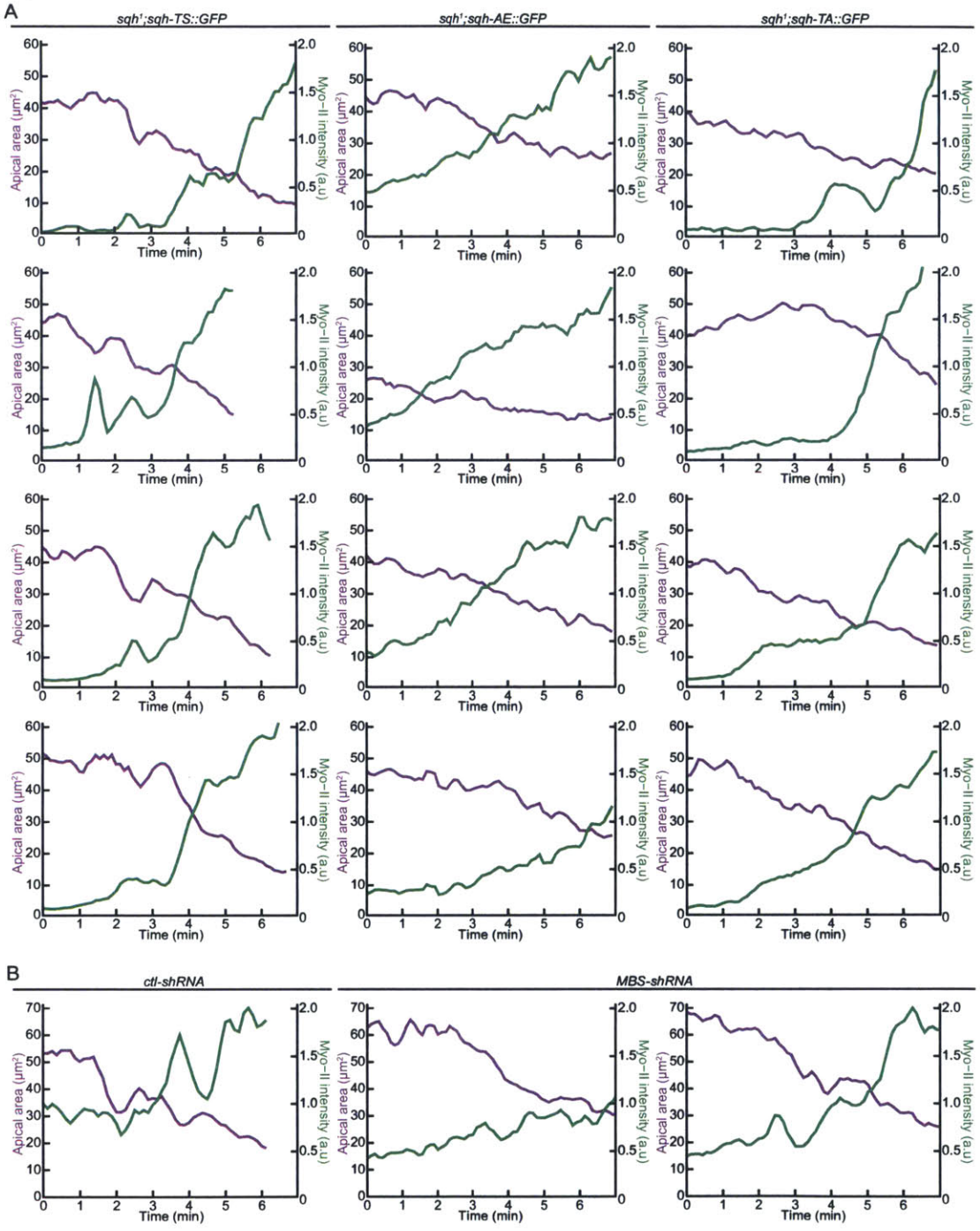

Figure S4 Phospho-mimetic *sqh* mutants and knock-down of MBS result in more continuous Myo-II accumulation and apical constriction. Examples of individual cell apical constriction in *sqh* phospho-mutants (A) and *ctl-shRNA* and *MBS-shRNA* mutants (B). Data plots show apical area and Myo-II intensity as a function of time for representative cells from *sqh*^{1} germline clones expressing the indicated Sqh phospho-mutants or embryos expressing the indicated shRNAs. Starting time corresponds to 1-2 minutes before the onset of mean apical constriction in the corresponding embryo.

Myosin phosphatase localizes to the Myo-II contractile network and is required for contractile pulses

Continuous Myo-II accumulation in the phospho-mimetic mutants suggested that Myo-II dephosphorylation plays a critical role in remodeling Myo-II pulses. Myosin phosphatase is a multi-subunit enzyme that includes a catalytic protein phosphatase 1c δ (PP1cδ; also referred to as PP1cβ in *Drosophila*) and a myosin-binding subunit (MBS) that targets PP1cβ to Myo-II (Hartshorne et al., 1998). Previous studies showed that the *Drosophila* homologs of MBS and PP1cβ regulate the phosphorylation state of Myo-II during multiple developmental stages (Majumder et al., 2012; Ong et al., 2010; Sun et al., 2011; Tan et al., 2003). Therefore, we determined whether MBS could catalyze the dynamic remodeling of Myo-II that occurs during pulsing. During cellularization, MBS localizes to Rok/Myo-II-containing furrow canals (Fig. 1 B and S1 F). In addition, MBS localizes to basal Myo-II particles in *sqh-TS* mutants and to basal aggregates in *sqh-AE* mutants, providing further evidence that phospho-mimetic mutants convert Myo-II into an active conformation that undergoes oligomerization (Fig. S1 F). During ventral furrow formation, MBS is present in the apical cytoplasm of all cells and is enriched in the apical cortex of ventral furrow cells (Fig. 6 A). MBS co-localized with both apical Myo-II and Rok foci throughout the process of ventral furrow formation (Fig. 6, B and C). To determine whether MBS is required for Myo-II pulses, we knocked-down MBS using maternal expression of a small hairpin RNA (shRNA) that targets MBS (Ni et al., 2011) (Fig. S1 G). MBS knock-down resulted in apical Myo-II assembly that exhibited a defect in medioapical coalescence, reminiscent of Myo-II organization in phospho-mimetic mutants (Fig. 6, D-F). While periods of rapid Myo-II accumulation did occur in MBS knock-downs (Fig. 6 G), changes in Myo-II signal were not well correlated with constriction (Fig. 6H). These data suggest that Myo-II dynamics in MBS knock-down cells is uncoupled from area constriction, indicating that there is a defect in the pulsing behavior compared to wild-type cells. Consistent with this atypical Myo-II behavior,

cells in MBS knock-down embryos exhibited more persistent Myo-II accumulation and constriction (Fig. 6, E; and S4 B). Thus, MBS is recruited to apical Myo-II where it is required to polarize Myo-II accumulation and to generate cycles of assembly and disassembly.

Figure 6

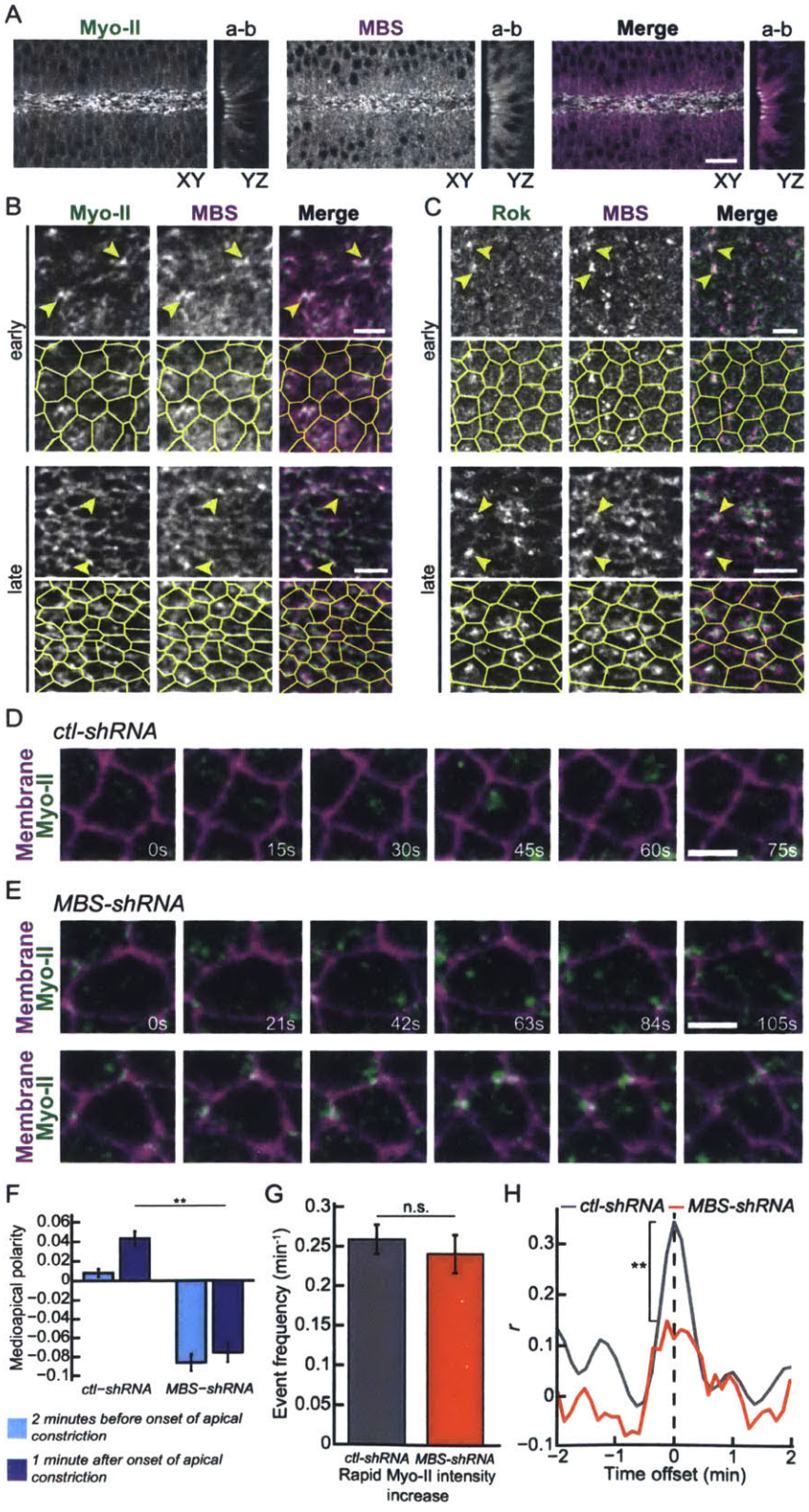

Figure 6 Myo-II contractile pulses require MBS. (A) MBS is apically enriched in ventral furrow cells. Images of XY semi-sagittal and YZ cross-sections for fixed *sqh::GFP* embryos stained for MBS. Scale bar = 10 µm. (B) MBS structures co-localize with Myo-II foci and the supracellular Myo-II meshwork (arrowheads). Images are from fixed *sqh::GFP* embryos stained for MBS. Scale bars = 5 µm. Segmented cell-outlines are from subapical *sqh::GFP* signal. (C) MBS co-localizes with Rok foci (arrowheads). Images are from fixed *GFP::Rok* embryos stained for MBS. Scale bars = 5 µm. Segmented cell-outlines are from subapical Rok signal. (D-E) MBS knock-down inhibits Myo-II pulses. Time-lapse images are cells from embryos expressing *control-shRNA* (*ctl-shRNA*) (D) or *MBS-shRNA* (E), *sqh::GFP* (Myo-II) and Memb::Cherry (membrane). (F) Quantification of Medioapical polarity in Myo-II organization (*ctl-shRNA* n=115 cells, 2 embryos; *MBS-shRNA* n= 123 cells, 2 embryos). Error bars are SEM. (G) Frequency of rapid increases of Myo-II intensity (*ctl-shRNA* n=82 cells, 2 embryos; *MBS-shRNA* = 70 cells, 3 embryos). Error bars are SEM. (H) Mean cross-correlation between constriction rate and change in Myo-II intensity for cells as a function of time offset (*ctl-shRNA* n=118 cells, 2 embryos; *MBS-shRNA* n= 84 cells, 3 embryos). P-values were calculated at 0 time offset. **, $p < 0.01$; n.s, not significant.

Myo-II pulses are important for maintaining tissue integrity during morphogenesis

It is unknown why cells undergo pulsatile, rather than continuous, contraction during tissue morphogenesis. Because we were able to disrupt contractile pulses and promote more persistent apical Myo-II accumulation using both Myo-II phospho-mutants and MBS depletion, we next investigated the consequences of continuous apical constriction on tissue invagination. Surprisingly, many of the phospho-mutants that disrupted contractile pulses (with the exception of the *sqh-AA* mutant) underwent apical constriction and tissue invagination (Fig. 7, A-C; and S5 A-C; data not shown). On average, the *sqh-AE* mutant cells constricted more slowly than wild-type *sqh-TS* control cells, suggesting that unregulated Myo-II may decrease the rate of apical constriction and tissue invagination (Fig. 7, A and C; and S5 B). However, phospho-mimetic mutations in other Myo-II RLCs have been shown to not fully recapitulate the ATPase activity of phosphorylated Myo-II *in vitro* (Kamisoyama et al., 1994). Importantly, MBS depletion, which also appears to trap Myo-II in the phosphorylated state, resulted in apical constriction with similar rates to control cells, despite greater heterogeneity in cell size (Fig. 7, D-F). Thus, while contractile pulses may enhance constriction rate, they do not appear to be required for individual cell apical constriction.

Although apical constriction and tissue invagination occur in Sqh phospho-mutants, the coordination of tissue invagination was perturbed. In wild-type ventral furrows, Myo-II foci in neighboring cells come together steadily to form a dense supracellular Myo-II meshwork across the entire tissue (Fig. 7 G). Furrows in Myo-II phospho-mimetic mutants underwent global contraction, but exhibited abnormal Myo-II separation events at late stages of furrow invagination, resulting in transient gaps in the supracellular Myo-II meshwork (Fig. 7 H; separations observed in 16/21 *sqh-AE* embryos and 14/14 *sqh-EE* embryos). These separations involved stretching of Myo-II structures into fibers and transient recoil between Myo-II structures in adjacent cells and between Myo-II and the junctional membrane (Fig. 7 H and J).

Furthermore, the phenotype of MBS knock-down resembled phospho-mimetic Myo-II mutants, also displaying Myo-II separations (Fig. 7, K and L; separations observed in 9/9 *MBS-shRNA* embryos). We did not observe frequent stretching of Myo-II fibers in the *sqh-TA* mutant, but we did observe dynamic separation between Myo-II foci, suggesting that high levels of phosphorylation and/or Myo-II remodeling are important to maintain strong intercellular coupling between actomyosin networks as the tissue invaginates (Fig. 7 I; separations observed in 7/15 *sqh-TA* embryos). Although the dynamic separation events are similar to tearing events that occur in mutants that reduce cell-cell adhesion (Martin et al., 2010), the *sqh-TA* and *sqh-AE* mutants exhibited normal apical E-cadherin localization (Fig. S5 D-F). Thus, dynamic Myo-II pulses appear to be important for coordinating apical constriction and the contractile force balance between cells such that inappropriate stretching and tearing events do not occur in the supracellular actomyosin meshwork that transmits tension across the ventral furrow tissue.

Figure 7

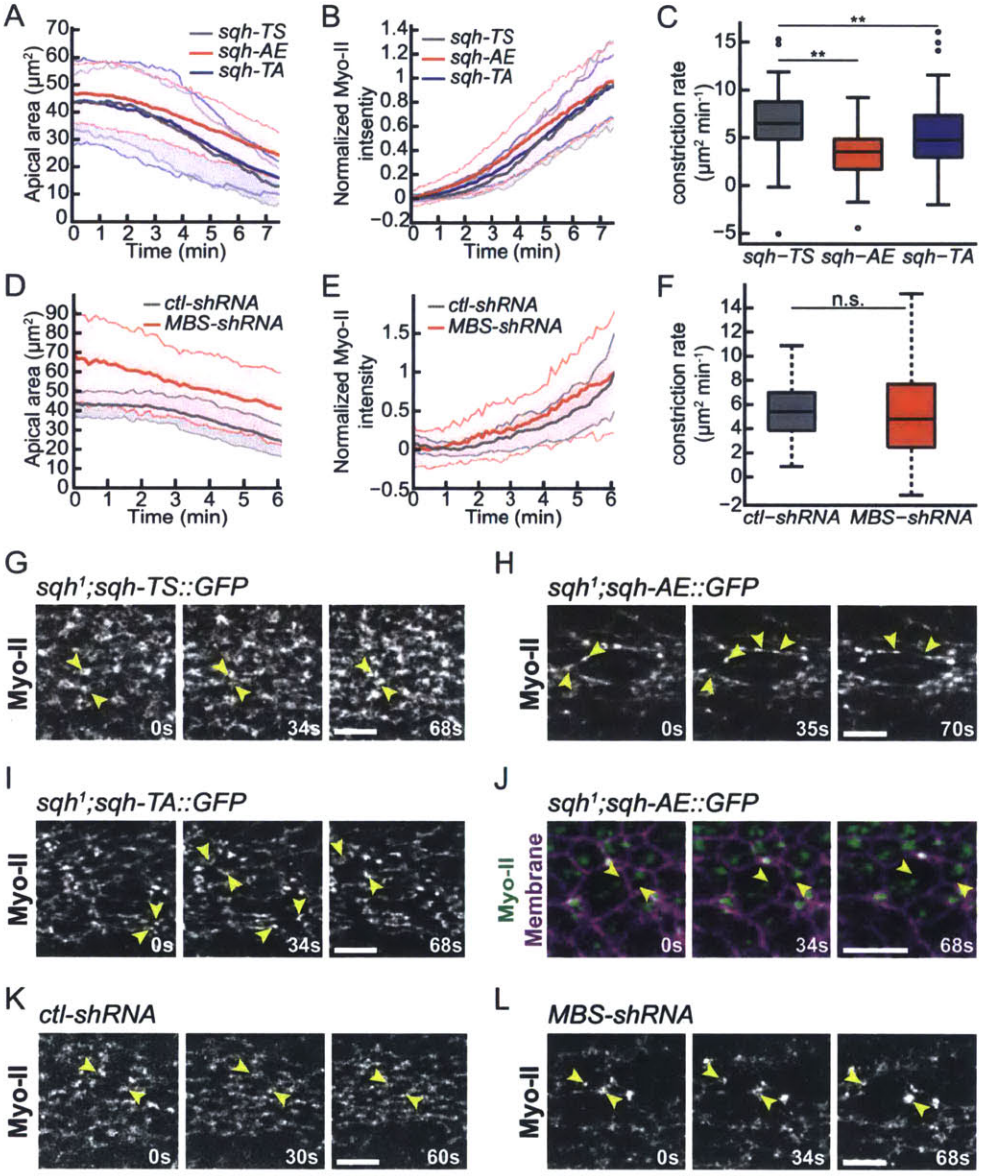

Figure 7 Defects in Myo-II pulsing disrupt the integrity of the supracellular actomyosin meshwork. (A-B) Mean apical area (A) and normalized mean cellular Myo-II intensity (B) for representative *sqh*^{1} germline clone embryos expressing the indicated phospho-mutants (*sqh-TS*, n=50 cells; *sqh-TA*, n=49 cells, and *sqh-AE*, n=50 cells). Shaded area is +/- 1 SD. (C) Box-and-Whisker plot of cell constriction rates for multiple *sqh*^{1} germline clone embryos expressing the indicated phospho-mutants (*sqh-TS* n=102 cells, 2 embryos; *sqh-AE* n=169 cells, 3 embryos; and *sqh-TA* n=189 cells, 3 embryos). (D-E) Mean apical area (D) and normalized mean cellular Myo-II intensity (E) for representative embryos expressing the indicated shRNA (*control-shRNA*, n=78 cells; *MBS-shRNA*, n=31 cells). Apical area of cells in *MBS-shRNA* knock-down embryos were more heterogenous and larger than that of *ctl-shRNA* embryos; however, they undergo apical constriction. Shaded area is +/- 1 SD. (F) Box-and-Whisker plot of constriction rates for multiple embryos expressing the indicated shRNA (*control-shRNA*, n=104 cells, 2 embryos; *MBS-shRNA*, n=78 cells, 3 embryos). (G-L) Myo-II phospho-mutants and MBS knock-down cause separation of Myo-II networks between cells. Time-lapse images are of representative cells from *sqh*^{1} germline clone embryos with the indicated phospho-mutants or from embryos expressing the indicated shRNA. Arrowheads indicate contraction of an intact supracellular Myo-II meshwork in control embryos (G and K) or instances of intercellular Myo-II network separation in mutants or knock-downs (H-J and L). Scale bars = 10 μm. Box-and-Whisker plots display median (central mark), 25th and 75th percentiles (box edges), the most extreme data points not considered outliers (whiskers), and outliers (plotted individually). **, $p < 0.01$; n.s., not significant.

Figure S5

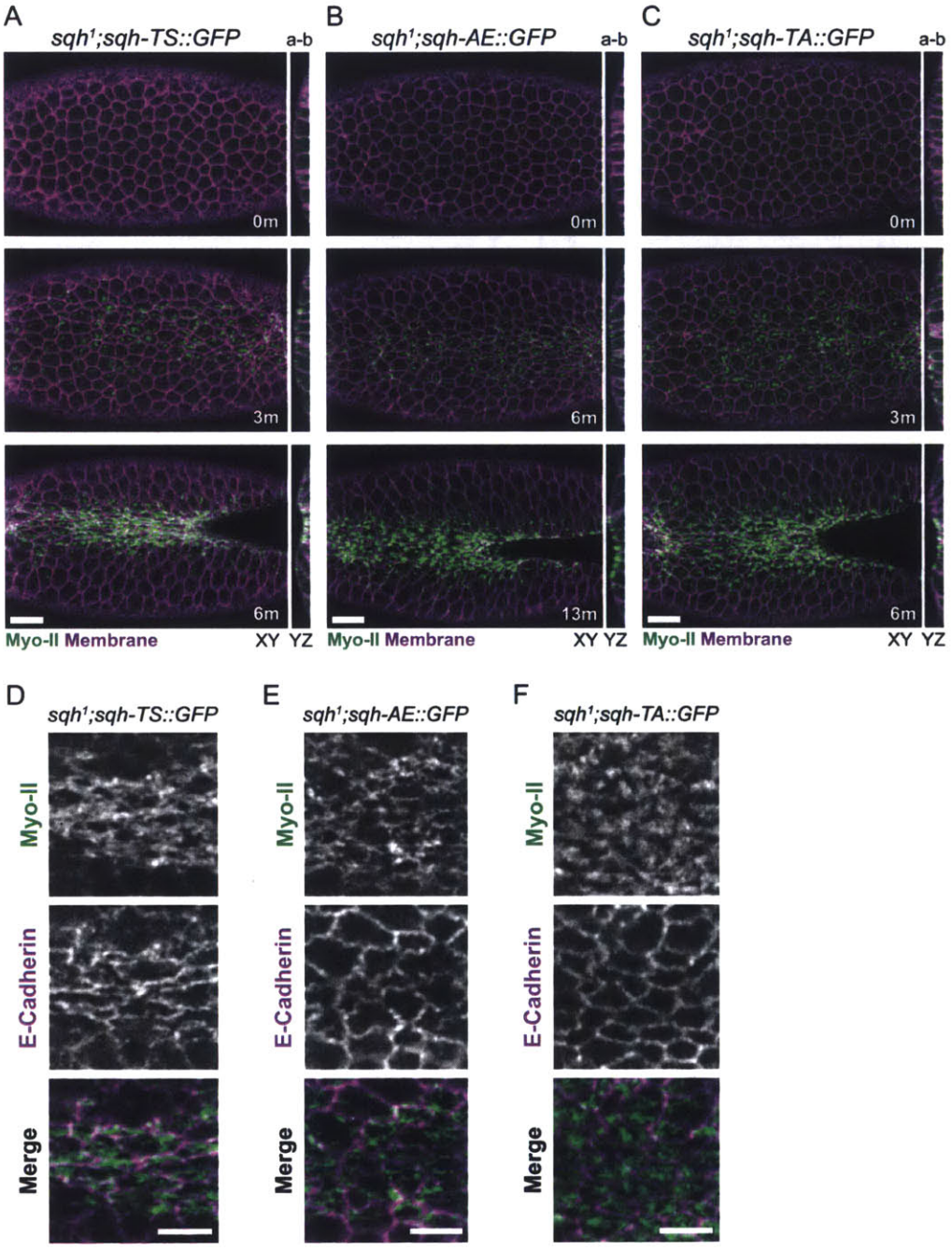

Figure S5 Tissue invagination and E-cadherin localization in Myo-II phospho-mutants.
(A-C) Activating and inactivating *sqh* serine-21 phospho-mutants rescue ventral furrow invagination. The *sqh-AE* allele exhibits delayed apical constriction and tissue invagination. Representative images of XY semi-sagittal sections and YZ cross-sections of live embryos from *sqh*^{1} GLCs expressing *sqh-TS::GFP* (A), *sqh-AE::GFP* (B), and *sqh-TA::GFP* (C). Embryos also express Gap43::mCherry as a membrane marker (magenta). a-b indicates apical-basal polarity. Scale bars = 10 μm. (D-F) Representative images of furrows of fixed *sqh*^{1} GLC embryos expressing *sqh-TS::GFP* (D), *sqh-AE::GFP* (E), and *sqh-TA::GFP* (F) and stained for E-cadherin. Scale bars = 5 μm.

Discussion

Recent studies demonstrated that pulsatile Myo-II contractions drive diverse morphogenetic processes, including *C. elegans* embryo polarization (Munro et al., 2004), *Drosophila* gastrulation (He et al., 2014; Martin et al., 2009; Roh-Johnson et al., 2012), dorsal closure (Azevedo et al., 2011; Blanchard et al., 2010; David et al., 2010), germband extension (Fernandez-Gonzalez and Zallen, 2011; Rauzi et al., 2010; Sawyer et al., 2011), oocyte elongation (He et al., 2010), and *Xenopus* convergent extension (Kim and Davidson, 2011; Shindo and Wallingford, 2014; Skoglund et al., 2008). Although Rok, and likely Myo-II activation via Rok phosphorylation, is required for contraction (Dawes-Hoang et al., 2005; He et al., 2010; Kim and Davidson, 2011; Mason et al., 2013), it was not clear whether Myo-II activation simply regulates cortical Myo-II levels or whether coupling between Myo-II activity and its regulators organizes contractile pulses in space and time. Furthermore, why cells undergo pulsatile, rather than continuous, contraction to drive tissue morphogenesis was unknown. We were able to answer these questions by visualizing the consequences of uncoupling Myo-II activation from upstream signaling pathways on cell and tissue dynamics.

Dynamic Myo-II phospho-regulation organizes contractile pulses

We identified dynamic Myo-II phosphorylation as a key mechanism that regulates contractile pulses. We found that Myo-II pulses are associated with dynamic medioapical Rok foci and myosin phosphatase. In addition, the phospho-mimetic *sqh-AE* and *sqh-EE* mutants, which exhibited constitutive cytoplasmic Myo-II assembly *in vivo,* exhibited defects in two properties of contractile pulses. First, phospho-mimetic mutants did not initially condense apical Myo-II or F-actin into medioapical foci, resulting in Myo-II accumulation across the apical domain and thus a defect in Myo-II radial cell polarity. Second, phospho-mimetic mutants continuously

accumulated Myo-II in the apical cortex, lacking clear cycles of Myo-II remodeling that are observed in wild-type embryos. Although the phospho-mimetic alleles are predicted to partially activate the Myo-II motor's ATPase activity compared to normal phosphorylation (Kamisoyama et al., 1994), the similarity of the MBS knock-down phenotype suggests that the changes in Myo-II organization and dynamics in phospho-mimetic mutants reflect defects in the control over Myo-II dynamics rather than a reduction in motor activity. The consequence of persistent Myo-II assembly across the apical surface in phospho-mimetic mutants and MBS knock-down is a more continuous, rather than incremental, apical constriction, demonstrating that pulsatile cell shape change results from temporal and spatial regulation of Myo-II activity via a balance between kinase (Rok) and phosphatase (myosin phosphatase) activity.

Mutants that decrease Myo-II phosphorylation affected contractile pulses in a manner that was distinct from the phospho-mimetic alleles. Both the *sqh-AA* and the *sqh-TA* mutants exhibited Myo-II assembly into apical foci, potentially mediated by phosphorylation of low levels of endogenous Sqh or phosphorylation of threonine-20, respectively. For the *sqh-TA* mutant, Myo-II assembly was correlated with constriction, suggesting that Myo-II motor activity is not rate-limiting to initiate a contractile pulse. However, Myo-II foci in *sqh-TA* and *sqh-AA* mutants were not efficiently remodeled after assembly and coalescence. The persistence of cortical Myo-II foci in *sqh-AA* and *sqh-TA* mutants was surprising given that *rok* mutants and injection of Rok inhibitor reduce cortical localization of Myo-II (Dawes-Hoang et al., 2005; Mason et al., 2013; Royou et al., 2004; Royou et al., 2002). One explanation is that high levels of Myo-II activity induce actomyosin turnover and thus could be required to remodel the actomyosin network after contraction (Murthy and Wadsworth, 2005; Wilson et al., 2010). Alternatively, apical recruitment of myosin phosphatase or proteins that negatively regulate Rok could depend on Myo-II phosphorylation or actomyosin contraction (David et al., 2013). While future work is needed to address the role of Myo-II motor activity in contractile pulses, the phenotypes of

alleles that constitutively reduce phosphorylation further suggest that cycling between high and low phosphorylation states is required for proper Myo-II pulses.

We propose a model for contractile pulses in the ventral furrow where, in combination with unknown cortical cues that apically localize Myo-II, local pulses of apical Rok activity within the medioapical cortex polarize Myo-II assembly and coalescence (Fig. 8 A). Rok foci could polarize actomyosin condensation by generating an intracellular gradient of minifilament assembly and tension that results in inward centripetal actomyosin network flow (Fig. 8 A, red arrows) (Bray and White, 1988; Mayer et al., 2010; Munro et al., 2004). In addition, local Myo-II activation by Rok foci combined with broader myosin phosphatase activity throughout the apical cytoplasm could generate a gradient of Myo-II turnover that will concentrate Myo-II into medioapical foci (Fig. 8 A). MBS is required to restrict phosphorylated Myo-II to specific cell-cell interfaces during dorsal closure, demonstrating that the balance between Myo-II kinases and phosphatase can generate spatial patterns of Myo-II activation in epithelial cells (Mizuno et al., 2002). Myo-II remodeling after coalescence could result from local decreases in Rok activity and enrichment of apical myosin phosphatase with Myo-II structures (Fig. 8 A). Thus, coupling Myo-II activation to dynamic signals that regulate Myo-II phosphorylation organizes contractile pulses in space and time to drive incremental apical constriction.

Polarized actomyosin contraction, pulses, and flows generate force and organize the actin cortex in a variety of cellular and developmental contexts (Lecuit et al., 2011; Salbreux et al., 2012). In contrast to the ratchet-like constriction of ventral furrow cells, some cell types undergo extended periods of actomyosin pulsing and area fluctuations without net reduction in area (Blanchard et al., 2010; He et al., 2010; Solon et al., 2009). Furthermore, directional rearrangement of cell contacts, such as during convergent-extension in the *Drosophila* germband, can be achieved through planar polarized accumulation of junctional Rok and Myo-II (Bertet et al., 2004; Blankenship et al., 2006; Simoes et al., 2010) in conjunction with planar polarized medioapical actomyosin flows (Levayer and Lecuit, 2013; Rauzi et al., 2010).

Modulating the spatial and temporal regulation of Myo-II phosphorylation and dephosphorylation provides a possible mechanism to tune contractile dynamics and organization to generate diverse cell shape changes (Mason and Martin, 2011). Thus, it will be important to define the principles that control Myo-II activity and dynamics and how tuning Myo-II dynamics impacts force generation and tissue movement.

Role of pulsatile Myo-II contractions during tissue morphogenesis

Myo-II phospho-mutants resulted in a more continuous apical Myo-II assembly and apical constriction, enabling us to investigate the role of pulsation during tissue morphogenesis. Continuous Myo-II assembly and contraction in the *sqh-AE* mutant resulted in a slower mean rate of apical constriction and thus delayed tissue invagination. This delay suggested that pulsing might be important for the efficiency of apical constriction. However, phospho-mimetic mutants might not fully recapitulate the ATPase activity of phosphorylated Myo-II. The *sqh-TA* mutant, which also perturbs Myo-II remodeling, constricted ventral furrow cells at a rate that is only slightly slower than wild-type. In addition, MBS knock-down, which disrupted Myo-II pulses, exhibited a more variable constriction rate, but with an average rate comparable to control embryos. Our finding is distinct from studies in other cell types where loss of MBS results in excessive phosphorylated Myo-II accumulation and cell invagination (Corrigall et al., 2007; Lee and Treisman, 2004). Thus, MBS can regulate Myo-II organization and dynamics without causing a significant increase in apical Myo-II levels. We conclude that Myo-II pulses are not absolutely required for individual cell apical constriction.

Although phospho-mimetic mutant cells constrict and undergo tissue invagination, the coordination of invagination and the stability of the supracellular actomyosin meshwork were perturbed. Continuous apical constriction was associated with abnormal stretching and tearing events between Myo-II structures, resulting in gaps or holes in the supracellular Myo-II

meshwork. Tearing events were also observed in MBS knock-downs, where Myo-II networks separated at cell-cell interfaces. Thus, continuous Myo-II assembly and a lack of Myo-II dynamics during apical constriction appear to sensitize the tissue to loss of intercellular integrity during morphogenesis (Fig. 8 B). While loss of cytoskeletal continuity in phospho-mimetic mutants does not block tissue invagination, we speculate that dynamic Myo-II pulses are important to make tissue invagination robust to changes in tensile stress. One possible function of Myo-II pulses is to attenuate tissue tension or stiffness during morphogenetic movements (Fischer et al., 2014). Because pulsed Myo-II contractions are staggered between neighboring cells, pulsation could serve as a mechanism to coordinate contractile force generation across the tissue such that cell junctions are buffered from high levels of tension (Fig. 8 B). Indeed, reducing adherens junction proteins sensitizes the intercellular connections between cytoskeletal networks to tensile forces generated in ventral furrow cells (Martin et al., 2010; Sawyer et al., 2011; Spahn et al., 2012). Alternatively, remodeling of actomyosin networks that occurs during pulses could be required to adapt the cytoskeletal organization such that forces transmitted between cells accommodate the changing pattern of tissue-scale forces during the course of morphogenesis. In either case, our data suggest that Myo-II pulsing and remodeling are important for collective cell behavior by ensuring proper force transmission between cells in a tissue undergoing morphogenesis.

Figure 8

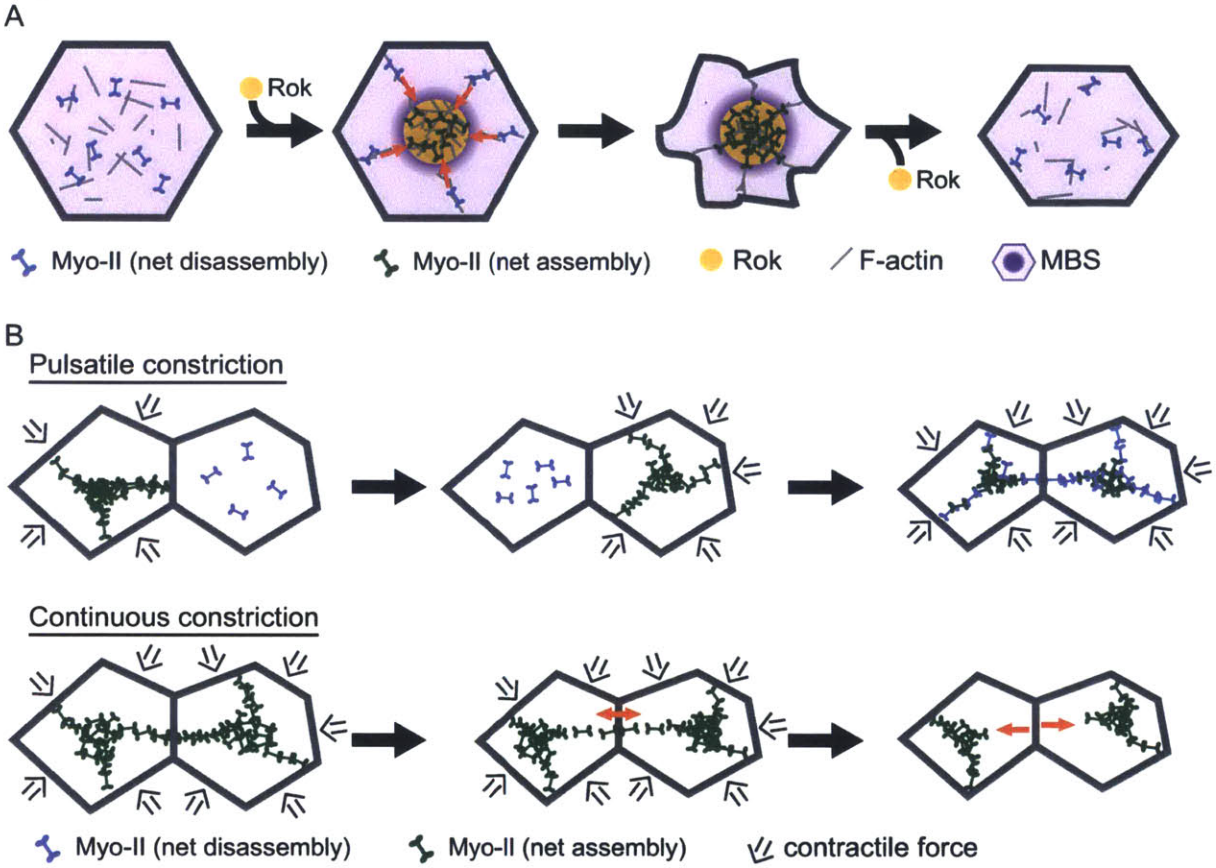

Figure 8 Model for mechanism and function of contractile pulses. (A) Myo-II dynamics during a contractile pulse. The contractile pulse is initiated by a local increase in Rok activity that elevates Myo-II phosphorylation and activity. Myo-II coalescence into medioapical foci results from: 1) cortical flow (red arrows) resulting from a gradient in cortical tension, and 2) net Myo-II minifilament assembly (dark green) at Rok foci with net minifilament disassembly (light blue) in regions of low Rok by myosin phosphatase (purple). Decreased Rok activity after Myo-II coalescence results in Myo-II dephosphorylation followed by remodeling of the contracted cortex. (B) Contractile pulses are required to maintain tissue integrity. Pulsatile Myo-II contraction occurs asynchronously in adjacent cells, which reduces stress at adherens junctions. In addition, Myo-II remodeling allows cells to adjust contacts to maintain stable intercellular cytoskeletal connections. Continuous Myo-II assembly and apical constriction decreases ability of actomyosin networks to dynamically adjust to changes in tissue mechanics, resulting in stretching of Myo-II structures and loss of intercellular connections (red arrows).

Materials and Methods

Fly Stocks and Genetics

Stocks used in this investigation are listed in Table S1. Germline clones were generated using the FLP-DFS technique by heat-shocking mutant/ovo^D larvae for two hours at 37°C for three to four days (Chou and Perrimon, 1992). For two-channel imaging of *Venus::Rok* (UAS-driven) (Simoes et al., 2010) and *sqh::mCherry* (sqh promoter), rok^2 FRT/FM7;;*mat15 sqh::mCherry*/TM3 females were crossed to ovo^D FRT/Y; *hsFlp UAS-Venus::Rok*/CyO males and embryos from heat shocked rok^2 FRT/ ovo^D FRT; *hsFlp UAS-Venus::Rok*/+; *mat15 sqh::mCherry*/+ females were collected for live imaging. For *sqh::GFP* rescue of sqh^1 germline clones, sqh^1 FRT/FM7; *sqh-XX::GFP*/CyO females were crossed to ovo^D FRT/Y; *hsFlp* males, the resulting larvae were heat shocked, and sqh^1 FRT/ ovo^D FRT; *sqh-XX::GFP/ hsFlp* females were crossed to OreR to collect embryos that resulted from germline clones. All *sqh-XX::GFP* transgenes were expressed via the endogenous *sqh* promoter. *Sqh* phosphomutants were recombined with *Gap43::mCherry* (Memb::Cherry, plasma membrane marker, driven by *sqh* promoter) (Martin et al., 2010) or with *Utr::mCherry* (F-actin marker, driven by *sqh* promoter) (Rauzi et al., 2010). For *sqh-EE::GFP* suppression of *rok* mutant germline clones, rok^1 FRT/FM7; *sqh-EE::GFP*/CyO females were crossed to ovo^D FRT/Y; *hsFlp* males and heat shocked. rok^1 FRT/ ovo^D FRT; *sqh-EE::GFP/ hsFlp* females were crossed to OreR males to collect embryos. In all cases, control crosses lacking heat shock were performed to verify the presence of the ovo^D allele. To generate MBS knock-down embryos, females containing a UAS-driven shRNA against MBS (*MBS-shRNA*) or the *white* gene (control) were crossed to males containing a double-maternal driver line with both *sqh::GFP* and *Gap43::mCherry*. Both UAS stocks are gifts from N. Perrimon, L. Perkins and the TRiP, Harvard Medical School, Boston, MA). The resulting larvae were raised at 25°C and females that maternally expressed *MBS-*

shRNA or *ctl-shRNA* and both fluorescent markers were crossed to OreR males, and the resulting embryos were imaged.

Construction of GFP-tagged *sqh* phospho-mutants

Substitution of threonine-20 and serine-21 with alanine or glutamate prevented or mimicked phosphorylation, respectively (Jordan and Karess, 1997; Winter et al., 2001). The *sqh* gene, including 5' promoter sequences and 3' termination sequences, was tagged at the carboxy-terminus with eGFP. The *sqh::GFP* sequence is identical to the previously used *sqh::mCherry* construct with the exception of the fluorescent protein sequence (Martin et al., 2009). Site-directed mutagenesis of residues threonine-20 and/or serine-21 was performed on *sqh::GFP* in the pBluescript vector using QuikChange II XL site-directed mutagenesis kit (Agilent Technologies). The 3.5 kb KpnI/XbaI *sqh::GFP* fragments were cloned into the pTiger transformation vector containing an attB site (pTiger courtesy of S. Ferguson, State University of New York at Fredonia, Fredonia, NY). These constructs were sent to BestGene Inc. for integration into either the attP1 or attP40 landing sites (see Table S1) using the ϕC31 integrase system (Groth et al., 2004). Transgenes integrated at these chromosome II landing sites were crossed to the sqh^1 mutant. The *sqh-TS::GFP* transgene could rescue sqh^1 mutant flies to adulthood, however, homozygous sqh^1 adult flies were not observed with any of the *sqh::GFP* phosphomutants (including *sqh-AE* and *sqh-EE*), demonstrating that dynamic myosin phosphorylation is required for development.

Generation of full-length Sqh antibody and Western blotting

Full-length Sqh cDNA was cloned and purified from E. coli by GenScript (GenScript USA Inc., Piscataway, NJ). Rabbit sera were obtained using the full-length Sqh as antigen (Panigen, Inc., Blanchardville, WI). Polyclonal anti-Sqh antibody was affinity purified using standard biochemical procedures. Briefly, purified Sqh was coupled to CNBr-Activated Sepharose 4B

(Amersham Pharmacia), the Sqh-coupled resin was incubated with sera, the resin was washed and the antibody was eluted with Glycine, pH 2.5.

Western blotting was performed by grinding embryos directly in sample buffer and running samples on 12% SDS-PAGE gels. Protein was transferred to 0.45 μm Nitrocellulose membrane (Bio-Rad Laboratories, Hercules, CA) and the indicated primary antibodies were detected using horseradish peroxidase labeled secondary antibodies (Jackson ImmunoResearch Laboratories, Inc., West Grove, PA).

Immunohistochemistry

Antibodies and corresponding concentrations used in this investigation are listed in Table S2. For fixed imaging, all embryos were first dechorionated in 50% bleach and then either methanol/ heat-fixed or paraformaldehyde (PFA) fixed. Embryos stained with α-zipper (Gift from E. Wieschaus, Princeton Univeristy, Princeton, NJ) and α-neurotactin were methanol/heat-fixed (Fig. 3), all other immunostainings used PFA-fixed embryos. For methanol/heat-fixations, embryos were placed in boiling Triton salt solution (0.03% Triton X-100 and 0.4% NaCl in water), cooled on ice and then devitellinized in a 1:1 heptane:methanol solution. PFA-fixed embryos were fixed in a 1:1 solution of 8% paraformaldehyde in 0.1M phosphate buffer pH 7.4 and heptane for 30 minutes, transferred to a petri dish and manually devitellinized using a syringe needle. Following immunostaining, heat-fixed embryos were placed on a slide in mounting medium (4% N-propyl-galate in 80% glycerol) and sliced using a syringe blade to create cross-sections. PFA-fixed embryos were mounted in AquaPolymount (Polysciences, Inc.). Images were acquired on a Zeiss LSM 710 confocal microscope with a 40x/1.2 Apochromat water objective (Zeiss), using an argon ion, 561nm diode, 594nm HeNe, and 633nm HeNe lasers. In Fig. 1 and 6 endogenous GFP fluorescence was used to visualize Myo-II and Rok, respectively.

Time-Lapse Imaging

Embryos were dechorionated in 50% bleach, mounted ventral side up on a slide coated with "embryo glue" (double-sided tape soaked in heptane). No. 1.5 coverslips were used as spacers and to create a chamber for the mounted embryo. A No. 1 coverslip completes the top of the chamber, and the chamber was filled with Halocarbon 27 oil. All imaging occurred at room temperature (~23°C) on a Zeiss LSM 710 confocal microscope with 40x/1.2 Apochromat water objective (Zeiss), argon ion and 561nm diode lasers, and a pinhole setting between 1-2 Airy units. Simultaneous excitation was used for live two-channel imaging of GFP/mCherry or Venus/mCherry. The band-pass filters for Venus/mCherry were set at 519-578 nm and ~599-696 nm, respectively. For Venus/mCherry two-channel imaging we confirmed that there was minimal spectral bleed-through between channels. The band-pass selected for GFP was ~488-558 nm and for mCherry was ~573-696 nm. All images were acquired using Zen (Zeiss) software.

Image Processing and Analysis

Images were processed using Fiji (http://fiji.sc/wiki/index.php/Fiji) and MATLAB (MathWorks).

A Gaussian filter (σ=0.5-0.7) was applied to images. Apical images are maximum intensity projections of ~2-5μm. Subapical image and membrane images are single sections ~1-2 μm below the apical projection.

To quantify Rok and Myo-II intensity over time, we generated kymographs of pulses and acquired intensity values along a linear trace through the kymographs. To determine the phase relationship between Rok and Myo-II signals, a Pearson correlation was calculated for various time offsets where the Rok and Myo-II signals were shifted relative to each other.

We used custom MATLAB software, EDGE (Embryo Development Geometry Explorer) (Gelbart et al., 2012) to segment images for quantification of apical area and Myo-II intensities. EDGE automatically segmented cell membranes, however we manually corrected cells with errors in segmentation. Segmented cell membranes were subapical to the Myo-II signal. Embryos were aligned in time using the mean apical area signals of each embryo by choosing the time where the tissue begins to constrict. For quantification of junctional and medioapical Myo-II intensity in Fig. 4, we used a maximum intensity projection of the raw apical Myo-II signal and applied EDGE to segment images. The medioapical domain of a cell is defined by shrinking the cell's segmented contour by 2 pixels width; the pixel intensity in this area was used to define "medioapical Myo-II" and "junctional Myo-II" was defined as the difference between the Myo-II intensity in the entire cell and the intensity in the medioapical area (see equations below). We then calculated "Medioapical polarity" as shown below.

P_T = total number of pixels in cell apex
P_m = number of pixels in medial region of cell
I_k = intensity of pixel k
N_c = number of cells

$$\text{total Myo-II} = \frac{\sum_{k=1}^{P_T} I_k}{P_T}$$

$$\text{medial Myo-II} = \frac{\sum_{k=1}^{P_m} I_k}{P_m}$$

$$\text{junctional Myo-II} = \frac{\sum_{k=1}^{P_T} I_k - \sum_{k=1}^{P_m} I_k}{P_T - P_m}$$

$$\text{p} = \frac{\text{medial Myo-II} - \text{junctional Myo-II}}{\text{total Myo-II}}$$

$$\text{Medioapical polarity} = \frac{\sum_{i=1}^{N_c} \text{p}_i}{N_c}$$

To quantify Myo-II dynamics in Fig. 5-7, raw Myo-II images were pre-processed to remove cytoplasmic Myo-II by clipping intensity values 2.5 standard deviations above the mean intensity of cytoplasmic Myo-II. A Gaussian filter was applied (σ=0.5) and maximum intensity z-projections were made for the top two highest intensity values of Myo-II and imported into

EDGE. To compare the frequency of instances of rapid Myo-II intensity increase or instances of rapid area reduction between embryos (Fig. 5 D-E, and 6 G), we first smoothed signals for apical area and mean Myo-II intensity and calculated instantaneous rates for each time point. Rapid Myo-II intensity increases or rapid area reductions were defined as instances where the Myo-II accumulation rate (for Fig. 5 D and 6 G) or the constriction rate (for Fig. 5 E), respectively, exceed a threshold of 1 standard deviation above the mean rate for all control cells (*sqh-TS* for Fig. 5 and *ctl-shRNA* for Fig. 6). To compare maximum constriction rates between control and mutants (Fig. 5 F), we identified the instance of where the constriction rate of each cell was maximal. The identified maximum constriction rates were averaged for control and mutant embryos. The time-resolved cross-correlation between constriction rate and Myo-II accumulation rate (Fig. 5 G and 6 F) was measured by calculating the Pearson correlation between constriction rate and Myo-II accumulation rate for different time offsets. Mean Myo-II intensity displayed in Fig. 7, A and D were normalized such that the minimum and maximum intensity values were 0 and 1, respectively. We calculated the mean constriction rate for Fig. 7 C and F, by taking the negative slope of the apical area between the time apical constriction initiates and 3 minutes later for each cell.

Statistics

Statistical analyses were preformed using the MATLAB statistics toolbox. p-values were calculated using a two-tailed unpaired t-test in Fig. 4-7.

Acknowledgments

We thank E. Wieschaus, J. Zallen, S. Simões, R. Fernandez-Gonzalez, T. Lecuit, Y. Bellaiche, and the Bloomington Stock Center for fly stocks and antibodies used in this study. Additionally, we thank N.Perrimon, L. Perkins, and the TRiP at Harvard Medical School (NIH/NIGMS R01-GM084947) for providing transgenic RNAi fly stocks used in this study. The Neurotactin and E-cadherin antibodies, developed by Goodman, C. and Uemura, T., respectively, were obtained from the Developmental Studies Hybridoma Bank, created by the NICHD of the NIH and maintained at the University of Iowa, Deparment of Biology, Iowa City, IA 52242. Finally, we thank A. Sokac, I. Cheeseman, J. Zallen, K. Kasza, and members of the Martin lab for their helpful comments and discussion on this manuscript. This work was supported by grant R00GM089826 and R01GM105984 to A.C.M. from the National Institute of General Medical Sciences and by NIH Pre-Doctoral Training Grant T32GM007287. The authors declare no competing financial interests.

References

Amano, M., Ito, M., Kimura, K., Fukata, Y., Chihara, K., Nakano, T., Matsuura, Y., and Kaibuchi, K. (1996). Phosphorylation and activation of myosin by Rho-associated kinase (Rho-kinase). J Biol Chem *271*, 20246-20249.

Azevedo, D., Antunes, M., Prag, S., Ma, X., Hacker, U., Brodland, G.W., Hutson, M.S., Solon, J., and Jacinto, A. (2011). DRhoGEF2 regulates cellular tension and cell pulsations in the Amnioserosa during Drosophila dorsal closure. PLoS One *6*, e23964.

Bardet, P.L., Guirao, B., Paoletti, C., Serman, F., Leopold, V., Bosveld, F., Goya, Y., Mirouse, V., Graner, F., and Bellaiche, Y. (2013). PTEN controls junction lengthening and stability during cell rearrangement in epithelial tissue. Dev Cell *25*, 534-546.

Barrett, K., Leptin, M., and Settleman, J. (1997). The Rho GTPase and a putative RhoGEF mediate a signaling pathway for the cell shape changes in Drosophila gastrulation. Cell *91*, 905-915.

Bertet, C., Sulak, L., and Lecuit, T. (2004). Myosin-dependent junction remodelling controls planar cell intercalation and axis elongation. Nature *429*, 667-671.

Blanchard, G.B., Murugesu, S., Adams, R.J., Martinez-Arias, A., and Gorfinkiel, N. (2010). Cytoskeletal dynamics and supracellular organisation of cell shape fluctuations during dorsal closure. Dev *137*, 2743-2752.

Blankenship, J.T., Backovic, S.T., Sanny, J.S., Weitz, O., and Zallen, J.A. (2006). Multicellular rosette formation links planar cell polarity to tissue morphogenesis. Dev Cell *11*, 459-470.

Bray, D., and White, J.G. (1988). Cortical flow in animal cells. Science *239*, 883-888.

Bresnick, A.R., Wolff-Long, V.L., Baumann, O., and Pollard, T.D. (1995). Phosphorylation on threonine-18 of the regulatory light chain dissociates the ATPase and motor properties of smooth muscle myosin II. Biochemistry *34*, 12576-12583.

Chou, T.B., and Perrimon, N. (1992). Use of a yeast site-specific recombinase to produce female germline chimeras in Drosophila. Genetics *131*, 643-653.

Corrigall, D., Walther, R.F., Rodriguez, L., Fichelson, P., and Pichaud, F. (2007). Hedgehog signaling is a principal inducer of Myosin-II-driven cell ingression in Drosophila epithelia. Dev Cell *13*, 730-742.

David, D.J., Tishkina, A., and Harris, T.J. (2010). The PAR complex regulates pulsed actomyosin contractions during amnioserosa apical constriction in Drosophila. Dev *137*, 1645-1655.

David, D.J., Wang, Q., Feng, J.J., and Harris, T.J. (2013). Bazooka inhibits aPKC to limit antagonism of actomyosin networks during amnioserosa apical constriction. Dev *140*, 4719-4729.

Dawes-Hoang, R.E., Parmar, K.M., Christiansen, A.E., Phelps, C.B., Brand, A.H., and Wieschaus, E.F. (2005). folded gastrulation, cell shape change and the control of myosin localization. Dev *132*, 4165-4178.

Fernandez-Gonzalez, R., and Zallen, J.A. (2011). Oscillatory behaviors and hierarchical assembly of contractile structures in intercalating cells. Physical biology *8*, 045005.

Fischer, S.C., Blanchard, G.B., Duque, J., Adams, R.J., Arias, A.M., Guest, S.D., and Gorfinkiel, N. (2014). Contractile and mechanical properties of epithelia with perturbed actomyosin dynamics. PLoS One *9*, e95695.

Gelbart, M.A., He, B., Martin, A.C., Thiberge, S.Y., Wieschaus, E.F., and Kaschube, M. (2012). Volume conservation principle involved in cell lengthening and nucleus movement during tissue morphogenesis. PNAS *109*, 19298-19303.

Groth, A.C., Fish, M., Nusse, R., and Calos, M.P. (2004). Construction of transgenic Drosophila by using the site-specific integrase from phage phiC31. Genetics *166*, 1775-1782.

Hacker, U., and Perrimon, N. (1998). DRhoGEF2 encodes a member of the Dbl family of oncogenes and controls cell shape changes during gastrulation in Drosophila. Genes Dev *12*, 274-284.

Hartshorne, D.J., Ito, M., and Erdodi, F. (1998). Myosin light chain phosphatase: subunit composition, interactions and regulation. J Muscle Res Cell Motil *19*, 325-341.

He, B., Doubrovinski, K., Polyakov, O., and Wieschaus, E. (2014). Apical constriction drives tissue-scale hydrodynamic flow to mediate cell elongation. Nature *508*, 392-396.

He, L., Wang, X., Tang, H.L., and Montell, D.J. (2010). Tissue elongation requires oscillating contractions of a basal actomyosin network. Nature cell biology *12*, 1133-1142.

Heisenberg, C.P., and Bellaiche, Y. (2013). Forces in tissue morphogenesis and patterning. Cell *153*, 948-962.

Hildebrand, J.D. (2005). Shroom regulates epithelial cell shape via the apical positioning of an actomyosin network. J Cell Sci *118*, 5191-5203.

Jordan, P., and Karess, R. (1997). Myosin light chain-activating phosphorylation sites are required for oogenesis in Drosophila. J Cell Biol *139*, 1805-1819.

Kamisoyama, H., Araki, Y., and Ikebe, M. (1994). Mutagenesis of the phosphorylation site (serine 19) of smooth muscle myosin regulatory light chain and its effects on the properties of myosin. Biochemistry *33*, 840-847.

Karess, R.E., Chang, X.J., Edwards, K.A., Kulkarni, S., Aguilera, I., and Kiehart, D.P. (1991). The regulatory light chain of nonmuscle myosin is encoded by spaghetti-squash, a gene required for cytokinesis in Drosophila. Cell *65*, 1177-1189.

Kawano, Y., Fukata, Y., Oshiro, N., Amano, M., Nakamura, T., Ito, M., Matsumura, F., Inagaki, M., and Kaibuchi, K. (1999). Phosphorylation of myosin-binding subunit (MBS) of myosin phosphatase by Rho-kinase in vivo. J Cell Biol *147*, 1023-1038.

Kim, H.Y., and Davidson, L.A. (2011). Punctuated actin contractions during convergent extension and their permissive regulation by the non-canonical Wnt-signaling pathway. J Cell Sci *124*, 635-646.

Kimura, K., Ito, M., Amano, M., Chihara, K., Fukata, Y., Nakafuku, M., Yamamori, B., Feng, J., Nakano, T., Okawa, K., *et al.* (1996). Regulation of myosin phosphatase by Rho and Rho-associated kinase (Rho-kinase). Science *273*, 245-248.

Lecuit, T., Lenne, P.F., and Munro, E. (2011). Force generation, transmission, and integration during cell and tissue morphogenesis. Annual review of cell and developmental biology *27*, 157-184.

Lee, A., and Treisman, J.E. (2004). Excessive Myosin activity in mbs mutants causes photoreceptor movement out of the Drosophila eye disc epithelium. Mol Biol Cell *15*, 3285-3295.

Lee, J.Y., and Harland, R.M. (2007). Actomyosin contractility and microtubules drive apical constriction in Xenopus bottle cells. Dev Biol *311*, 40-52.

Lee, J.Y., Marston, D.J., Walston, T., Hardin, J., Halberstadt, A., and Goldstein, B. (2006). Wnt/Frizzled signaling controls C. elegans gastrulation by activating actomyosin contractility. Curr Biol *16*, 1986-1997.

Leptin, M. (2005). Gastrulation movements: the logic and the nuts and bolts. Dev Cell *8*, 305-320.

Leptin, M., and Grunewald, B. (1990). Cell shape changes during gastrulation in Drosophila. Development *110*, 73-84.

Levayer, R., and Lecuit, T. (2013). Oscillation and Polarity of E-Cadherin Asymmetries Control Actomyosin Flow Patterns during Morphogenesis. Developmental cell *26*, 162-175.

Majumder, P., Aranjuez, G., Amick, J., and McDonald, J.A. (2012). Par-1 controls myosin-II activity through myosin phosphatase to regulate border cell migration. Curr Biol *22*, 363-372.

Martin, A.C., Gelbart, M., Fernandez-Gonzalez, R., Kaschube, M., and Wieschaus, E.F. (2010). Integration of contractile forces during tissue invagination. J Cell Biol *188*, 735-749.

Martin, A.C., and Goldstein, B. (2014). Apical constriction: themes and variations on a cellular mechanism driving morphogenesis. Dev *141*, 1987-1998.

Martin, A.C., Kaschube, M., and Wieschaus, E.F. (2009). Pulsed contractions of an actin-myosin network drive apical constriction. Nature *457*, 495-499.

Mason, F.M., and Martin, A.C. (2011). Tuning cell shape change with contractile ratchets. Current opinion in genetics & development *21*, 671-679.

Mason, F.M., Tworoger, M., and Martin, A.C. (2013). Apical domain polarization localizes actin-myosin activity to drive ratchet-like apical constriction. Nat Cell Biol *15*, 926-936.

Mayer, M., Depken, M., Bois, J.S., Julicher, F., and Grill, S.W. (2010). Anisotropies in cortical tension reveal the physical basis of polarizing cortical flows. Nature *467*, 617-621.

Mizuno, T., Tsutsui, K., and Nishida, Y. (2002). Drosophila myosin phosphatase and its role in dorsal closure. Development *129*, 1215-1223.

Munro, E., Nance, J., and Priess, J.R. (2004). Cortical flows powered by asymmetrical contraction transport PAR proteins to establish and maintain anterior-posterior polarity in the early C. elegans embryo. Dev Cell *7*, 413-424.

Murthy, K., and Wadsworth, P. (2005). Myosin-II-dependent localization and dynamics of F-actin during cytokinesis. Curr Biol *15*, 724-731.

Nance, J., Munro, E.M., and Priess, J.R. (2003). C. elegans PAR-3 and PAR-6 are required for apicobasal asymmetries associated with cell adhesion and gastrulation. Development *130*, 5339-5350.

Ni, J.Q., Zhou, R., Czech, B., Liu, L.P., Holderbaum, L., Yang-Zhou, D., Shim, H.S., Tao, R., Handler, D., Karpowicz, P., *et al.* (2011). A genome-scale shRNA resource for transgenic RNAi in Drosophila. Nature methods *8*, 405-407.

Nishimura, T., and Takeichi, M. (2008). Shroom3-mediated recruitment of Rho kinases to the apical cell junctions regulates epithelial and neuroepithelial planar remodeling. Dev *135*, 1493-1502.

Ong, S., Foote, C., and Tan, C. (2010). Mutations of DMYPT cause over constriction of contractile rings and ring canals during Drosophila germline cyst formation. Dev Biol *346*, 161-169.

Rauzi, M., Lenne, P.F., and Lecuit, T. (2010). Planar polarized actomyosin contractile flows control epithelial junction remodelling. Nature *468*, 1110-1114.

Roh-Johnson, M., Shemer, G., Higgins, C.D., McClellan, J.H., Werts, A.D., Tulu, U.S., Gao, L., Betzig, E., Kiehart, D.P., and Goldstein, B. (2012). Triggering a cell shape change by exploiting preexisting actomyosin contractions. Science *335*, 1232-1235.

Royou, A., Field, C., Sisson, J.C., Sullivan, W., and Karess, R. (2004). Reassessing the role and dynamics of nonmuscle myosin II during furrow formation in early Drosophila embryos. Mol Biol Cell *15*, 838-850.

Royou, A., Sullivan, W., and Karess, R. (2002). Cortical recruitment of nonmuscle myosin II in early syncytial Drosophila embryos: its role in nuclear axial expansion and its regulation by Cdc2 activity. J Cell Biol *158*, 127-137.

Salbreux, G., Charras, G., and Paluch, E. (2012). Actin cortex mechanics and cellular morphogenesis. Trends Cell Biol *22*, 536-545.

Sawyer, J.K., Choi, W., Jung, K.C., He, L., Harris, N.J., and Peifer, M. (2011). A contractile actomyosin network linked to adherens junctions by Canoe/afadin helps drive convergent extension. Molecular biology of the cell *22*, 2491-2508.

Sawyer, J.M., Harrell, J.R., Shemer, G., Sullivan-Brown, J., Roh-Johnson, M., and Goldstein, B. (2010). Apical constriction: A cell shape change that can drive morphogenesis. Dev Biol, 1-15.

Sellers, J.R. (1991). Regulation of cytoplasmic and smooth muscle myosin. Curr Opin Cell Biol *3*, 98-104.

Shindo, A., and Wallingford, J.B. (2014). PCP and septins compartmentalize cortical actomyosin to direct collective cell movement. Science *343*, 649-652.

Simoes, S.d.M., Blankenship, J.T., Weitz, O., Farrell, D.L., Tamada, M., Fernandez-Gonzalez, R., and Zallen, J.A. (2010). Rho-kinase directs Bazooka/Par-3 planar polarity during Drosophila axis elongation. Dev Cell *19*, 377-388.

Skoglund, P., Rolo, A., Chen, X., Gumbiner, B., and Keller, R. (2008). Convergence and extension at gastrulation require a myosin IIB-dependent cortical actin network. Development *135*, 2435-2444.

Solon, J., Kaya-Copur, A., Colombelli, J., and Brunner, D. (2009). Pulsed forces timed by a ratchet-like mechanism drive directed tissue movement during dorsal closure. Cell *137*, 1331-1342.

Spahn, P., Ott, A., and Reuter, R. (2012). The PDZ-GEF protein Dizzy regulates the establishment of adherens junctions required for ventral furrow formation in Drosophila. J Cell Sci *125*, 3801-3812.

Sun, Y., Yan, Y., Denef, N., and Schupbach, T. (2011). Regulation of somatic myosin activity by protein phosphatase 1beta controls Drosophila oocyte polarization. Development *138*, 1991-2001.

Sweeton, D., Parks, S., Costa, M., and Wieschaus, E. (1991). Gastrulation in Drosophila: the formation of the ventral furrow and posterior midgut invaginations. Development *112*, 775-789.

Tan, C., Stronach, B., and Perrimon, N. (2003). Roles of myosin phosphatase during Drosophila development. Development *130*, 671-681.

Wheatley, S., Kulkarni, S., and Karess, R. (1995). Drosophila nonmuscle myosin II is required for rapid cytoplasmic transport during oogenesis and for axial nuclear migration in early embryos. Development *121*, 1937-1946.

Wilson, C.A., Tsuchida, M.A., Allen, G.M., Barnhart, E.L., Applegate, K.T., Yam, P.T., Ji, L., Keren, K., Danuser, G., and Theriot, J.A. (2010). Myosin II contributes to cell-scale actin network treadmilling through network disassembly. Nature *465*, 373-377.

Winter, C.G., Wang, B., Ballew, A., Royou, A., Karess, R., Axelrod, J.D., and Luo, L. (2001). Drosophila Rho-associated kinase (Drok) links Frizzled-mediated planar cell polarity signaling to the actin cytoskeleton. Cell *105*, 81-91.

Young, P.E., Pesacreta, T.C., and Kiehart, D.P. (1991). Dynamic changes in the distribution of cytoplasmic myosin during Drosophila embryogenesis. Development *111*, 1-14.

Supplementary Information

Table S1: Fly Stocks

Genotype	Source
OreR	2
sqh^{AX3};P{w^+ sqh::GFP}42	2
ovo^D FRT^{19A}; hsFLP UAS-Venus::Rok/CyO	4,5
rok^2 FRT^{19A}; mat15 sqh::$mCherry^{A11}$	1
y w; P{w^+ sqh-TS::GFP}attP1	1
y w; P{w^+ sqh-AA::GFP}attP1	1
y w; P{w^+ sqh-TA::GFP}attP1	1
y w; P{w^+ sqh-AS::GFP}attP1	1
y w; P{w^+ sqh-TE::GFP}attP1	1
y w; P{w^+ sqh-AE::GFP}attP1	1
y w; P{w^+ sqh-EE::GFP}attP1	1
y w; P{w^+ sqh-TS::GFP}attP40	1
y w; P{w^+ sqh-EE::GFP}attP40	1
ovo^{D1} FRT^{101}/Y; hsFLP-38/hsFLP-38	2
sqh^1 FRT^{101}/FM7; P{w^+ sqh-TS::GFP}attP1/CyO	1
sqh^1 FRT^{101}/FM7; P{w^+ sqh-AA::GFP}attP1/CyO	1
sqh^1 FRT^{101}/FM7; P{w^+ sqh-TA::GFP}attP1/CyO	1
sqh^1 FRT^{101}/FM7; P{w^+ sqh-AS::GFP}attP1/CyO	1
sqh^1 FRT^{101}/FM7; P{w^+ sqh-TE::GFP}attP1/CyO	1
sqh^1 FRT^{101}/FM7; P{w^+ sqh-AE::GFP}attP1/CyO	1
sqh^1 FRT^{101}/FM7; P{w^+ sqh-EE::GFP}attP1/CyO	1
sqh^1 FRT^{101}/FM7; P{w^+ sqh-TS::GFP}attP40/CyO	1
sqh^1 FRT^{101}/FM7; P{w^+ sqh-TS::GFP}attP1 P{w^+ Gap43::mCherry}attP40/CyO	1
sqh^1 FRT^{101}/FM7; P{w^+ sqh-TA::GFP}attP1 P{w^+ Gap43::mCherry}attP40/CyO	1
sqh^1 FRT^{101}/FM7; P{w^+ sqh-AE::GFP}attP1 P{w^+ Gap43::mCherry}attP40/CyO	1
Utr::mCherry	3
sqh^1 FRT^{101}/FM7; P{w^+ sqh-TS::GFP}attP1 Utr::mCherry/CyO	1
sqh^1 FRT^{101}/FM7; P{w^+ sqh-TA::GFP}attP1 Utr::mCherry/CyO	1
sqh^1 FRT^{101}/FM7; P{w^+ sqh-AE::GFP}attP1 Utr::mCherry/CyO	1

rok^{2} FRT^{19A}/FM7; P{w^{+} sqh-TS::GFP}attP1	1
rok^{2} FRT^{19A}/FM7; P{w^{+} sqh-EE::GFP}attP40	1
P{Ubi-GFP::Rok}	6
y[1] sc[*] v[1]; P{y[+t7.7] v[+t1.8]=TRiP.GL00094}attP2 (*ctl-shRNA*)	7
y[1] v[1]; P{y[+t7.7] v[+t1.8]=TRiP.GL01207}attP40 (*MBS-shRNA*)	7
y[1]w[1118]; P{w^{+} sqh::GFP}42, mat67; P{Gap43:mCherry}, mat15/TM3	1
y[1]w[1118]; P{w^{+} sqh::GFP}42; P{Gap43:mCherry}, mat15/TM3	1

sqh-XX = *sqh* promoter and ORF with site-directed mutagenesis at T20 and S21 as noted below.
Gap43 = *sqh* promoter with N-terminal 20 amino acids of rat Gap43 gene which contains a myristoylation sequence.
Utr = *sqh* promoter with Utrophin actin-binding domain

name	**mutation**
TS	*T20,S21*
TA	*T20,S21A*
AS	*T20A,S21*
TE	*T20,S21E*
AE	*T20A,S21E*
EE	*T20E,S21E*

Sources

1. This study
2. Bloomington Drosophila Stock Center
3. (Rauzi et al., 2010) Gift from T. Lecuit (IBDM, Marseille, France).
4. (Mason et al., 2013)
5. Gifts from J. Zallen, S. Simões (Sloan Kettering Institute, New York, NY), and R. Fernandez-Gonzalez (Univ. of Toronto, Toronto, ON).
6. (Bardet et al., 2013) Gift from Y. Bellaiche (Institut Curie, Paris, France).
7. Gifts from Norbert Perrimon, Liz Perkins, and the TRiP (Harvard Medical School, Boston, MA

Table S2: Antibodies used and concentrations

Antibody	Use	Concentration	Source
R anti-Zipper	HF & PFA	1:500	Wieschaus Lab (Princeton Univ., Princeton, NJ)
R anti-MBS	PFA	1:500	Tan Lab (Univ. of Missouri, Columbia, MO)
R anti-ECad2	PFA	1:50	DSHB
M anti-Neurotactin	HF	1:100	DSHB
R anti-Sqh	WB	1:5000	This study
M anti-GFP	WB	1:1000	Roche
M anti-tubulin	WB	1:5000	Sigma

R = rabbit, M = mouse

HF = heat-fixation, PFA = paraformaldehyde fixation, WB = western blot

DSHB = Developmental Studies Hybridoma Bank

Chapter 3: *Drosophila* Myosin ATPase activity limits the rate of tissue folding

Authors: Claudia G. Vasquez[1], Sarah Heissler[2], James R. Sellers[2], Adam C. Martin[1]
[1]Department of Biology, Massachusetts Institute of Technology, Cambridge, Massachusetts
[2]Laboratory of Molecular Cardiology, NHLBI, National Institutes of Health, Bethesda, Maryland
SH carried out myosin ATPase assays. CV performed in vivo experiments and wrote manuscript.

Abstract

The actomyosin cytoskeleton is responsible for cell and tissue shape change. Epithelial sheets of cells with defined apical and basal sides can fold to form tubes in an organism. During early *Drosophila* development and neural tube formation, apical constriction of cells promotes folding of an epithelial sheet into a tube. Although, non-muscle myosin II (myosin) functions as a molecular motor, recent studies have questioned the importance of motor function and the importance of any myosin function in epithelial sheet folding. Here, we quantitatively characterize the activity of several mutants affecting the myosin regulatory light chain phosphorylation sites both biochemically and *in vivo*. Phosphomimetic mutants of the *Drosophila* myosin regulatory light chain are defective in motor activity. Cells expressing the phosphomimetic myosin mutant constrict more slowly than wildtype cells. Additionally, epithelial tension is decreased in the myosin phosphomutant tissue compared to wildtype tissue, consistent with myosin motor activity being required to generate epithelial tension. Overall, myosin ATPase activity and constriction rate are correlated for several mutants, suggesting that myosin ATPase activity increases the rate of cell contraction and tissue folding in developing embryos.

Introduction

During the development of an organism, tissues are sculpted into different three-dimensional forms. Cell shape changes and cell movement drive these tissue-scale rearrangements. While the molecular motor non-muscle myosin II (myosin) is thought to drive many of these cell shape changes, it is debated whether the motor function of myosin is actually required for epithelial folding (Escuin et al., 2015). Myosin is a molecular motor that can couple the hydrolysis of ATP with binding and translocation of actin filaments. A myosin hexamer is composed of two myosin heavy chains, two regulatory light chains (RLCs), and two essential light chains. The N-terminal domain of the myosin heavy chain is the motor domain that binds actin and hydrolyzes ATP. The C-terminal tail of the myosin heavy chain associates with the tails of other myosin heavy chains and promotes assembly of the myosin hexamer into bipolar mini-filaments. In mammals, phosphorylation of the RLC at conserved serine and threonine sites activates myosin ATPase activity and promotes mini-filament formation. Myosin light chain kinase (MLCK), Rho-associated protein kinase (ROCK), and Citron kinase are all known activators of myosin activity via direct phosphorylation of the RLC (Amano et al., 1996; Kamm and Stull, 1985; Yamashiro et al., 2003). Actin filament polarity and myosin assembly into bipolar mini-filaments can result in plus-end directed-movement of myosin filaments along anti-parallel actin filaments to generate filament sliding (Huxley, 1963).

The canonical model of myosin-driven cellular contraction uses myosin as a motor protein. In this model, contraction is driven by myosin motor activity-dependent translocation of actin filaments. Activation of myosin results in its translocation along actin filament plus-ends to contract actin network by filament sliding. Recent studies have questioned the importance of myosin motor function in cellular force-generation processes. An alternative model for myosin-driven cellular contraction does not necessitate myosin motor activity, but instead, relies on the load-dependent actin-binding property of myosin (Kovacs et al., 2007). Application of load to

myosin alters the kinetics of the ATPase cycle, favoring a state where myosin is bound to actin, compared to when there is no load (Kovacs et al., 2007). In migrating cells, polarity defects caused by depletion of myosin isoforms (myosin IIA and myosin IIB) are partially rescued by expression of a myosin motor mutant that can bind but not translocate actin filaments, suggesting that cell polarity does not require myosin motor activity, but its ability to cross-link filaments (Kim, 2005; Vicente-Manzanares et al., 2007). Consistent with this motor-independent function of myosin, defects in vertebrate cytokinesis following depletion of myosin IIB (the major myosin isoform in the studied cells) were rescued by expression of the same myosin motor mutant that can bind but not translocate actin filaments (Hu et al., 2002; Kim, 2005; Ma et al., 2012). These results provide evidence for a mode of contraction that does not require myosin motor activity, but requires myosin to function as a tension-dependent cross-linker. Recently, it has been suggested that myosin motor is not required for contraction of epithelial cells that results in the folding of epithelial tissues, such as the neural tube. In this case, it has been proposed that actin depolymerization plays the predominant role (Escuin et al., 2015).

Defining the importance of myosin motor activity requires mutants with precisely characterized motor defects and quantitative analysis of cell and tissue shape changes. We study a tissue invagination process in the early *Drosophila* embryo, which is amenable to genetic modification and quantitative live imaging. The *Drosophila* embryo is initially an ellipsoid composed of a single epithelial sheet surrounding a yolk. To initiate the formation of multiple embryonic germ layers, a subset of cells on the ventral-most side of the embryo change from columnar-shaped cells to wedge-shaped cells through a process known as apical constriction (the apical surface faces outwards). Apical constriction of ventral cells promotes invagination and folding of the sheet into a tube inside the embryo. Ventral cells constrict in a step-wise manner; these contractions are driven by cycles of assembly and disassembly of an apical myosin network, or pulses of myosin (Martin et al., 2009). ROCK, the upstream regulator of myosin, localizes and pulses with myosin, and its activity is required for apical myosin

accumulation and cellular constriction (Mason et al., 2013; Vasquez et al., 2014). Previously, we made a series of RLC that substituted the threonine-20 and serine-21 phosphorylation sites with alanine, as an unphosphorylatable residue or glutamate, as a phosphomimetic. RLC mutants that uncouple myosin from its upstream regulators abolished pulsatile behavior of myosin. Furthermore, depletion of the myosin binding subunit of the myosin phosphatase also suppressed myosin pulsing. Thus, pulsatile behavior of myosin relies on cycles of phosphorylation and dephosphorylation of the myosin RLC (Vasquez et al., 2014). While the importance of upstream regulation of myosin for myosin dynamics has been shown, whether myosin motor activity or other properties of myosin are driving apical constriction has not been studied.

Here we find that myosin RLC phosphomutants have measureable motor activity defects, providing us with an allelic series of motors with varying defects in motor activity. Decreased motor activity is associated with slower cellular contractions and an apparent decrease in tension generation in the ventral tissue. These results suggest that myosin motor activity is important for efficient apical constriction. Furthermore, caution should be used when interpreting results using phosphomimetic alleles of the myosin RLC, because these mutants do not fully mimic the phosphorylated state of the myosin motor.

Results

Myosin RLC phosphomutants have reduced actin-activated ATPase activity

We and others have used myosin RLC phosphomutants to show that myosin localization and dynamics depend on cycles of myosin phosphorylation and dephosphorylation (Kasza et al., 2014; Vasquez et al., 2014). Previously, others have suggested that phosphomimetic alleles of the RLC (*RLC-EE*) could suppress mutation or inhibition of the *Drosophila* ROCK (Bertet et al., 2004; Winter et al., 2001). We found that while expression of *RLC-EE* rescued cortical localization myosin in *rock* mutants, *RLC-EE* did not contract the actomyosin network or constrict cells. The failure to contract is likely to result, in part, from lack of proper spatiotemporal regulation of myosin (Kasza et al., 2014; Vasquez et al., 2014); however, another contributing factor could be that the phosphomimetic RLC does not activate the myosin motor to wildtype levels/full extent.

To characterize the biochemical properties of myosin phosphomutants, we purified the full-length wildtype and phosphomutant *Drosophila* myosin complexes, and performed *in vitro* analyses of myosin motor activity. For all RLC phosphomutants the basal ATPase activity (k_{basal}), ATPase activity in the absence of actin, was ~0.10 s^{-1}, which is comparable to basal ATPase rates of human non-muscle myosin II isoforms (Sarah Heissler and James Sellers personal communication)(Billington et al., 2013). Like many other myosin RLCs, rabbit MLCK can phosphorylate *Drosophila* RLC threonine and serine phosphorylation sites (S.H. and J.S. personal communication). Consistent with findings in human non-muscle myosin IIs, phosphorylation of wildtype RLC (RLC-TS) by MLCK increased actin-activated myosin ATPase activity by almost 7-fold, from 0.10 s^{-1} to 0.82 s^{-1} (S.H. and J.S. personal communication) (Billington et al., 2013). Addition of MLCK to myosin in complex with RLC-TA, which still contains the secondary phosphorylation site, threonine-20, increased the ATPase activity 3-fold, demonstrating that this mutant is still regulated by phosphorylation (S.H. and J.S. personal

communication). As expected, for RLC mutants that could not be phosphorylated at either site, addition of MLCK did not significantly alter the actin-activated ATPase activity of the myosin motor (fold activation: RLC-AA—1.4, RLC-AE—1.1, RLC-EE—1.1)(S.H. and J.S. personal communication). Surprisingly, the phosphomimetic mutants RLC-AE and RLC-EE display a similar steady-state ATPase activity as the unphosphorylatable RLC-AA mutant, which was only 27-28% of the activity of myosin with phosphorylated RLC (RLC-TS) (S.H. and J.S. personal communication). These results demonstrate that myosin in complex with RLC-AE or RLC-EE have myosin ATPase activity that is uncoupled from upstream regulators; however, due to their low ATPase activities, these motors do not recapitulate the activity of phosphorylated wildtype myosin. Thus, RLC-AE and RLC-EE, do not behave like true RLC phosphomimetics and cannot be classified as constitutively active myosin mutants; however, these mutants could be useful to determine the importance of myosin ATPase activity during tissue morphogenesis.

Myosin RLC phosphomutants have slower cellular contractions than wildtype myosin

Biochemical characterization of myosin with the different RLC phosphomutants revealed that myosin phosphomutants had defects in motor activity. These results allowed us to determine the contribution of myosin ATPase activity to apical constriction and tissue tension. Previously this experiment has been technically challenging due to the insensitivity of *Drosophila* myosin to blebbistatin, a widely used myosin activity inhibitor (Heissler et al., 2015; Straight, 2003). While blebbistatin is an effective inhibitor of myosin ATPase activity, it also locks the motor domain in a state with low actin affinity *in vitro*. Consequently, when using blebbistatin the effects of ATPase inhibition cannot be uncoupled from the loss of actin-binding and thus the cross-linking behavior of myosin (Kovacs et al., 2004).

Previously, we reported that cells expressing *RLC-AE* constricted more slowly on average and delayed tissue invagination than the wildtype (*RLC-TS*) control (Figure 1A) (Vasquez et al., 2014). In light of our biochemical measurements, the decrease in constriction rate could be due to differences in motor activity between the *RLC-AE* myosin and wildtype myosin (*RLC-TS*). The amount of apical myosin accumulation in a cell correlates with the strength of the consequent contraction; thus, myosin can be used as proxy for force generation (Xie and Martin, 2015). Additionally, tissues expressing RLC phosphomutants exhibit normal apical-basal localization of myosin (Vasquez et al., 2014). Thus, if phosphomutant myosin can generate as much contractile force as wildtype myosin, then at instances of comparable myosin accumulation rates, the constriction rate would be comparable. We identified instances of rapid myosin accumulation, where the rate of myosin accumulation was between one and two standard deviations above the mean rate of constriction of all control cells (*RLC-TS*). At these instances we calculated the constriction rate. However, even with enrichment for constriction rates caused by high myosin accumulation rates, cells expressing *RLC-AE* or *RLC-TA* constricted significantly slower than wildtype cells (*RLC-TS*) (Figure 1B). Furthermore, on

average, cells expressing *RLC-AE* constricted slower than those expressing *RLC-TA* (Figure 1B). These results suggest that there is a direct relationship between myosin motor activity and constriction rate (Figure 1C).

Figure 1

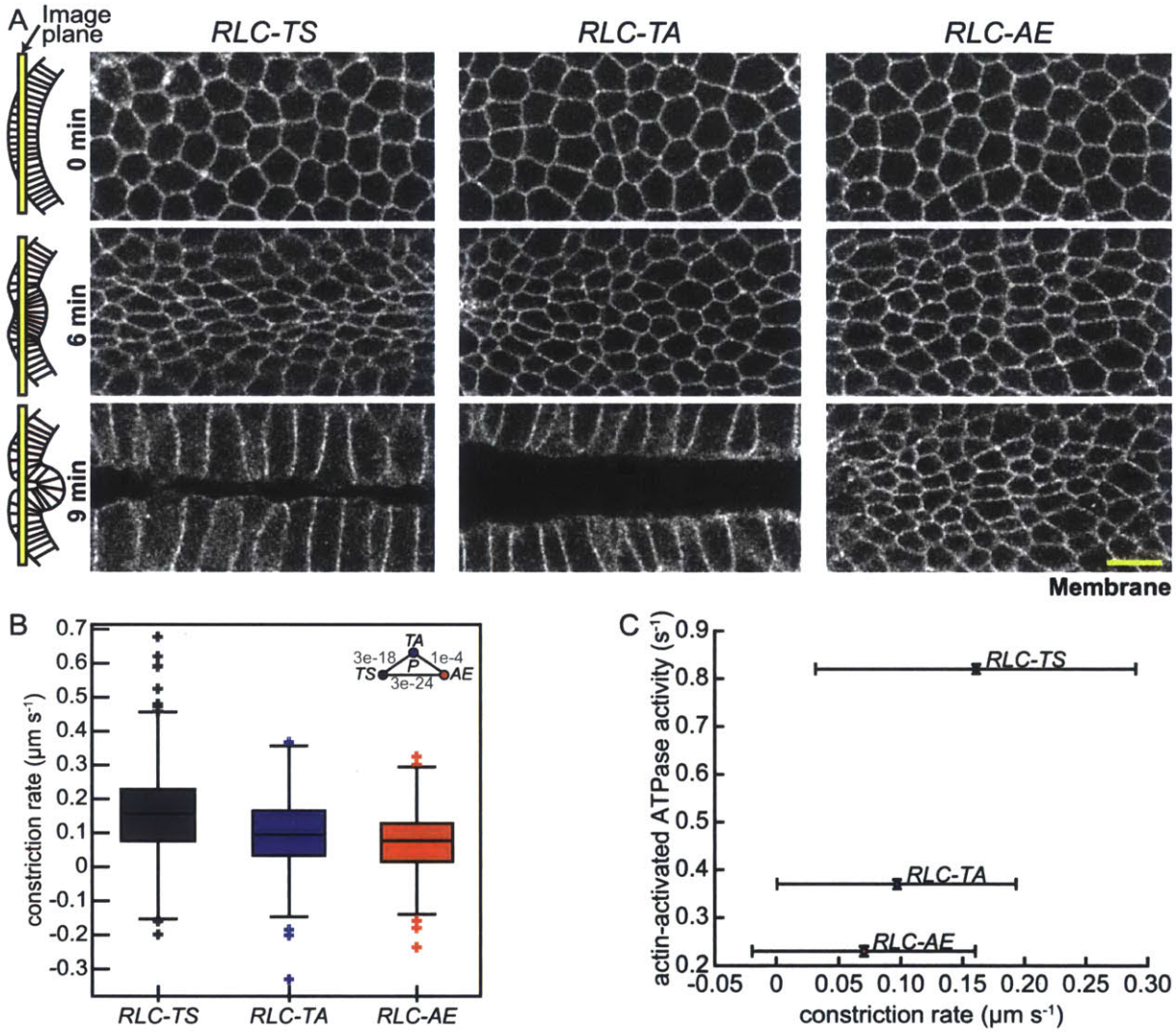

Figure 1 Cellular constrictions in myosin RLC phosphomutants are weaker than in wildtype cells **(A)**Tissue invagination and apical constriction is delayed in *RLC-AE* mutant. Time-lapse images are representative tissues from embryos expressing the indicated RLC phosphomutant and Membrane::Cherry (membrane). Schematics illustrate plane images were acquired in. **(B)** *RLC-TA* and *RLC-AE* generate weaker constrictions than wildtype (*RLC-TS*) myosin. Central line in box plot is the median, the box edges are the 25th and 75th percentiles, and the whiskers represent the distribution minima and maxima, not considered outliers; outliers are plotted individually (n = 426 constriction instances identified from 138 cells from 2 embryos for *RLC-TS*; n = 757 constriction instances identified from 268 cells from 3 embryos for *RLC-TA*; n = 310 constriction instances identified from 157 cells from 3 embryos for *RLC-AE*). **(C)** Constriction rate corresponds with actin-activated ATPase activity. Bars correspond to the standard deviation of the measurements. Scale bars = 10 µm.

Myosin ATPase activity contributes to tissue tension

Tissue-cutting techniques have been used to infer the mechanical properties of many living tissues (Fabry et al., 2001; Fernandez-Gonzalez et al., 2009; Fischer et al., 2014; Ma et al., 2009; Mayer et al., 2010). In response to a cut, tissue edges will initially recoil quickly away from the cut, and then move more slowly away from the cut site, before the wound begins to heal and close. The initial displacement of the tissue, the initial recoil velocity, is proportional to the tension in the tissue just prior to the cut.

We made cuts 8.5 μm in length oriented perpendicular to the length of the furrow at equivalently staged embryos and tracked the displacement of the wound edge relative to the cut (Figure 2A and 2B). Qualitatively, it appeared that the wound responses for tissue expressing either *RLC-TA* or *RLC-AE* were less pronounced (Figure 2A). This difference could be due to differences in tissue tension or differences in tissue viscosity; for the same tension, increased viscosity of the tissue would dampen the initial recoil velocity, while decreased viscosity would increase the initial recoil velocity. To determine if the material properties of the tissues expressing differing myosin phosphomutants were similar, we fit the initial displacement of the wound response to a power law function. The exponent (alpha) of the power law gives information on the energy of the system. If alpha is zero then the tissue is behaving like a purely elastic solid (lower energy), if alpha is 1 then the tissues is behaving like a purely viscous fluid (higher energy) (Fabry et al., 2001). For the wildtype tissue (*RLC-TS*) the mean power law exponent was 0.3, which is on par with alpha-values calculated other *Drosophila* embryonic tissues (Fischer et al., 2014; Ma et al., 2009). We also found that the mean alpha-values for *RLC-TA* and *RLC-AE* were 0.3 and 0.4, respectively. Pair-wise comparisons of all distributions from the three RLC phosphomutants found that they were not significantly different (Figure 2C). These results suggest that tissues expressing different RLC phosphomutants have similar viscoelastic properties.

Since the general viscoelasticity is consistent among tissues, we compared the initial recoil velocities from different tissues, and could infer the relative tension in the tissues prior to the cut. Importantly, using tissue-cutting experiments we cannot calculate the absolute values of tensile force in the different tissues, we can only make relative comparisons using the initial recoil velocities. To calculate the initial recoil velocity of the cut we fit the displacement curve to a Kelvin-Voigt model, which defines the tissue as a spring (the elastic component) and a dashpot (the viscous component) in parallel. The initial recoil velocity of a Kelvin-Voigt tissue is equivalent to the tensile force in the tissue prior to the cut over the viscous coefficient of the dashpot. Because the viscoelastic properties of the phosphomutant tissues are comparable, we assumed that the tissues had the same viscous coefficient and compared the initial recoil velocities to infer the relative tensions in the different tissues. Tissues expressing either *RLC-TA* or *RLC-AE* display lower initial recoil velocities than wildtype tissues (*RLC-TS*), suggesting that tissues expressing phosphomutant myosin do not hold as much tension as wildtype tissues and that myosin motor activity may play a role in force-generation. Just like with the contractile properties of myosin RLC, a decrease in myosin motor activity corresponded with a decrease in the initial recoil velocity of the wound, and possibly the pre-existing tension in the tissue (Figure 2E).

Figure 2

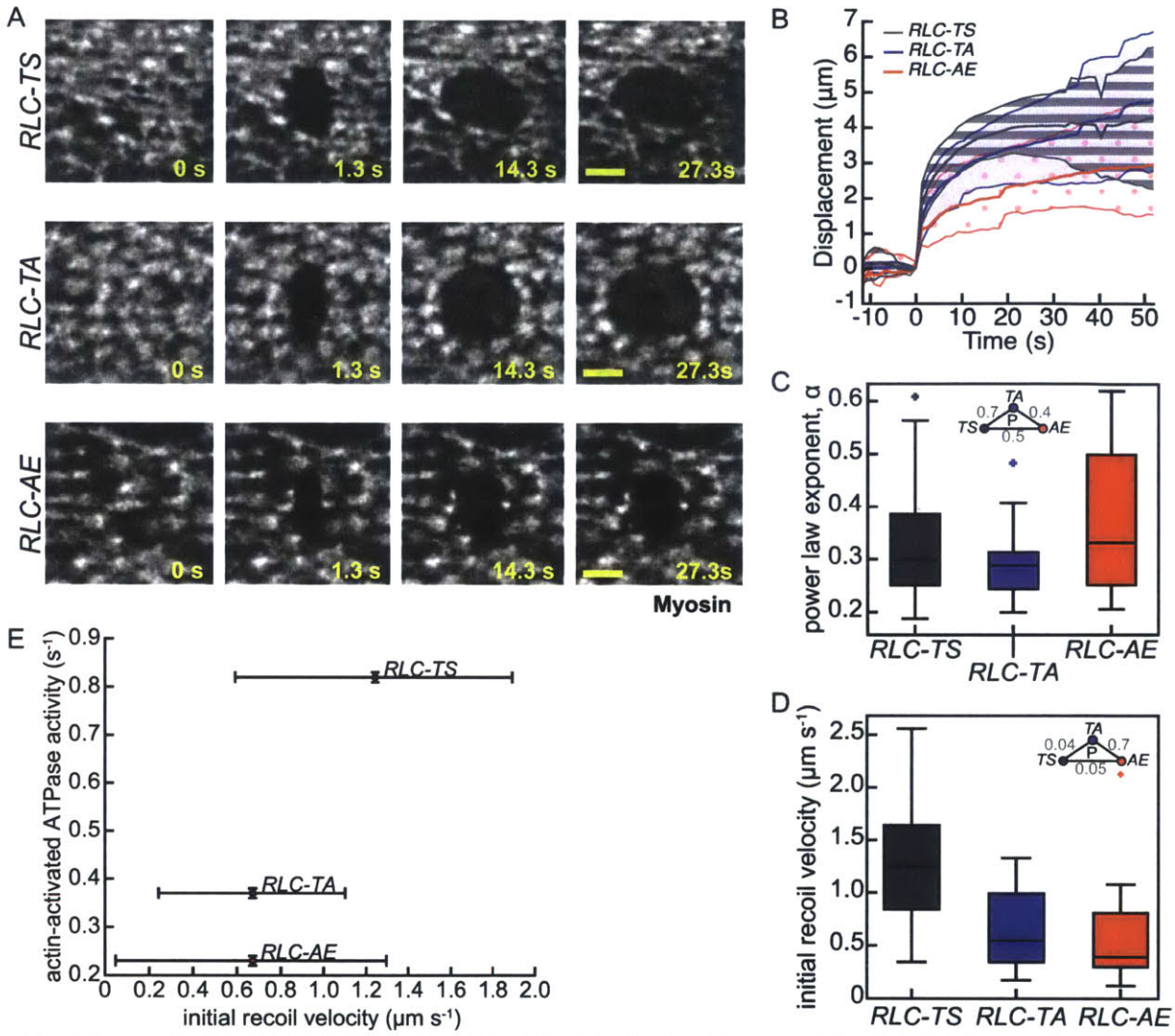

Figure 2 RLC phosphomutants build less tissue tension than wildtype myosin. **(A)** Initial wound recoil appears less severe in tissues expressing phosphomutant myosin than in the wildtype tissue. Time-lapse images of embryos expressing indicated RLC phosphomutant. Between time 0 s and 1.3 s an 8.5 μm incision in the tissue was made. **(B)** Mean displacement of wound edge following tissue ablation (n = 15 *RLC-TS* embryos, n = 11 *RLC-TA* embryos, n = 10 *RLC-AE* embryos). Shaded area is +/- standard deviation. **(C)** Viscoelastic properties of tissues expressing different RLC phosphomutants are comparable. Displacement curves were fit with a power law function. (n = 15 *RLC-TS* embryos, n = 10 *RLC-TA* embryos, n = 8 *RLC-AE* embryos). **(D)** Initial recoil velocity is highest in wildtype tissue (*RLC-TS*). The initial recoil velocity was calculated by fitting the displacement to a Kelvin-Voigt model and taking the derivative of the fit at time zero. (n = 14 *RLC-TS* embryos, n = 10 *RLC-TA* embryos, n = 9 *RLC-AE* embryos). **(E)** Initial recoil velocity scales with actin-activated ATPase activity. Bars correspond to the standard deviation of the measurements. Scale bars = 5 μm. For all box plots, the central line is the median, the box edges are the 25th and 75th percentiles, and the whiskers represent the distribution minima and maxima, not considered outliers; outliers are plotted individually.

Discussion

The role of myosin during tissue morphogenesis has not been clearly defined. We provide evidence that high myosin ATPase activity is required for strong cellular contractions and to generate high epithelial tension during ventral furrow formation. We combine *in vitro* biochemical analysis of myosin phosphomutants with *in vivo* characterization of force-generation by these myosin phosphomutants at the cellular- and tissue-scales.

Measurement of full-length myosin ATPase activity with wildtype and phosphomutant myosin RLCs demonstrated that all mutants that were thought to be uncoupled from upstream regulation had motor activity that was independent of the presence of MLCK. In agreement with measurements made in smooth muscle myosin, substitution of phosphorylation sites with negatively charged residues (*RLC-AE* and *RLC-EE*), yielded MLCK-independent activation of myosin ATPase activity (Kamisoyama et al., 1994). However, the magnitude of activation of these so-called phosphomimetic mutants was much lower than that of activated wildtype myosin (17% in (Kamisoyama et al., 1994), and 27% in this study). These results demonstrate that the negative charges from these acidic residues are not sufficient to mimic the negative charges of the phosphate moieties. Thus, it might be interesting to see if the addition of more acidic residues in this region of the RLC would result in constitutive motor activity with activation comparable to wildtype motor activity.

Comparison of contraction rate of instances with equivalent amounts of myosin signal demonstrated that there is a correlation between motor activity and the extent of contraction myosin can generate. The effect myosin phosphomutants have on cellular contraction is less severe than the effect on myosin motor activity; tissues expressing *RLC-TS* or *RLC-AE* could generate contractions at 56% and 44% of the wildtype (*RLC-TS*) tissue. Additionally, relative to wildtype (*RLC-TS*) tissues, tissues expressing *RLC-TS* or *RLC-AE* build less tissue tension.

This difference suggests that while myosin ATPase activity is rate-limiting, other motor activity-independent properties of myosin, like cross-linking, could be contributing to force-generation.

This work demonstrates that interpretation of experiments using myosin RLC phosphomutants should be aware of the low motor activity of these mutants, which do not recapitulate the activity of myosin with phosphorylated RLCs. Additionally, this study demonstrates that RLC phosphomutants can be used as a tool to modulate myosin motor activity. Previously, in *Drosophila*, studying the role of myosin motor activity has been technically difficult due to the insensitivity of *Drosophila* myosin to the pharmacological inhibitor of myosin, blebbistatin (Heissler et al., 2015; Straight, 2003). In the future it will be important to determine if other properties of myosin, like actin cross-linking and actin disassembly, are required for tissue morphogenesis.

Materials and Methods

Fly stocks and genetics

Fly stocks used in this study are listed in Table S1. *spaghetti squash* (*sqh*) is the *Drosophila* gene name for the myosin RLC. Briefly, we used *sqh-XX::GFP* alone and *sqh-XX::GFP* recombined with *Gap43::mCherry* (a plasma membrane) phosphomutant stocks crossed into the sqh^1 hypomorph background, generated in (Vasquez et al., 2014). Germline clones were generated using the FLP-DFS technique by heat shocking mutant/ovo^D larvae for 2 h at 37°C for 3–4 d (Chou and Perrimon, 1992). *sqh::GFP* rescue of sqh^1 germline clones, sqh^1 FRT/FM7; *sqh-XX::GFP*/CyO females were crossed to ovo^D FRT/Y; *hsFlp* males, the resulting larvae were heat shocked, and sqh^1 FRT/ovo^D FRT; *sqh-XX::GFP/hsFlp* females were crossed to OreR to collect embryos that resulted from germline clones.

Time-lapse imaging

Embryos were dechorionated in 50% bleach, mounted ventral side upon a slide coated with "embryo glue" (double-sided tape soaked in heptane). No. 1.5 coverslips were used as spacers and a No. 1 coverslip was used as a cover to create a chamber for the embryo. The chamber was filled with Halocarbon 27 oil. All imaging occurred at room temperature on a Zeiss LSM 710 confocal microscope with a 40x/1.2 Apochromat water objective. Argon ion and 561 nm diode lasers were used for excitation. The band-pass selected for GFP was ~488-558 nm and for mCherry was ~573-696 nm. All images were acquired using Zen (Zeiss) software.

Tissue-cutting

Ablations were performed using a Chameleon Ultra II femtosecond pulsed-IR laser (set at 800nm and 24% intensity) attached to a Zeiss LSM710 with a 40X water immersion objective.

To perform ablations, the laser was targeted to a region of interest (8.5 μm line). Image stacks were collected every 1.3 seconds.

Image analysis

Images were processed using Fiji and MATLAB (Mathworks).

Constriction rate analysis

We used custom MATLAB software, EDGE (Embryo Development Geometry Explorer) (Gelbart et al., 2012) to segment images for quantification of apical area and myosin intensities. Segmented cell membranes were ~1 μm below the myosin signal. Embryos were aligned in time using the mean apical area signals of each embryo and choosing the time when the tissue begins to constrict. The myosin signal was pre-processed to remove cytoplasmic myosin by only using the maximum intensity z-projection for the two highest myosin intensity values that were greater than 2.5 standard deviations above the mean cytoplasmic myosin intensity. A Gaussian filter (σ=0.5) was applied to this signal. To identify instances of rapid cellular constriction (Figure 2C), we first smoothed signals for apical area and mean myosin intensity and calculated instantaneous rates for each time point. Instances of rapid myosin intensity increases were identified as instances where the myosin accumulation rate was between one and two standard deviations above the mean rate for all control cells (*RLC-TS*). The constriction rate was calculated at these instances.

Tissue-cutting analysis

In Fiji, for each ablation experiment, a maximum projection was made from both z-slices. Kymographs were taken along the center 4.25 μm of the laser incision. The image was converted to binary mode and a maximum projection was made from these kymographs. Images were imported into MATLAB, the built-in function bwmorph was used to remove outlier points. The distance between the wound edges was calculated for each time point. The

displacement was this distance divided by two. The initial recoil velocity was calculated by fitting the displacement to a Kelvin-Voigt model of tissue displacement using the MATLAB built-in function lsqcurvefit (Equation 1).

$$x(t) = \frac{T}{\zeta}(1 - e^{-\frac{\zeta t}{\eta}}) \quad \textbf{(1)}$$

Where t indicates time, $x(t)$ is the displacement of the wound edge, T is the tensile force in the tissue prior to the cut, ζ is the stiffness of the spring, and η is the viscous coefficient of the dashpot. Only fits with R-squared values greater than 50% were used in the subsequent calculations of initial recoil velocity. The initial recoil velocity (v_0) is described by the derivative of the displacement at time zero, which is the tension over the viscous coefficient of the dashpot (Equation 2).

$$v_0 = \frac{dx(0)}{dt} = \frac{T}{\eta} \quad \textbf{(2)}$$

Statistics

All statistics were performed in MATLAB. *P*-values were calculated using the built-in ranksum function, which performs the Mann-Whitney U test.

Acknowledgements

We thank Sarah Heissler and James Sellers (NIH, Bethesda, Maryland, USA) for sharing results of *Drosophila* phosphomutant myosin ATPase assays. We also thank the W.M. Keck Microscopy Facility and Wendy Salmon for assistance with use of the 2-photon laser and confocal microscope used in tissue-cutting experiments.

Supplementary Information

Table S1: Fly Stocks

Genotype	Source
OrR	2
ovo^{D1} FRT^{101}/Y; hsFLP-38/hsFLP-38	2
sqh^{1} FRT^{101}/FM7; P{w^{+} sqh-TS::GFP}attP1/CyO	1
sqh^{1} FRT^{101}/FM7; P{w^{+} sqh-TA::GFP}attP1/CyO	1
sqh^{1} FRT^{101}/FM7; P{w^{+} sqh-AE::GFP}attP1/CyO	1
sqh^{1} FRT^{101}/FM7; P{w^{+} sqh-TS::GFP}attP1 P{w^{+} Gap43::mCherry}attP40/CyO	1
sqh^{1} FRT^{101}/FM7; P{w^{+} sqh-TA::GFP}attP1 P{w^{+} Gap43::mCherry}attP40/CyO	1
sqh^{1} FRT^{101}/FM7; P{w^{+} sqh-AE::GFP}attP1 P{w^{+} Gap43::mCherry}attP40/CyO	1

sqh-XX = *sqh* promoter and ORF with site-directed mutagenesis at T20 and S21 as noted below (*spaghetti squash*, *sqh* is the *Drosophila* RLC gene name).

Gap43 = *sqh* promoter with N-terminal 20 amino acids of rat Gap43 gene which contains a myristoylation sequence (membrane marker).

name	mutation
TS	*T20,S21*
TA	*T20,S21A*
AE	*T20A,S21E*

Sources

1. (Vasquez et al., 2014)
2. Bloomington Drosophila Stock Center

References

Amano, M., Ito, M., Kimura, K., Fukata, Y., Chihara, K., Nakano, T., Matsuura, Y., and Kaibuchi, K. (1996). Phosphorylation and activation of myosin by Rho-associated kinase (Rho-kinase). J Biol Chem *271*, 20246-20249.

Billington, N., Wang, A., Mao, J., Adelstein, R.S., and Sellers, J.R. (2013). Characterization of three full-length human nonmuscle myosin II paralogs. J Biol Chem *288*, 33398-33410.

Chou, T.B., and Perrimon, N. (1992). Use of a yeast site-specific recombinase to produce female germline chimeras in Drosophila. Genetics *131*, 643-653.

Escuin, S., Vernay, B., Savery, D., Gurniak, C.B., Witke, W., Greene, N.D., and Copp, A.J. (2015). Rho-kinase-dependent actin turnover and actomyosin disassembly are necessary for mouse spinal neural tube closure. J Cell Sci *128*, 2468-2481.

Fabry, B., Maksym, G.N., Butler, J.P., Glogauer, M., Navajas, D., and Fredberg, J.J. (2001). Scaling the microrheology of living cells. Phys Rev Lett *87*, 148102.

Fernandez-Gonzalez, R., Simoes Sde, M., Roper, J.C., Eaton, S., and Zallen, J.A. (2009). Myosin II dynamics are regulated by tension in intercalating cells. Dev Cell *17*, 736-743.

Fischer, S.C., Blanchard, G.B., Duque, J., Adams, R.J., Arias, A.M., Guest, S.D., and Gorfinkiel, N. (2014). Contractile and mechanical properties of epithelia with perturbed actomyosin dynamics. PLoS One *9*, e95695.

Gelbart, M.A., He, B., Martin, A.C., Thiberge, S.Y., Wieschaus, E.F., and Kaschube, M. (2012). Volume conservation principle involved in cell lengthening and nucleus movement during tissue morphogenesis. PNAS *109*, 19298-19303.

Heissler, S.M., Chinthalapudi, K., and Sellers, J.R. (2015). Kinetic characterization of the sole nonmuscle myosin-2 from the model organism Drosophila melanogaster. FASEB J *29*, 1456-1466.

Hu, A., Wang, F., and Sellers, J.R. (2002). Mutations in human nonmuscle myosin IIA found in patients with May-Hegglin anomaly and Fechtner syndrome result in impaired enzymatic function. J Biol Chem *277*, 46512-46517.

Huxley, H.E. (1963). Electron Microscope Studies on the Structure of Natural and Synthetic Protein Filaments from Striated Muscle. J Mol Biol *7*, 281-308.

Kamisoyama, H., Araki, Y., and Ikebe, M. (1994). Mutagenesis of the phosphorylation site (serine 19) of smooth muscle myosin regulatory light chain and its effects on the properties of myosin. Biochemistry *33*, 840-847.

Kamm, K.E., and Stull, J.T. (1985). The function of myosin and myosin light chain kinase phosphorylation in smooth muscle. Annual Rev Pharm Toxic *25*, 593-620.

Kasza, K.E., Farrell, D.L., and Zallen, J.A. (2014). Spatiotemporal control of epithelial remodeling by regulated myosin phosphorylation. PNAS *111*, 11732-11737.

Kim, K. (2005). Disease-associated Mutations and Alternative Splicing Alter the Enzymatic and Motile Activity of Nonmuscle Myosins II-B and II-C. J Biol Chem *280*, 22769-22775.

Kovacs, M., Thirumurugan, K., Knight, P.J., and Sellers, J.R. (2007). Load-dependent mechanism of nonmuscle myosin 2. PNAS *104*, 9994-9999.

Kovacs, M., Toth, J., Hetenyi, C., Malnasi-Csizmadia, A., and Sellers, J.R. (2004). Mechanism of blebbistatin inhibition of myosin II. J Biol Chem *279*, 35557-35563.

Ma, X., Kovacs, M., Conti, M.A., Wang, A., Zhang, Y., Sellers, J.R., and Adelstein, R.S. (2012). Nonmuscle myosin II exerts tension but does not translocate actin in vertebrate cytokinesis. PNAS *109*, 4509-4514.

Ma, X., Lynch, H.E., Scully, P.C., and Hutson, M.S. (2009). Probing embryonic tissue mechanics with laser hole drilling. Phys Biol *6*, 036004.

Martin, A.C., Kaschube, M., and Wieschaus, E.F. (2009). Pulsed contractions of an actin-myosin network drive apical constriction. Nature *457*, 495-499.

Mason, F.M., Tworoger, M., and Martin, A.C. (2013). Apical domain polarization localizes actin-myosin activity to drive ratchet-like apical constriction. Nat Cell Biol *15*, 926-936.

Mayer, M., Depken, M., Bois, J.S., Julicher, F., and Grill, S.W. (2010). Anisotropies in cortical tension reveal the physical basis of polarizing cortical flows. Nature *467*, 617-621.

Munjal, A., Philippe, J.M., Munro, E., and Lecuit, T. (2015). A self-organized biomechanical network drives shape changes during tissue morphogenesis. Nature *524*, 351-355.

Straight, A. (2003). Dissecting Temporal and Spatial Control of Cytokinesis with a Myosin II Inhibitor. Science *299*, 1743-1747.

Vasquez, C.G., Tworoger, M., and Martin, A.C. (2014). Dynamic myosin phosphorylation regulates contractile pulses and tissue integrity during epithelial morphogenesis. J Cell Biol *206*, 435-450.

Vicente-Manzanares, M., Zareno, J., Whitmore, L., Choi, C., and Horwitz, A. (2007). Regulation of protrusion, adhesion dynamics, and polarity by myosins IIA and IIB in migrating cells. J Cell Biol *176*, 573-580.

Xie, S., and Martin, A.C. (2015). Intracellular signalling and intercellular coupling coordinate heterogeneous contractile events to facilitate tissue folding. Nat Comm *6*, 7161.

Yamashiro, S., Totsukawa, G., Yamakita, Y., Sasaki, Y., Madaule, P., Ishizaki, T., Narumiya, S., and Matsumura, F. (2003). Citron kinase, a Rho-dependent kinase, induces di-phosphorylation of regulatory light chain of myosin II. Mol Biol Cell *14*, 1745-1756.

Zhao, F.Q., Padron, R., and Craig, R. (2008). Blebbistatin stabilizes the helical order of myosin filaments by promoting the switch 2 closed state. Biophy J *95*, 3322-3329.

Chapter 4: Discussion

Key conclusions of this thesis

Myosin pulsing is regulated by cycles of myosin phosphorylation and dephosphorylation

Contractile myosin pulses have been observed in many developing systems; however, how these pulses are dynamically regulated was not known. The results presented in this thesis demonstrate that assembly and disassembly of contractile pulses of myosin require dynamic phosphorylation of the myosin RLC. Furthermore, coalescence of myosin in the medioapical domain requires signaling between myosin and its upstream activator, ROCK. Previous studies have observed myosin pulses and medioapical localization of myosin and ROCK but had not determined the mechanism underlying the dynamics and precise localization of myosin (Martin et al., 2009; Mason et al., 2013). The results presented here demonstrate that dynamic signaling by ROCK, an activating kinase, and myosin phosphatase, an inactivating phosphatase, are required to organize properly contractile myosin and to generate contractile pulses, thereby promoting efficient and coherent tissue invagination.

Cellular force-generation depends on myosin motor activity

Whether myosin ATPase activity, and thus myosin motor-driven translocation of actin filaments, is involved in cellular constriction and tissue morphogenesis is not well understood. Some studies have suggested that certain cellular contractions do not require myosin motor activity (Escuin et al., 2015; Ma et al., 2012). The results presented in this thesis provide evidence for a requirement for myosin motor activity during apical constriction in the *Drosophila* epithelium. Biochemical analysis of myosin phosphomutants demonstrate that so-called phosphomimetic mutants are constitutively active, above basal ATPase levels. However, the ATPase activity of the phosphomimetic myosin mutant does not reach the level of ATPase activity of phosphorylated myosin, and thus do not faithfully mimic the phosphorylated, activated myosin

state. *In vivo* analysis demonstrates that decreased myosin motor activity negatively affects the ability of cells to constrict and of tissue to generate tension, leading us to propose a model where force-generation scales with myosin ATPase activity.

Unanswered questions and future directions

The results presented in this thesis provide evidence for a mode of regulation of pulsatile myosin, and a requirement for myosin motor activity to generate efficient cellular contractions. Many open questions, discussed below, remain to be addressed to fully understand the regulation and importance of pulsatile myosin during tissue morphogenesis.

What are the dynamics of the myosin binding subunit of the myosin phosphatase?

We demonstrate that the myosin binding subunit (MBS) of the myosin phosphatase (MP) is required to generate pulsatile myosin, incremental apical constriction, and to limit myosin localization to the medial domain of the apical cell surface. While we know that MBS co-localizes with myosin puncta and myosin meshworks in fixed tissues, the spatial and temporal dynamics of MBS are not well understood (Vasquez et al., 2014). During *Drosophila* germband extension, the morphogenetic event that follows ventral furrow invagination, germband cells contract along their dorsal-ventral axis and elongate along their anterior-posterior axis in a process known as convergent-extension. Germband cells also display medial pulses; in these pulses, a 2 second delay between the peak intensity of myosin and the peak intensity of MBS was observed (Munjal et al., 2015; Rauzi et al., 2010). Though MBS was overexpressed at non-physiological levels, these results suggest the existence of a delayed negative feedback loop, where myosin intensity increases, produces a contractile event, and then MP (with MBS) remodels the myosin network so a new pulsatile cycle can begin. Characterization of how MBS temporal dynamics regulate pulsing and cell shape changes in the ventral furrow require generation of a fluorescently-tagged MBS probe expressed at physiological levels. To understand the relationship between MP and myosin, preliminary results indicate that the catalytic subunit of MP (PP1c∂, Flapwing in *Drosophila*) pulses with myosin, without any

observable temporal delay in the ventral furrow (data not shown). Characterization of MBS pulses in relation to myosin will help determine if there is a temporal delay in ventral furrow pulses. The absence of a temporal offset between myosin and MBS pulses would suggest that the nature of pulsatile myosin in apically constricting cells is different from cells undergoing convergent extension.

Additionally, the behavior of MBS pulses could be correlated with different classes of contractile events. Ratcheted contractile events are defined by a decrease in apical area and stabilization of this new area; these events are characterized by high amplitude myosin pulses and more persistent myosin (Xie and Martin, 2015). Unratcheted and unconstricting contractile events, defined by the relaxation of a constriction and no constriction, respectively, have low amplitude myosin pulses and less persistent myosin(Xie and Martin, 2015). One model that could account for difference in myosin persistence in ratcheted contractions compared to unratcheted and unconstricting contractions, is that the MBS pulse intensity or persistence is lower in ratcheted events than unratcheted and unconstricted events. Using a computational framework to classify pulses and contractile events, we can determine the relationship between MBS intensity and force generation.

Does ROCK regulate MP activity via MBS phosphorylation during apical constriction?

ROCK can activate myosin directly, by phosphorylating the myosin RLC, or indirectly, by phosphorylating MBS (Amano et al., 1996; Kawano et al., 1999; Kimura et al., 1996). Phosphorylation of MBS at a conserved threonine site (threonine-594) inhibits the catalytic activity of MP, and thus promotes the activated state of myosin (Kawano et al., 1999). While the importance of ROCK in apical myosin maintenance and stabilization of constriction has been shown, it remains unknown if either or both of these ROCK-dependent mechanisms of myosin activation are required for apical constriction (Mason et al., 2013). One way to determine if

ROCK stabilizes myosin via inhibition of MP activity during constriction is to express a version of MBS that is uncoupled from regulation by ROCK. The first 300 amino acids of MBS (MBS^{N300}) removes the inhibitory phosphorylation site but retains the domains required to interact with the catalytic subunit of MP, constitutively activating MP activity (Hirano et al., 1997; Tanaka et al., 1998). In cultured cells, expression of MBS^{N300} results in decreased myosin RLC phosphorylation and the absence of stress fibers and focal adhesion (Totsukawa et al., 2000). In *Drosophila,* overexpression of MBS^{N300} during germband extension decreased levels of apical myosin and generated shorter-lived myosin pulses, corroborating our results that MBS regulates pulsing and suggests that MBS^{N300} could be a great tool to uncouple MBS activity from regulation of ROCK (Munjal et al., 2015).

To test whether ROCK-inhibition of MBS is required during apical constriction, we will express MBS^{N300} during ventral furrow formation. Our preliminary results have found that overexpression of MBS^{N300} results in loss of pulsatile myosin behavior. Instead, myosin accumulates persistently, forming condensed foci in the medioapical domain of cells (data not shown). These results suggest a model where ROCK stabilizes myosin networks by protecting myosin from MP-induced disassembly. This model predicts that in the presence of MBS^{N300} there would be an increased overlap between myosin and ROCK intensity signals compared to wildtype tissues. Additionally, the formation of a connected supracellular myosin meshwork, which occurs in wildtype tissues and correlates with ratchet-like contractions, would be delayed or abnormal (Martin et al., 2009). These experiments will determine if MBS is an important ROCK target during apical constriction and provide further insight on the regulation of pulsatile myosin. Furthermore, by characterizing MBS dynamics during apical constriction (see above) and the importance of ROCK-dependent inhibition of MBS, we can determine if ROCK is regulating the stabilization phase of ratcheted constrictions by protein myosin networks from MP-induced disassembly.

What are upstream regulators of MBS?

Aside from negative regulation by ROCK, upstream regulation of MP and MBS during tissue morphogenesis is not well known. Two candidates, BIG1 and BIG2 (Arf guanine nucleotide-exchange factors), were found to bind MBS and the MP catalytic subunit and promote de-phosphorylation of the myosin RLC in cultured cells (Le et al., 2013). Depletion of the *Drosophila* homolog of BIG1/2, Sec71, resulted in persistent accumulation of apical myosin in the ventral furrow, which is reminiscent of the observed phenotype following depletion of MBS, suggesting that Sec71 could have a role in recruiting MP during apical constriction (data not shown)(Vasquez et al., 2014).

To identify other potential regulators of MBS, we will immuno-precipitate MBS from embryo lysates and perform mass-spectrometry on these purifications using protocols developed in our lab. The role of candidate interactors identified by our screen could be further investigated by live imaging of embryos depleted of a candidate gene via shRNA and comparing its phenotype to the phenotypes of MBS depletion and constitutive activation of MBS. Additionally, to determine if candidates are acting in the same pathway or signaling complex as MBS, we can see if depletion of MBS or expression of constitutively active MBS can suppress depletion of candidate gene phenotype.

Concluding Remarks

Previously, it was not known whether phospho-regulation of myosin contributed to pulsatile cell shape changes. The work presented in this thesis increased our understanding of the mechanisms of myosin pulsing. Cycles of apical myosin network assembly and consequent remodeling are required for incremental apical constriction and ventral tissue integrity as it invaginates. Pulsatile myosin-driven cellular contractions drive other processes during *Drosophila* development and are also observed in other animals (Maitre et al., 2015; Martin et al., 2009; Roh-Johnson et al., 2012; Solon et al., 2009). The modes of regulation of pulsatile myosin found in this thesis will likely inform us on how myosin generates force throughout various morphogenetic processes.

References

Amano, M., Ito, M., Kimura, K., Fukata, Y., Chihara, K., Nakano, T., Matsuura, Y., and Kaibuchi, K. (1996). Phosphorylation and activation of myosin by Rho-associated kinase (Rho-kinase). J Biol Chem *271*, 20246-20249.

Hirano, K., Phan, B.C., and Hartshorne, D.J. (1997). Interactions of the subunits of smooth muscle myosin phosphatase. J Biol Chem *272*, 3683-3688.

Kawano, Y., Fukata, Y., Oshiro, N., Amano, M., Nakamura, T., Ito, M., Matsumura, F., Inagaki, M., and Kaibuchi, K. (1999). Phosphorylation of myosin-binding subunit (MBS) of myosin phosphatase by Rho-kinase in vivo. J Cell Biol *147*, 1023-1038.

Kimura, K., Ito, M., Amano, M., Chihara, K., Fukata, Y., Nakafuku, M., Yamamori, B., Feng, J., Nakano, T., Okawa, K., *et al.* (1996). Regulation of myosin phosphatase by Rho and Rho-associated kinase (Rho-kinase). Science *273*, 245-248.

Le, K., Li, C.C., Ye, G., Moss, J., and Vaughan, M. (2013). Arf guanine nucleotide-exchange factors BIG1 and BIG2 regulate nonmuscle myosin IIA activity by anchoring myosin phosphatase complex. PNAS *110*, E3162-3170.

Maitre, J.L., Niwayama, R., Turlier, H., Nedelec, F., and Hiiragi, T. (2015). Pulsatile cell-autonomous contractility drives compaction in the mouse embryo. Nat Cell Biol*17*, 849-855.

Martin, A.C., Kaschube, M., and Wieschaus, E.F. (2009). Pulsed contractions of an actin-myosin network drive apical constriction. Nature *457*, 495-499.

Mason, F.M., Tworoger, M., and Martin, A.C. (2013). Apical domain polarization localizes actin-myosin activity to drive ratchet-like apical constriction. Nat Cell Biol *15*, 926-936.

Munjal, A., Philippe, J.M., Munro, E., and Lecuit, T. (2015). A self-organized biomechanical network drives shape changes during tissue morphogenesis. Nature *524*, 351-355.

Rauzi, M., Lenne, P.F., and Lecuit, T. (2010). Planar polarized actomyosin contractile flows control epithelial junction remodelling. Nature *468*, 1110-1114.

Roh-Johnson, M., Shemer, G., Higgins, C.D., McClellan, J.H., Werts, A.D., Tulu, U.S., Gao, L., Betzig, E., Kiehart, D.P., and Goldstein, B. (2012). Triggering a cell shape change by exploiting preexisting actomyosin contractions. Science *335*, 1232-1235.

Solon, J., Kaya-Copur, A., Colombelli, J., and Brunner, D. (2009). Pulsed forces timed by a ratchet-like mechanism drive directed tissue movement during dorsal closure. Cell *137*, 1331-1342.

Tanaka, J., Ito, M., Feng, J., Ichikawa, K., Hamaguchi, T., Nakamura, M., Hartshorne, D.J., and Nakano, T. (1998). Interaction of myosin phosphatase target subunit 1 with the catalytic subunit of type 1 protein phosphatase. Biochemistry *37*, 16697-16703.

Totsukawa, G., Yamakita, Y., Yamashiro, S., Hartshorne, D.J., Sasaki, Y., and Matsumura, F. (2000). Distinct roles of ROCK (Rho-kinase) and MLCK in spatial regulation of MLC

phosphorylation for assembly of stress fibers and focal adhesions in 3T3 fibroblasts. J Cell Biol *150*, 797-806.

Vasquez, C.G., Tworoger, M., and Martin, A.C. (2014). Dynamic myosin phosphorylation regulates contractile pulses and tissue integrity during epithelial morphogenesis. J Cell Biol *206*, 435-450.

Xie, S., and Martin, A.C. (2015). Intracellular signalling and intercellular coupling coordinate heterogeneous contractile events to facilitate tissue folding. Nat Commun *6*, 7161.